DECOUPLED ACCOMMODATION AND SEDIMENT SUPPLY IN THE LATE CRETACEOUS CORDILLERAN BASIN OF SOUTHERN UTAH: AN EXTRABASINAL AFFAIR

by

Jonathan William Primm

A thesis submitted to the faculty of
The University of Utah
in partial fulfillment of the requirements for the degree of

Master of Science

in

Geology

Department of Geology and Geophysics

The University of Utah

December 2016

The University of Utah Graduate School

STATEMENT OF THESIS APPROVAL

The thesis of **Jonathan William Primm**

has been approved by the following supervisory committee members:

Cari Johnson	, Chair	**07/15/2016** Date Approved
Lauren P. Birgenheier	, Member	**07/15/2016** Date Approved
Michael Andrew Stearns	, Member	**07/15/2016** Date Approved

and by **Thure E. Cerling**, Chair/Dean of

the Department/College/School of **Geology and Geophysics**

and by David B. Kieda, Dean of The Graduate School.

ABSTRACT

The Turonian-Coniacian Smoky Hollow Member of the Straight Cliffs Formation (Kaiparowits basin, southern Utah) records a transition from isolated fluvial channel bodies to increasingly amalgamated channel belts, capped by a highly amalgamated coarse-grained fluvial unit known as the Calico bed. Previous studies have interpreted Smoky Hollow Member architecture in terms of decreased accommodation due to eustasy, tectonics, or some combination of both. This regional stratigraphic outcrop study tests these and alternative hypotheses by combining detailed facies and architectural observations with paleocurrent analysis and provenance data (sandstone petrography and detrital zircon U-Pb geochronology). The Smoky Hollow Member displays upsection increases in average grain size, bed thickness amalgamation, and net-to-gross, and a planform fan-shaped morphology with a distal increase in sinuosity. These features are diagnostic of prograding distributive fluvial system. The progradation of this system oriented to the northeast based on thickness and facies patterns, and paleocurrent indicators. This basin-axial trend (i.e., approximately parallel to the fold-thrust belt at this latitude) is also supported by provenance data including detrital zircons derived mainly from the Mogollon Highlands and Cordilleran magmatic arc to the south rather than the more proximal Sevier fold-thrust belt to the west. An upsection increases in the modal percent of quartz and potassium-feldspar grains relative to lithic grains also signals these source terranes, but records episodic input from transverse drainages. Despite relatively

static eustatic sea-level and continuous tectonic subsidence, the data suggest that progradation persisted and was controlled by some combination of autogenic processes and increased extrabasinal sediment supply from the south, rather than changes in accommodation. Progradation of the Smoky Hollow Member fluvial system culminated in an unconformity of ~2-3 My at the top of the lower Calico bed interval, and a correlation with the Ferron Sandstone (Notom delta) 80 km northeast in the Henry Basin, is suggested based on facies relationships and geochronology. The Calico bed unconformity is interpreted to have been caused regional tilting and erosion, which is observed in both basins.

TABLE OF CONTENTS

LIST OF FIGURES

LIST OF TABLES

ACKNOWLEDGEMENTS

This research was supported by the Rocks2Models research consortium run by Cari Johnson and Lisa Stright (Colorado State University), with funding from Chevron, ConocoPhillips, Hess Corporation, Shell, and Statoil. Jonathan Primm received additional funding from the University of Utah Department of Geology and Geophysics through the ConocoPhillips Graduate Fellowship and Department Research Grant. Thanks to the Bureau of Land Management, the Grand Staircase Escalante National Monument, and the Dixie National Forest for permits to conduct research in the Kaiparowits Plateau region. Detrital zircon geochronology was performed at the University of Utah Department of Geology and Geophysics LA-ICP-MS Laboratory, run by Diego Fernandez. Thanks to T. Szwarc, Q. Sahratian, C. Beno, and G. Mackey for help during the processing and analysis of detrital zircon samples. Special thanks to Paul B. Anderson for valuable feedback. Lastly, thanks to B. Chentnik, G. Ferguson, C. Johnson, S. McMullen, K. Mika, T. Morrill, J. Mulhern, R. Purcell, G. Rea-Downing, S. Rosendahl, G. St. Pierre, and D. Wheatley for their assistance during fieldwork.

INTRODUCTION

Terrestrial strata in foreland basins commonly record a cyclical pattern in fluvial architecture that transitions between isolated channel bodies and highly amalgamated fluvial sheets (Burbank et al., 1996; DeCelles and Giles, 1996; Brozovic and Burbank, 2000; Catuneanu et al., 2001; Catuneanu, 2001; Cleveland et al., 2007; Fanti and Catuneanu, 2010; Aschoff and Steel, 2011; Miall, 2014). Amalgamated fluvial sheets, typically very coarse-grained sand to gravel deposits, have previously been interpreted as the foreland basin record of allogenic processes, such as eustasy (Shanley and McCabe, 1991, 1993; Wright and Marriott, 1993; Olsen et al., 1995; Van Wagoner, 1995) or tectonics (Burbank et al., 1988; Heller et al., 1988; Little, 1997; Horton et al., 2004), or climate (Newell et al., 1999; Amorosi et al., 2008; Lawton et al., 2014), with sediment supply coupled to one or more of these processes (Currie, 1997; Ethridge et al., 1998; Catuneanu, 2004; Allen and Heller, 2012).

These models suggest that allogenic processes alter the ratio of accommodation to sediment supply (A:S) such that fluvial architecture transitions between the more isolated (high A:S) and more amalgamated (low A:S) end members (cf. Allen, 1978; Leeder, 1978; Bridge and Allen, 1979). However, the relationship between channel belt amalgamation and A:S assumes constant avulsion frequency, whereas variable stratigraphic architecture has been documented under conditions of variable avulsion frequency and other considerations (Bryant et al., 1995; Colombera et al., 2015).

Alternatively, many studies have shown that autogenic processes can cause these architectural variations without the influence of allogenic controls (Sheets et al., 2007; Hajek et al., 2010, 2012; Chamberlin et al., 2016). Recent work suggests that distributive fluvial systems (DFSs), may be a dominant fluvial form in the rock record, and proposes that DFSs can prograde through the autogenic avulsion of active depositional lobes during static accommodation creation and sedimentation rates (Hartley et al., 2010; Weissmann et al., 2010, 2011, 2013).

Foreland basin depositional models are additionally complicated by the oversimplification of source-to-sink relationships for sediment transport. Typically, models imply a direct link between accommodation, generated by flexural loading in the orogenic belt, and sediment supply, controlled by exhumation and redistribution of sediment into the foredeep (Shanley and McCabe, 1994; Van Wagoner, 1995; DeCelles and Giles, 1996; DeCelles and Cavazza, 1999). Orogen-transverse drainages are thus inferred to be the primary sediment transport mechanism, feeding basin-axial drainages in the foredeep during rapid active subsidence, and prograding across most of the foreland during periods of high erosion rates in the thrust front (c.f. Heller et al., 1988; Burbank, 1992; Jordan, 1995). Recent work, however, has shown that basin-axial drainage systems likely play a large, if not primary, role in the organization of fluvial strata within some ancient foreland basins (DeCelles and Cavazza, 1999; Brozovic and Burbank, 2000; Garcia-Castellanos, 2002; Miall, 2006; Raines et al., 2013; Lawton et al., 2014; Szwarc et al., 2015). Therefore, it cannot assumed that ancient foreland basin fill is directly coupled with activity in the proximal thrust front. Furthermore, changes in fluvial architecture cannot be assumed to reflect signals from the fold-thrust belt (Dickinson and Gehrels,

2008b).

The Turonian-Coniacian Smoky Hollow Member of the Upper Cretaceous Straight Cliffs Formation is the basal member of a series of cyclical fluvial successions preserved along the Kaiparowits Plateau in southern Utah, USA **(**Figure 1; Eaton and Nations, 1991; Schmitt et al., 1991; Goldstrand, 1994; Little, 1997; Roberts, 2007; Lawton et al., 2014; Szwarc et al., 2015; Gooley et al., 2016). These strata were deposited along the western margin of the Western Interior Seaway and proximal to the Sevier fold-thrust belt, approximately 70-175 km to the west (DeCelles, 2004). The Straight Cliffs Formation preserves offshore marine to terrestrial strata in a series of transgressive-regressive cycles, with fluvial strata most common in the western study area (Figure 2; Peterson et al., 1969a, 1969b; Shanley and McCabe 1991, 1993; Allen and Johnson 2010a, 2010b, 2011; Johnson et al., 2011; Dooling, 2012; Pettinga, 2013; Chentnik et al., 2015; Szwarc et al., 2015; Gooley et al., 2016; Mulhern et al., in press; Purcell et al., in press). Due to the proximity to the Western Interior Seaway, the Straight Cliffs Formation is the basis for a widely-known sequence stratigraphic model that attributes the cyclicity in fluvial strata to downstream fluctuations in eustatic sea-level (Shanley and McCabe, 1994). In this model, more isolated channel bodies represent deposition during highstands and amalgamated sheets represent deposition during lowstands and early transgression. Alternatively, more recent studies of the John Henry and Drip Tank Members of the upper Straight Cliffs Formation interpret shifts in fluvial architecture to reflect the evolution of competing axial and transverse drainages, which broadly reflect tectonic and/or climatic drivers in distinct source terranes (Lawton et al., 2014; Szwarc et

Figure 1. Map illustrating outcrop extent of Smoky Hollow Member along the Kaiparowits Plateau in southern Utah along with measured section (sxn) locations, locations of detrital zircon (DZ) sampling, and the extent of interpreted aerial photographs. AW=Alvey Wash, BH=Buck Hollow, CC=Coal Canyon, COY=Coyote Road, CR=Croton Road, KG=Kelly Grade, LHC=Left Hand Collet, MC=Main Canyon, RHC=Rock House Cove, SH=Smoky Hollow, SM=Shakespeare Mine, TC=Tibbet Canyon, TG= Tibbet Gate.

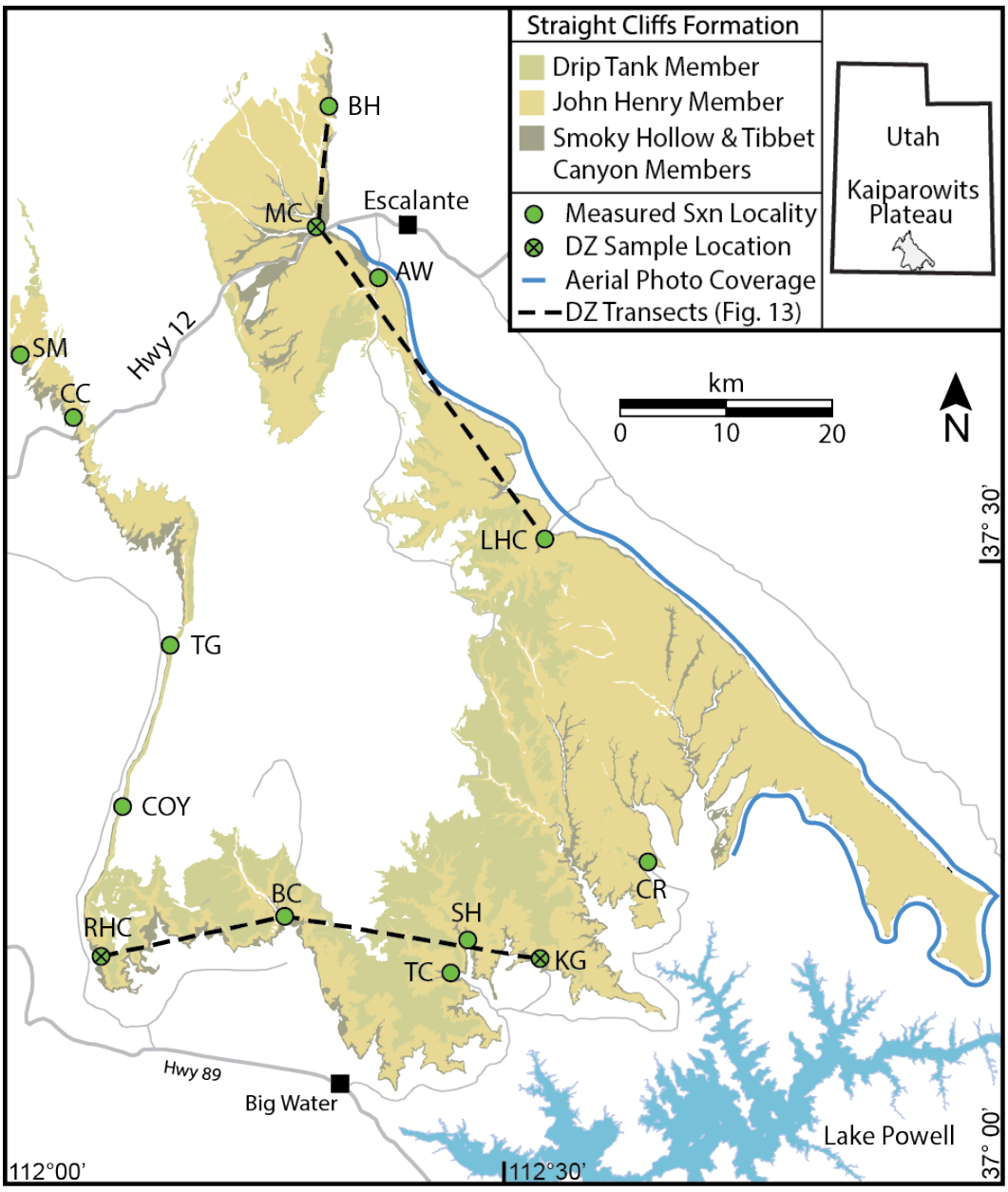
Straight Cliffs Formation
Drip Tank Member
John Henry Member
Smoky Hollow & Tibbet Canyon Members
Measured Sxn Locality
DZ Sample Location
Aerial Photo Coverage
DZ Transects (Fig. 13)
Utah
Kaiparowits Plateau
km
0
10
20
N
BH
MC
Escalante
AW
SM
CC
Hwy 12
LHC
TG
COY
BC
RHC
SH
TC
KG
CR
Hwy 89
Big Water
Lake Powell
37° 30'
37° 00'
112°00'
112°30'

Figure 2. Generalized stratigraphic column for the Straight Cliffs Formation in the Kaiparowits Plateau. Approximate ages of deposition, stratigraphic thicknesses, and depositional environment are labeled. Generalized sequence stratigraphic framework is from Shanley and McCabe (1994).

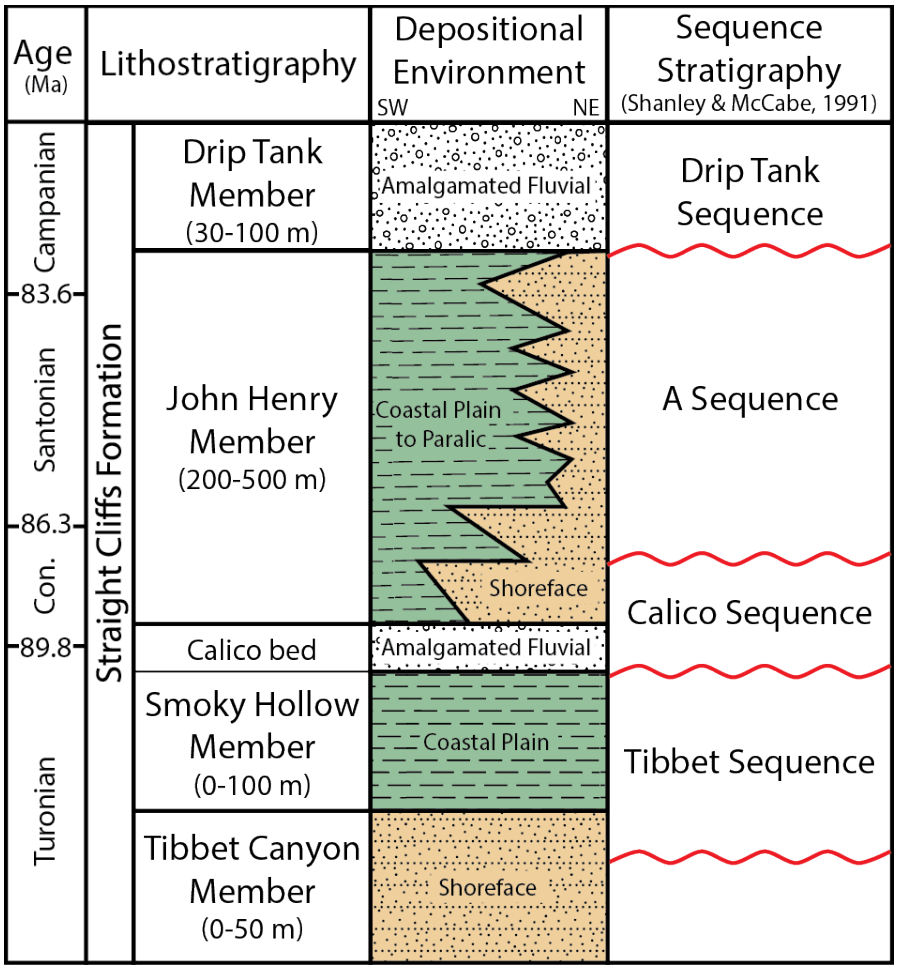
Age
(Ma)
Lithostratigraphy
Depositional Environment
SW
NE
Sequence Stratigraphy
(Shanley & McCabe, 1991)
Campanian
Santonian
Con.
Turonian
83.6
86.3
89.8
Straight Cliffs Formation
Drip Tank Member
(30-100 m)
John Henry Member
(200-500 m)
Calico bed
Smoky Hollow Member
(0-100 m)
Tibbet Canyon Member
(0-50 m)
Amalgamated Fluvial
Coastal Plain to Paralic
Shoreface
Amalgamated Fluvial
Coastal Plain
Shoreface
Drip Tank Sequence
A Sequence
Calico Sequence
Tibbet Sequence

al., 2015; Gooley et al., 2016). The Smoky Hollow Member is a relatively understudied but widespread fluvial section that provides additional opportunity to assess controls on sedimentation as this long-lived fluvial system was first established in the basin.

Previous studies of the Smoky Hollow Member are largely limited to its initial definition in the late 1960s (Peterson, 1969b), and later renewed interest in the early 1990s (Bobb, 1991; Shanley and McCabe 1991, 1993, 1995). Peterson (1969b) recognized the Smoky Hollow Member as a paludal to terrestrial fluvial unit that is topped by a regionally continuous, amalgamated coarse-grained fluvial unit known as the Calico bed. Furthermore, Peterson (1969b) interpreted an unconformity overlying the Calico bed spanning approximately the middle Turonian to middle Coniacian. Shanley and McCabe (1991, 1993, 1995) focused on placing the Straight Cliffs Formation within a sequence stratigraphic framework. In doing so, they interpreted the base of the Calico bed as a eustatic-driven sequence boundary (Figure 2), suggesting the coarse-grained Calico bed represented an abrupt, major seaward shift in facies. Bobb (1991) primarily focused on outcrops in the northern study area and reinterpreted the basal Calico bed sequence boundary as representing only a minor sea-level drop, the effects of which were suggested to be largely countered by high rates of subsidence. However, Bobb (1991) also suggested the coarse-grained Calico bed represented thrust-proximal sediment that was reworked into the basin due to slowed subsidence at this time. The present study provides the first detailed analysis of the Smoky Hollow Member across the Kaiparowits Plateau. This study presents facies and architectural interpretations combined with provenance and paleoflow data to both elucidate the depositional history and determine how potential allogenic and autogenic processes controlled deposition.

METHODS

This study employed both field- and lab-based methods to quantify the spatial and temporal variability in the Smoky Hollow Member's facies, architecture, and provenance. Eighteen detailed stratigraphic sections were measured from thirteen locations across the study area (Figure 1), typically measuring from the top of the Tibbet Canyon Member to the first prominent sandstone bed in the lower John Henry Member. Measured section descriptions included color, grain size, clast size, sorting, sedimentary structures, body and trace fossil occurrences, paleocurrent indicators, and bedding geometries. Lateral extent and maximum thickness of lenticular sandstone bodies were also recorded.

Paleocurrent and barform accretion data (n = 1950) were measured on sandstone beds throughout the Smoky Hollow Member. Paleocurrent data were measured using the axes of trough cross-stratification, tabular cross-stratification, and ripple lamination. The thickness of cross-set heights were recorded to estimate average channel dune height and mean bankfull water depth. Dune height is inferred to be 2.2 to 3.6 times the mean cross-set thickness, and mean bankfull water depth is inferred to be 6 to 10 times the dune height (Allen, 1984; Bridge and Tye, 2000; Leclair and Bridge, 2001). Where complete barform packages were preserved, these thicknesses were directly measured to compare to estimates. Accretion set orientation were compared to the paleocurrent orientations to distinguish between downstream and lateral accretion within channel bodies (McLaurin and Steel, 2007).

To supplement field observations between measured section locations and to better assess spatial variability in stratigraphic architecture at more remote locations of the study area, a series of low-angle aerial photographs (n = 217) were correlated over a distance of approximately 130 km by tracing key marker beds and sandstone packages along the eastern and southeastern study area (Figure 1). Due to the relatively low structural dip on these strata (<5°) and the distinctive nature of marker beds, approximate thicknesses were measured on these units using Google Earth. In addition to tracing marker beds, variations in fluvial architecture within the Smoky Hollow Member were noted, including relative changes in vertical and horizontal amalgamation, and the relative abundance of sandstone to mudstone and siltstone.

At each outcrop location, sandstone samples were collected (n = 38) from key horizons in order to assess temporal and spatial variations in composition. Sandstone samples were point conducted to determine modal mineral abundances using a modified Gazzi-Dickinson point counting method (Dickinson et al., 1983; Ingersoll et al., 1984; Zuffa, 1985). Five-hundred points were identified per sample. Framework grain identification focused on quantifying relative proportions of monocrystalline (Qm) and polycrystalline quartz (Qp), plagioclase (P) and potassium-feldspar (K), lithic fragments (L), and intergranular material when possible.

A total of ten sandstone samples were collected from Main Canyon, Rock House Cove, and Kelly Grade (Figure 1) for U-Pb detrital zircon geochronology. Zircons were isolated from the rocks by crushing and milling followed by magnetic (Sircombe and Stern, 2002) and density-separation techniques. The grains were mounted in 25 mm epoxy plugs. One hundred zircon grains were randomly selected from each sample for

analysis. The U-Pb dates were determined by laser-ablation inductively-coupled plasma mass spectrometry (LA-ICP-MS) at the University of Utah. Homogenous rim material was sampled using a Photon Machines® 193 nm excimer laser with a 24 µm laser beam diameter. Laser spots were placed with the aid of catholuminescene (CL) images for each grain, in order to target homogeneous crystal zonations. A standard-sample bracketing approach was employed using matrix matched primary and secondary reference materials. Laser-induced and downhole fractionation were characterized using the 91500 zircon (Wiedenbeck et al., 1995, 2004) as a primary reference material. Instrument drift and accuracy was monitored by measuring Plesovice zircon (Sláma, 2008) as a secondary reference material throughout the analytical run. Isotopic data were reduced using the Iolite v2.31 plugin for IgorPro (Paton et al., 2011), VizualAge (Petrus and Kamber, 2012), and Isoplot v3.75 plugin for Microsoft Excel (Ludwig, 2012). For each sample, additional error (~1–2%) was propagated to the secondary reference zircon to make it both accurate and a single population (MSWD = 1). This error was then added to each unknown analysis. A discordance filter of 10% was applied to data with ages greater than 500 Ma (Heumann et al., 2012; Szwarc et al., 2015).

RESULTS

Sedimentology and Stratigraphy

The Smoky Hollow Member contains fine- to coarse-grained fluvial and paralic deposits defined by 18 lithofacies following a classification scheme modified from Miall (1977, 1996). These lithofacies categories are primarily based on grain size and sedimentary structures, but also incorporate bedding geometries, architectural relationships, and trace and body fossils (Table 1). Lithofacies are grouped into two facies associations based on commonly observed assemblages, and these broadly reflect two depositional environments (Table 2).

Facies Association 1a Description

Facies association 1 is separated into two subdivisions, primarily reflecting mean grain size differences and dominant lithofacies. Facies association 1a is dominated by fine-grained lithofacies, including massive and laminated mudstone and siltstone (Fm, Fl), carbonaceous mudstone (Fc), and coal (C), with minor occurrences of sandstone lithofacies (Figure 3). The massive to laminated mudstone and siltstone units (Fm, Fl) occur in tabular beds that form bedsets typically 0.5 to 2.0 dm thick (Figure 3A). Colors include tan, grey-green, and purple, and mottling is rare to common. Sedimentary structures include rooting and blocky pedogenic structures. Coal beds are tabular, generally 0.1–2 m thick, and range in apparent grade from subbituminous to bituminous (Hettinger et al. 1996, 2000a). Carbonaceous mudstone beds are dark brown, weakly

Table 1

Observed lithofacies of upper Tibbet Canyon Member, Smoky Hollow Member, and lower John Henry Member

Code	Lithofacies	Description	Interpretation
Gm	Massive conglomerate	Structureless, clast-supported conglomerate; clasts are subangular to subrounded; clast size ranges from 2 to 40 mm in diameter with an average diameter of approximately 15 mm; matrix grain sizes range from medium to very coarse sand; bed thickness ranges from 0.1 to 0.5 m; often grades into Gp or Gm	Gravel sheet and channel lag deposits
Gt	Trough cross-stratified conglomerate	Clast-supported to matrix-supported conglomerate with trough cross-stratification; clasts are subangular to subrounded; clast size ranges from 2 to 20 mm in diameter with an average diameter of approximately 10 mm; matrix grain sizes range from fine to very coarse sand; foreset height ranges from 5 to 20 cm; bed thickness ranges from 0.1 to 1.5 m; often grades into Gp or St	Channel lag bedforms and barform deposits
Gp	Planar cross-stratified conglomerate	Clast-supported to matrix-supported conglomerate with planar cross-stratification; clasts are subangular to subrounded; clast size ranges from 2 to 40 mm in diameter with an average diameter of approximately 15 mm; matrix grain sizes range from from medium to very coarse sand; foreset height ranges from 2 to 15 cm; bed thickness ranges from 0.1 to 1 m; often grades into St or Sp	Channel lag bedforms and barform deposits
Se	Erosional sandstone	Irregularly-based, medium- to very-coarse grained sandstone with abundant pebble-sized clasts, wood material, and mud rip-up intraclasts; occur at the base of sandstone bedsets; often grades into St or Sp	Channel lag deposits during barform migration
Sm	Massive sandstone	Structureless, very fine- to very coarse-grained sandstone; pebble-sized clasts rare; bed are <0.5 m thick	Rapid sedimentation in channel-fill, levee, and splay deposits

Table 1 continued

Code	Lithofacies	Description	Interpretation
St	Trough cross-stratified sandstone	Fine- to very coarse-grained sandstone with trough cross-stratification; pebble-sized clasts rare to common; foreset height ranges from 1 to 15 cm; bed thickness ranges from 0.1 to 2.5 m; often grades into Sp, Sl or Sr	Migration of 3D unidirectional dune bedforms
Sp	Planar cross-stratified sandstone	Very fine- to very coarse-grained sandstone with planar cross-stratification; pebble sized clasts rare to common; foreset height ranges from 1 to 10 cm; bed thickness is <1 m; often grades into Sh or Sr	Migration of 2D unidirectional dune bedforms
Sh	Laminated sandstone	Very fine- to medium-grained planar laminated sandstone; often grades into Sr or Sb	Deposition during upper flow regime
Sr	Ripple-laminated sandstone	Very fine- to medium-grained sandstone with current ripples; ripple heights are <3 cm	Deposition during lower flow regime
Sf	Flaser-bedded sandstone	Very fine- to medium-grained sandstone with flaser ripples- sandstone ripples with mud and carbonaceous shale drapes; ripples are <2 cm thick	Deposition during fluctuating flow
Sc	Convolute-bedded sandstone	Fine- to coarse-grained sandstone with deformed bedding structures	Rapid sedimentation or post-depositional slumping or dewatering

Table 1 continued

Code	Lithofacies	Description	Interpretation
Sb	Bioturbated sandstone	Very fine- to very coarse-grained sandstone with original bedding structures altered or erased by bioturbation; observed traces include *Asthenopodichnium, Arenicolites, Diplocraterion, Lockeia, Ophiomorpha, Planolites, Skolithos, Taenidium, Teredolites, Thalassinoides*, and theropod tracks.	Biogenic reworking of sediments in crevasse splay, levee, and barform deposits
Fm	Massive mudstone/ siltstone	Structureless mudstone and siltstone; may contain organic matter and leaf impressions; often grades into Fl, Fc, or C	Waning flow of flooding events on floodplain or in abandoned channels
Fl	Laminated mudstone/ siltstone	Laminated mudstone and siltstone; may contain organic matter and leaf impressions; often grades into Fm, Fc, or C	Deposition from suspension and traction during waning flow of flooding events on floodplain or in abandonded channels
Fc	Carbonaceous mudstone	Laminated to structureless, dark brown to black shale; contains abundant plant material and coal fragments; closely associated with C	Floodplain deposition with high preservation of organic matter
C	Coal	Coal ranging in apparent grade from subbituminous to bituminous; closely associated with Fc	Peat development in poorly-drained flooplain or mire setting

Table 2

Facies associations for studied stratigraphic interval, including associated lithofacies, common architectural elements, facies association description, and interpretation

Facies Association	Lithofacies	Architectural Elements	Description	Interpretation	Depositional Environment
1a	C, Fc, Fm, Fl, Sm, Sr, Sh, Sb	Tabular beds; lenticular sandy bedforms	Massive mudstone and siltstone, laminated carbonaceous shale, 0.2-6 m thick coal beds, and minor thin (<1 m), very fine to medium sandstone beds	Overbank deposits and crevasse splays	Floodplain
1b	Fl, Sm, St, Sp, Sh, Sr, Gm, Gp, Gt	Lenticular and tabular sandy bedforms and gravel bedforms	0.1-2 m thick, fine- to very coarse-grained, fining-up sandstone and sandy conglomerate in 0.5-6 m bedsets; vertical amalgamation moderate to high; horizontal amalgamation moderate to high	Fluvial channel fill deposits including channel lag and barform deposits	Fluvial Channel
2	Fm, Fl, Sm, St, Sp, Sh, Sr, Sb, Sf, Gm, Gp	Lenticular fines; Lenticular and tabular sandy bedforms and gravel bedforms; Inclined heterolithic strata	0.1-1.5 m thick, very fine- to coarse-grained, fining-up sandstone and minor sandy conglomerate in 0.5-4 m bedsets; vertical amalgamation low to high; horizontal amalgamation low to high; abundant organic material; tidal indicators including: flaser bedding, *Teredolites* trace fossil occurences, inclined heterolithic strata, and double mud drapes	Fluvial channel fill deposits proximal to shoreline, including channel lag and barform deposits	Tide-Dominated Estuary Fill

Figure 3. Facies association 1. A. Interbedded mudstone/siltstone (Fc, Fm) and tabular sandstone beds (Sm, St) increasing in thickness and grain size upsection, representing crevasse deposits grading into the uppermost channel body sandstone; B. Theropod track on the base of a heavily bioturbated, fine-grained sandstone bed (Sb) including Psilonichnus (Ps) and Skolithos (Sk) burrows; C. Siderite nodule on the top of a massive, green, very fine-grained sandstone bed (Sm); D. Barform succession of lithofacies of (from bottom to top) erosive base (Se), trough cross-stratified sandstone (St), and convolute bedded/massive bedded sandstone (Sc, Sm); E. Typical expression of facies association 1b within the Calico bed showing coarse-grained bases (Gt, Se) grading into sandstone (St, Sp) and mudstone (Fm) lithofacies; F. Detail of gravel lithofacies in Calico bed including abundant white, gray, and black chert; G. Fluvial channel body (bottom) transitioning laterally into abandoned channel-fill (Fc). Note: staff is 1.5 m tall with 0.25 m (red and white) and 0.10 (gray) subdivision.

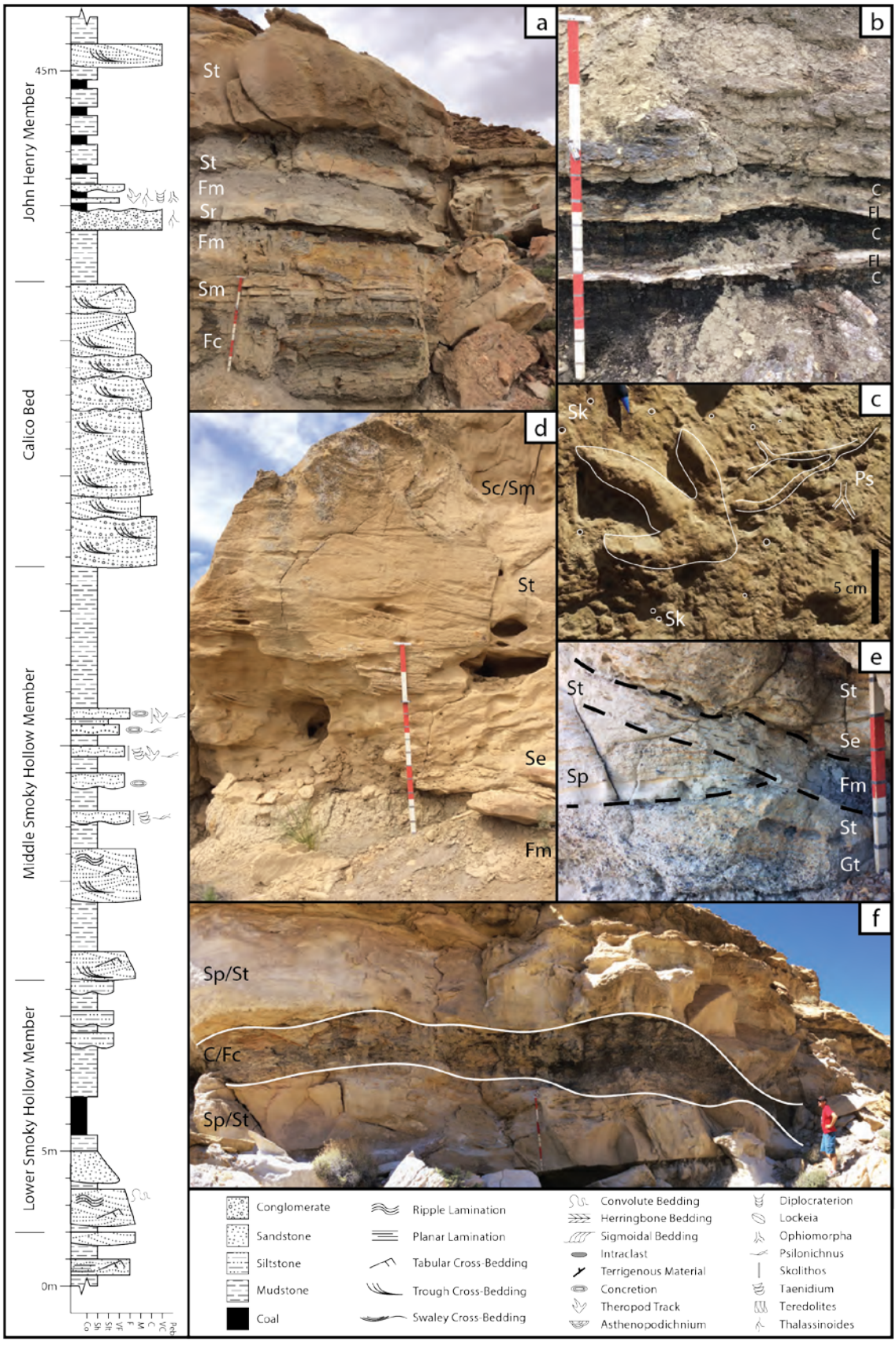
John Henry Member
Calico Bed
Middle Smoky Hollow Member
Lower Smoky Hollow Member
45m
5m
0m
a
St
St
Fm
Sr
Fm
Sm
Fc
b
C
Fl
C
Fl
C
c
Sk
Ps
5 cm
Sk
d
Sc/Sm
St
Se
Fm
e
St
St
Se
Sp
Fm
St
Gt
f
Sp/St
C/Fc
Sp/St
Conglomerate
Sandstone
Siltstone
Mudstone
Coal
Ripple Lamination
Planar Lamination
Tabular Cross-Bedding
Trough Cross-Bedding
Swaley Cross-Bedding
Convolute Bedding
Herringbone Bedding
Sigmoidal Bedding
Intraclast
Terrigenous Material
Concretion
Theropod Track
Asthenopodichnium
Diplocraterion
Lockeia
Ophiomorpha
Psilonichnus
Skolithos
Taenidium
Teredolites
Thalassinoides

laminated with abundant organic matter, typically within tabular beds that are <0.1–1 m thick (Figure 3A). Beds of all four lithofacies range in lateral extent from <1 m up to 100s of m. The fine-grained lithofacies are typically found interbedded with one another and have gradational contacts. Trace fossils, including *Thalassinoides* and theropod tracks, are common at the tops of coal beds at southern outcrops but absent in the north (Figure 3B). Leaf impressions are common throughout.

Sandstone lithofacies of facies association 1a are typically 0.1–2 m thick, very fine- to medium-grained lenticular or tabular sandstone beds. They are most commonly brown to tan colored, but are commonly drab-green in the southern outcrops (Figure 3A–C). Beds typically fine upward internally, within a series of subsequently coarser and thicker beds upsection (Figure 3A). They are primarily located beneath sandstone bodies of facies association 1b, but can occur adjacent to these sandstone bodies, or, rarely, as isolated units within mudstone facies of facies association 1a. Sedimentary structures include trough cross-stratification (St), rippled and planar lamination (Sr, Sh), convolute bedding (Sc), and heavy bioturbation (Sb; Figure 3A–C). These sandstone units range in width from 5–100s of m. Beds remove up to 2 m of underlying strata through incision and laterally truncate fine-grained beds. Trace fossils are common to abundant in these sandstone bodies, and include *Planolites, Skolithos*, *Taenidium, Psilonichnus,* and theropod tracks (Figure 3B). Siderite nodules are common in the south, occurring within the green siltstone and sandstone beds (Figure 3C).

Facies Association 1a Interpretation: Floodplain Deposits

The deposits of facies association 1a formed in floodplain environments separating active fluvial channels. The fine-grained lithofacies beds are overbank fines

that were deposited during levee-breaching flooding events, as well as minor paleosol development on interfluves. Overbank fines are mainly composed of carbonaceous mudstone and coal when sediment input is low enough to form a swamp or mire (McCabe and Parrish, 1992). Preservation of these deposits is mainly controlled by water table level (a function of rainfall and sea level fluctuations), clastic sediment input, and accommodation (Bohacs and Suter, 1997).

The coal and carbonaceous mudstone beds of the overlying John Henry Member were originally separated into four major coal zones by Peterson (1969a), and correlated across the plateau by Hettinger at al. (1996, 2009). These coal deposits were interpreted as raised mires by Shanley and McCabe (1992), forming as the result of peat accumulation on a coastal plain elevating the mires above adjacent floodplain deposits (Shearer et al., 1994). Peterson (1969b) only designated a basal coal zone in the Smoky Hollow Member, although coal beds can occur throughout the unit as isolated, lenticular beds. It is likely that the thick, laterally extensive coal beds of the Smoky Hollow Member occurred on raised coal mires, similar to the coal zones of the John Henry Member. The purple to green, mottled mudstone to siltstone beds with siderite nodules also suggest a poorly-drained, reducing environment (Kraus, 1999; Kraus and Hasiotis, 2006).

The sandstone lithofacies of facies association 1a represent crevasse deposits, i.e., the mud to sand-sized suspended and bed load of a channel that spills into the floodplain during levee-breaching flood events (Smith et al., 1989). Crevasse deposits typically occur adjacent to channel bodies where they thin and fine away from the channel body, or in a coarsening-, thickening-upward succession below channel bodies (Kraus and Wells,

1999). Both styles are present in facies association 1a, but the latter is most common.

Facies Association 1b Description

Facies association 1b is comprised almost entirely of sandstone and gravel lithofacies, with minor occurrences of fine-grained lithofacies. The sandstone and gravel lithofacies are found in lenticular to tabular beds of fine-grained sand to coarse pebbles. A single bed may contain both sand- and pebble-sized grains with poor to moderate sorting. These beds are typically dominated by trough and planar cross-stratification (Gt, Gp, St, Sp), but can be massive (Gm, Sm) or ripple laminated (Sr). There is a common vertical succession of these lithofacies from massive or erosive bases, to trough cross-stratified beds, to planar cross-stratified beds, with massive, laminated, or rippled tops (Figure 3D–E). Pebbles are generally concentrated along the erosive bases of beds and along large cross-sets and display upward fining into sand-sized grains (Figure 3E–F). Fine-grained lithofacies may also occur in this lithofacies succession, generally near the top as 0.1 to 3 m thick lenticular beds of massive to laminated mudstone (Fm, Fl; Figure 3G). This succession is the result of changing shear stress due to flooding and waning flow conditions along a barform (Jackson, 1976; Miall 1977, 1978). Beds show internal fining-up trends, and an overall fining-up in grain size within the barform. Cross-set heights are 0.1–2.0 m thick resulting in barforms that are 1–6 m thick (Figure 3A, D, G**)**. These barforms are also typically vertically amalgamated, resulting in 1–15 m thick packages that are composed of 1 to 6 barform successions (Figure 3). These packages can range from 10s m to >1000s m in lateral extent.

Facies Association 1b Interpretation: Fluvial Channel-Fill

Facies association 1b is interpreted to represent deposition in fluvial channels. Although rare, associated lenticular mudstone bodies are interpreted to represent abandoned channel fill, i.e., the result of fine-grained sediment depositing from suspension in lakes that formed due to chute or neck cutoff (Miall, 2006). Laterally amalgamated barforms are interpreted as a channel story representing barform accretion during the migration of a single channel (Friend, 1971). Accretion surfaces range from parallel to perpendicular to flow based on internal paleocurrent indicators and can represent both downstream and lateral accretion sets (McLaurin and Steel, 2007). Although limited in number compared to internal paleocurrent measurements, accretion set trends generally imply more lateral accretion in the lower Smoky Hollow Member transitioning to more downstream accretion in the Calico bed. Decompacted estimates for bankfull depths range from 1.8 to 4.9 m based on scaling of average cross-set thicknesses (Table 3; Allen, 1984; Bridge and Tye, 2000; Leclair and Bridge, 2001), and are consistent with 15 measurements of full barforms ranging from 1.9 to 6.3 m.

Facies Association 2 Description

Facies association 2 is primarily composed of sandstone with lesser amounts of gravel and fine-grained lithofacies. Sandstone lithofacies are similar to those of facies association 1b, occurring in 0.1 to 1.5 m thick lenticular to tabular beds. These beds are fine- to coarse-grained, showing upward fining trends. Sedimentary structures are dominantly trough and planar cross-stratification (St, Sp), but also include convolute bedding (Sc), climbing ripples, flaser bedding (Sf), ripple lamination (Sr), and sigmoidal cross-stratification (Figure 4A). Rare herringbone cross-stratification is also present in

Table 3

Calculated paleohydraulics for the lower and middle Smoky Hollow Member (LSHM, MSHM), lower and upper Calico bed (LCB, UCB), and lower John Henry Member (LJHM). Calculated paleohydraulics include estimated dune height and mean bankfull depth (from methods in Allen, 1984; Bridge and Tye, 2000; Leclair and Bridge, 2001), and standard deviation (StD) of paleocurrent flow meant to approximate sinuosity.

Region	Interval	Mean Cross-Set Thickness (m)	Estimated Dune Height (m)			Est. Bankfull Depth (m)			Paleocurrents	
			Min	Mid	Max	Min	Mid	Max	Mean	StD
North (Distal)	UCB	0.14	0.31	0.41	0.50	1.8	3.2	5.0	61.4	41.7
	LCB	0.23	0.51	0.67	0.83	3.0	5.3	8.3	46.7	40.3
	MSHM	0.14	0.31	0.41	0.50	1.8	3.2	5.0	71.7	32.4
	LSHM	0.12	0.26	0.35	0.43	1.6	2.8	4.3	78.4	27.9
South (Proximal)	LJHM	0.07	0.15	0.20	0.25	0.9	1.6	2.5	60.2	25.6
	LCB	0.13	0.29	0.38	0.47	1.7	3.0	4.7	55.5	31.3
	MSHM	0.13	0.29	0.38	0.47	1.7	3.0	4.7	90.6	28.3
	LSHM	0.12	0.26	0.35	0.43	1.6	2.8	4.3	102.7	28.4

Figure 4. Facies Assocation 2. A. Sigmoidal bedded and trough cross-stratified sandstone (Ss, St); B. Herringbone cross-stratification showing opposing paleocurrent indicators to the right (bottom) and left (top); C&D. Uninterpreted (left) and interpreted (right) sandstone with mud drapes; E. Ophiomorpha (Op) and Thalassinoides (Th) burrows on a vertical exposure; F. Diplocraterion burrows on the top of a heavily bioturbated sandstone bed (Sb); G. Asthenopodichnium burrows in a wood substrate with white arrows pointing to characteristic oblong u-shaped burrows; H. Teredolites burrows in a wood substrate. See Figure 3 for key.

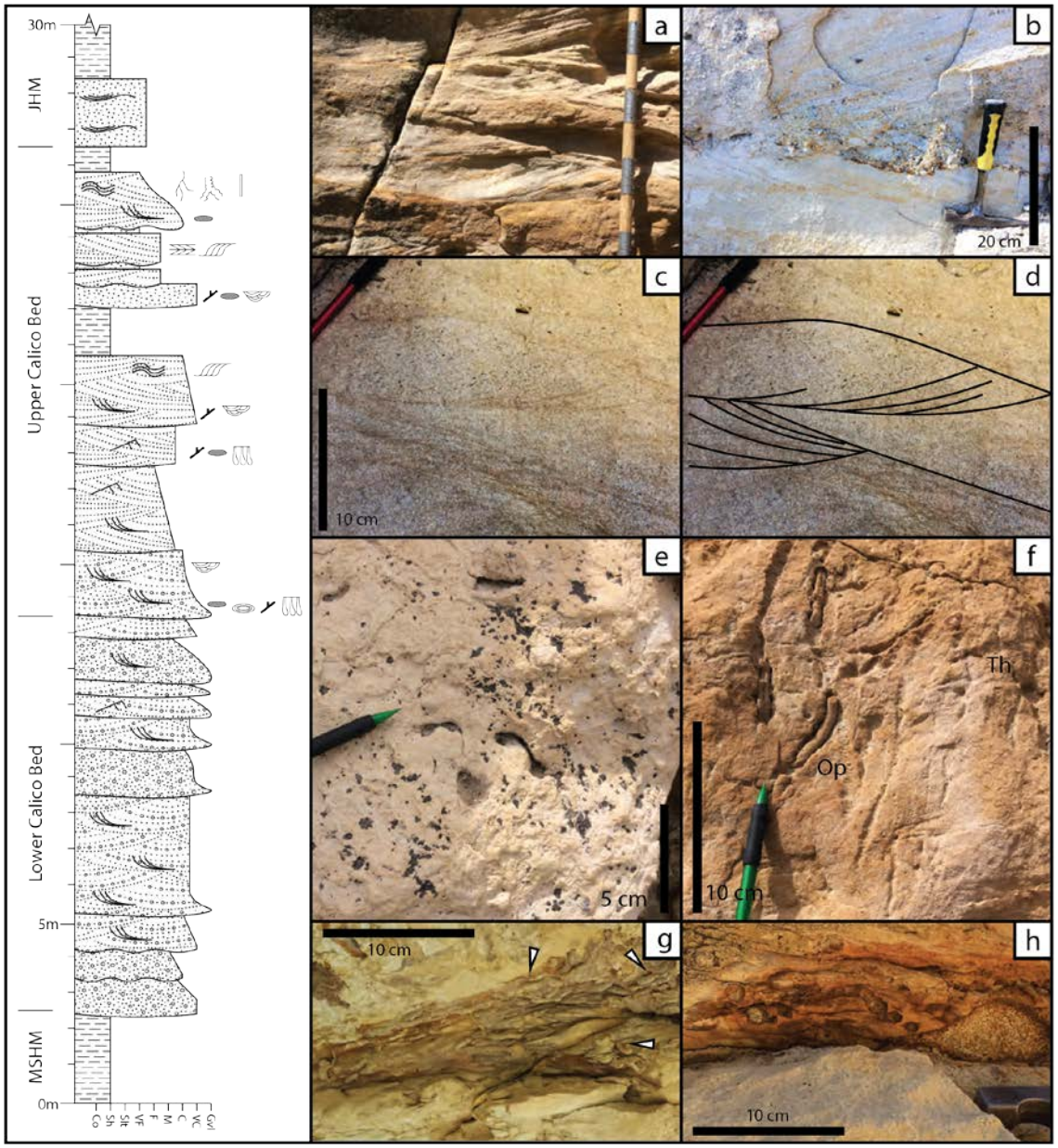
30m
JHM
Upper Calico Bed
Lower Calico Bed
5m
MSHM
0m
Cg
Sh
Sd
Vf
F
M
C
Vc
Gr
a
b
20 cm
c
10 cm
d
e
5 cm
f
Th
Op
10 cm
g
10 cm
h
10 cm

this facies association (Figure 4B). Gravel lithofacies are less common than sandstone, but occur at the base of bedsets as thin (0.1 – 0.5 m) massive or trough cross-stratified beds (Gm, Gt), or as lag deposits within erosional sandstone bases (Se; Figure 4B). Fine-grained lithofacies generally occur as mudstone or carbonaceous mudstone laminations (Fl, Fc) or organic-rich mud drapes (Figure 4C–D). Massive mudstone is also common as mud rip-up intraclasts and thin (< 0.5 m thick) lenses within sandstone packages.

Similar to facies association 1b, there is a typical lithofacies succession in sandstone bodies from erosive bases (Se) to trough and planar cross-stratification (St, Sp), to laminated or rippled tops (Sl, Sr). However, convolute bedding (Sc), bioturbation (Sb), and sigmoidal bedding (Ss) are much more common in facies association 2. Furthermore, these packages have common mudstone laminations and beds, occurring in flaser and rippled beds with mud drapes, and as inclined heterolithic strata (Figure 5). These packages represent barforms, and they range from 10's m to >1000s m wide due to lateral amalgamation. Vertical amalgamation ranges from 1 to 6 barforms, resulting in sand body thicknesses from 1 to 15 m thick. Trace fossils occurrences are widespread in this lithofacies association, with common occurrences of *Planolites*, *Skolithos*, *Thalassinoides*, *Ophiomorpha*, *Asthenopodichnium*, *Teredolites*, and theropod tracks, and rare occurrences of *Arenicolites*, *Diplocraterion*, and *Lockeia* (Figure 4E–H). Most of these traces occur within the top 0.5 m of bedsets except *Asthenopodichnium* and *Teredolites,* which are found in wood material throughout. Marine to brackish traces occur directly overlying the uppermost units of terrestrial facies association 1 at some localities in the southern field area, extending down into underlying fluvial sandstone and floodplain mudstone and coal beds (Figure 6E–F).

Figure 5. Photos showing the difference between the internal architecture of the Calico bed in the north (top) and the south (bottom). A. The lower Calico bed composed of 4-5 vertically and laterally amalgamated channel stories overlain by a paleosols and unconformity (red line), and the upper Calico bed composed of 4-6 vertically and laterally amalgamated channel stories, that display greater heterogeneity including prominent inclined hetetolithic strata (IHS); B. The lower Calico bed comprised of 2 vertically and laterally amalgamated channel stories (outlined in black) erosively overlain by a tidal bar of the lower John Henry Member (outlined in dashed black line). The red line marks the surface separating the Calico bed and John Henry Member.

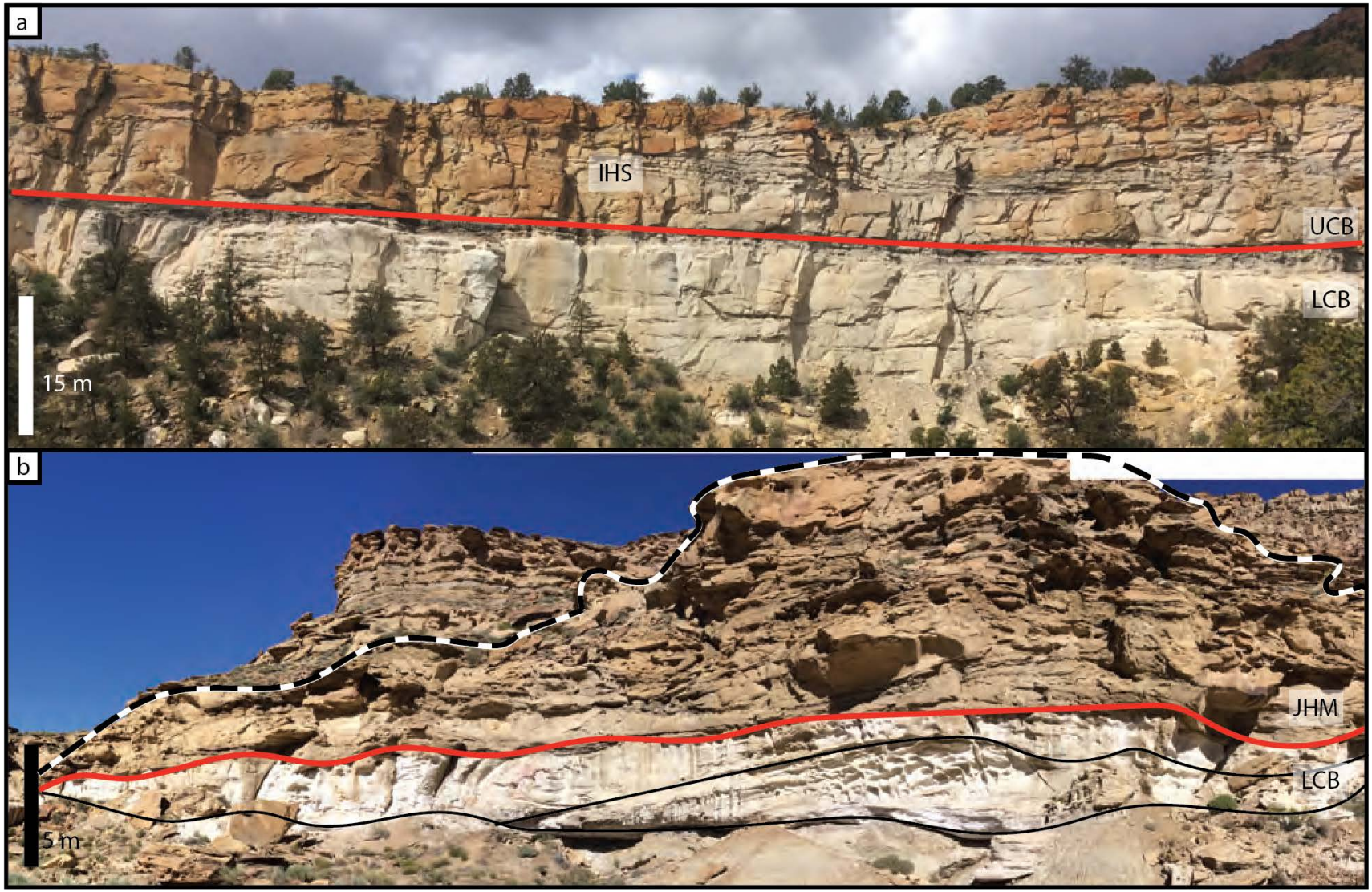
a
IHS
UCB
LCB
15 m
b
JHM
LCB
5 m

Figure 6: Photographs showing the variability in the surface (red dashed line) capping the lower Calico bed across the study area; A. Paleosol development showing gray mudstone grading into highly weather tan sandstone; B. Ferricrete layer separating lower and upper Calico bed; C. Iron concretion overlying Calico bed and underlying lower John Henry Member; D. Highly bioturbated top of lower Calico bed; E and F. Expression of Glossifungites surface overlying the Calico bed in the south including heavily bioturbated marine to brackish traces (D) and Thalassinoides on the sole of a bed (E) and within coal (F).

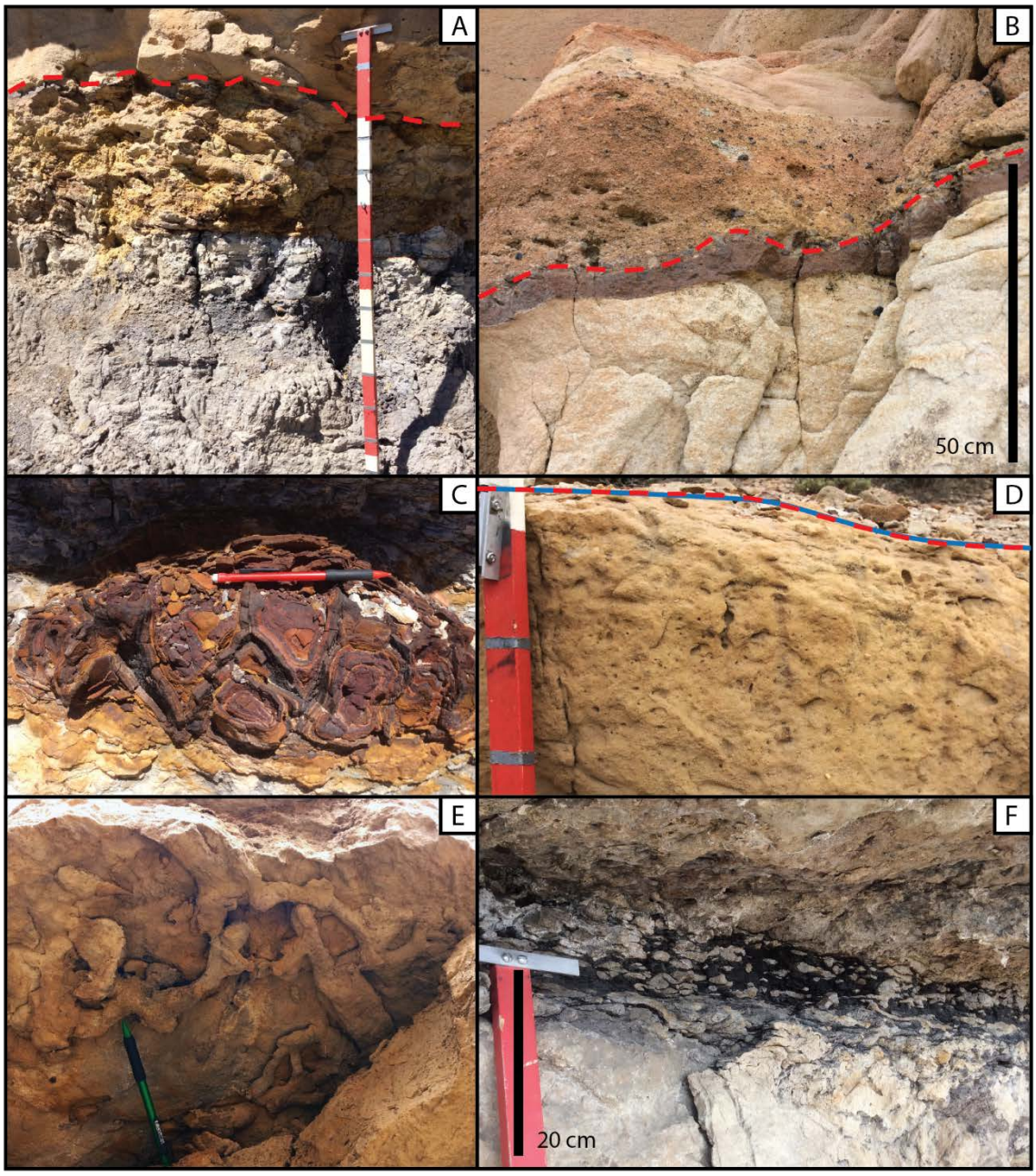
A
B
50 cm
C
D
E
F
20 cm

Facies Association 2 Interpretation: Tide-Dominated Estuary Fill

Facies association 3 is interpreted as tide-influenced fluvial channel fill due to the presence of both fluvial channel characteristics and tidal indicators. Observed sedimentary structures that are common tidal indicators include: flaser bedding (Reineck and Wunderlich, 1968), sigmoidal cross-stratification (Kreisa and Moiola, 1986), mud drapes within sandy cross-stratification, herringbone cross-stratification, and inclined heterolithic strata (Shanley et al., 1992; Davis, 2012). These deposits are the result of periodic waning to reversing flow causing dynamic bedding geometries and the deposition of suspended load fines interbedded with sand-sized beds (Davis, 2012). Both *Asthenopodichnium* and *Teredolites* form in wood substrates, but *Asthenopodichnium* is an insect trace that forms in freshwater conditions (Moran et al., 2010; Genise et al., 2012), whereas *Teredolites* is a shipworm burrow that forms in wood that has been inundated with brackish water, and is commonly used as a tidal indicator (Bromley et al., 1984; Shanley et al., 1992). The fact that these trace fossils are found interspersed throughout facies association 3 further suggests mixing of brackish and freshwater conditions.

The remaining suite of observed trace fossils in facies association 3 includes indicators of brackish water environments (Gingras and MacEachern, 2012). Specifically, *Ophiomorpha* is commonly found in brackish to marine environments, and *Thalassinoide*s is found in fully marine environments (Frey, 1978; Howard et al., 1984). *Diplocraterion* burrows are indicative of intertidal deposition (Fürsich, 1975). The presence of theropod tracks supports relatively shallow-water environments. These trace fossils are typically found near the tops of barform bedsets, similar to Campanian tidally-

influenced fluvial barform deposits of the Middle Castlegate Sandstone and Neslen Formation of northern Utah and western Colorado (Aschoff and Steel, 2011). In the southern study area, these trace fossils are abundant in the top 50 cm of the lower Calico bed (facies association 1b), forming what is interpreted as a *Glossifungites* surface (Figure 6).

Previous research recognized several of these tidal indicators within Smoky Hollow Member strata and interpreted them as "heterolithic estuarine strata" (Hettinger et al., 1993). Due to the strong fluvial influence recorded by facies association 3, however, it is suggested here that these strata are primarily within the tidal-fluvial transition of a tide-dominated estuary. The tidal-fluvial transition commonly shows a dominance of bedload with tidal indicators becoming more common seaward (Dalrymple and Choi, 2007). The tidal indicators listed herein are present only in the most eastern outcrop locations, Buck Hollow and Alvey Wash (Figure 1), supporting this interpretation. Furthermore, the extent of these deposits widen in extent from west to east and show a slight thickening in the seaward direction.

Stratigraphic and Spatial Variation

Although the internal contacts are typically gradational in nature, the Smoky Hollow Member is subdivided into four units based upon facies associations and architecture: the lower Smoky Hollow Member, the middle Smoky Hollow Member, a lower Calico bed, and an upper Calico bed (Figure 7). These informal units vary both stratigraphically and spatially across the study area.

Figure 7. Schematic diagrams highlighting the variation in Smoky Hollow Member architecture across the study area including changes in thickness, amalgamation, and facies associations; also shown are temporal variations in paleocurrent measurements for each area. TCM=Tibbet Canyon Member, LSHM=lower Smoky Hollow Member, MSHM=middle Smoky Hollow Member, LCB=lower Calico bed (CB), UCB=upper Calico bed, JHM=John Henry Member.

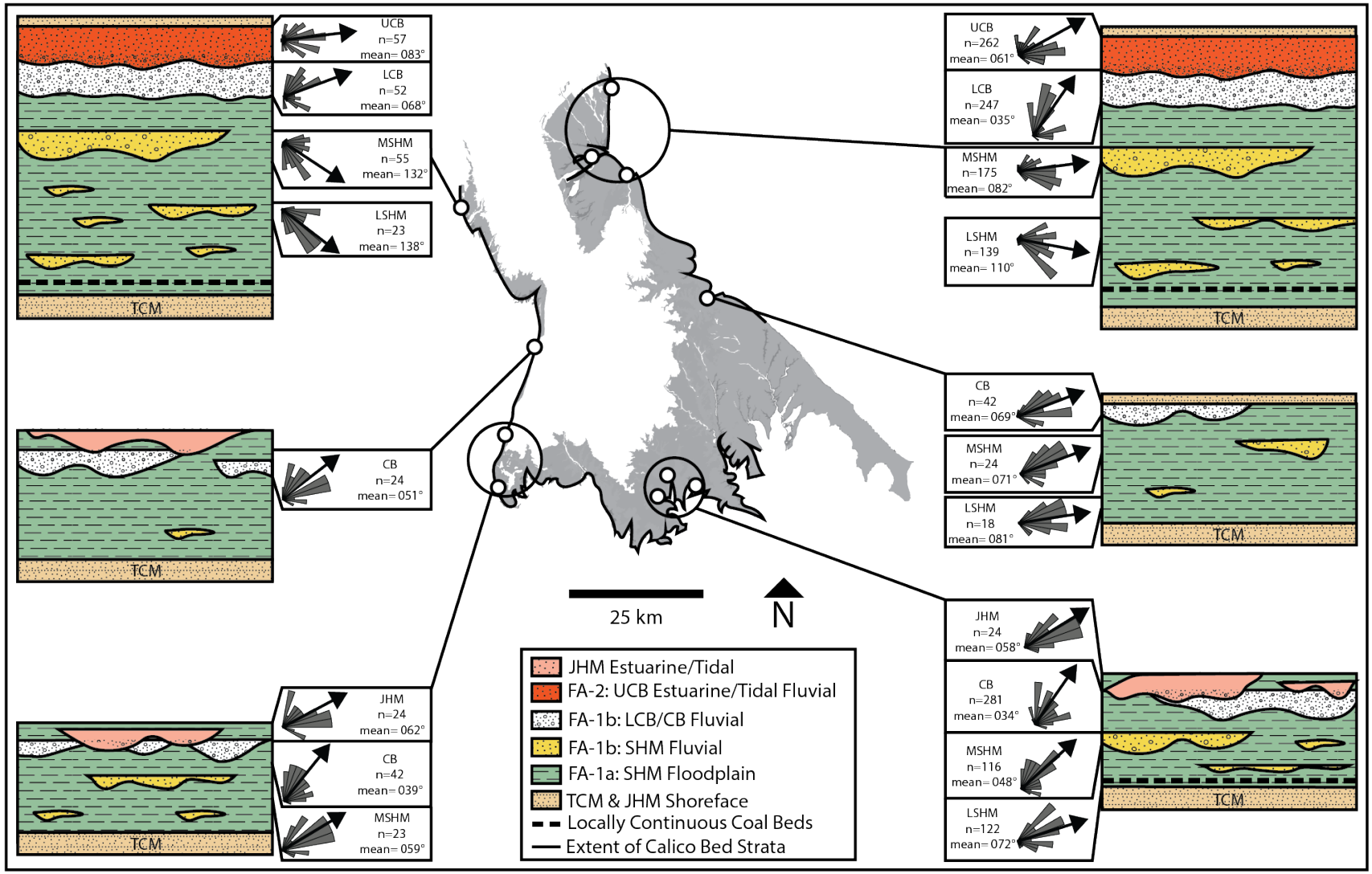
UCB
n=57
mean= 083°
LCB
n=52
mean= 068°
MSHM
n=55
mean= 132°
LSHM
n=23
mean= 138°
TCM
CB
n=24
mean= 051°
TCM
JHM
n=24
mean= 062°
CB
n=42
mean= 039°
MSHM
n=23
mean= 059°
TCM
UCB
n=262
mean= 061°
LCB
n=247
mean= 035°
MSHM
n=175
mean= 082°
LSHM
n=139
mean= 110°
TCM
CB
n=42
mean= 069°
MSHM
n=24
mean= 071°
LSHM
n=18
mean= 081°
TCM
JHM
n=24
mean= 058°
CB
n=281
mean= 034°
MSHM
n=116
mean= 048°
LSHM
n=122
mean= 072°
TCM
25 km
N
JHM Estuarine/Tidal
FA-2: UCB Estuarine/Tidal Fluvial
FA-1b: LCB/CB Fluvial
FA-1b: SHM Fluvial
FA-1a: SHM Floodplain
TCM & JHM Shoreface
Locally Continuous Coal Beds
Extent of Calico Bed Strata

Lower Smoky Hollow Member

The lower Smoky Hollow Member overlies the Tibbet Canyon Member, which is defined as cliff-forming sandstone that gradationally overlies the Tropic Shale (Peterson, 1969b). The Tibbet Canyon Member is generally a lower to upper shoreface sandstone with an incision surface in the upper half that places amalgamated fluvio-deltaic and estuarine sandstones on upper shoreface sandstones (Figure 8A-B; Peterson, 1969b; Shanley and McCabe 1991, 1993, 1995). This surface has been interpreted previously as either an unconformity marking a major base-level fall (i.e., Tibbet Canyon sequence boundary; Shanley and McCabe, 1991) or as a relatively conformable succession deposited during a more gradual regression (Peterson, 1969b). More recently, a bentonite collected 3.5 m below the Calico bed near the Tibbet Gate location of this study (Figure 1) was dated using U-Pb zircon and $^{40}Ar/^{39}Ar$ sanidine geochronology, with ages of 91.86 ± 0.34 Ma and 91.88 ± 0.70 Ma, respectively (Titus et al., 2013). These ages are within the *Prionocyclus hyatti* biostratigraphic range of the Tibbet Canyon Member, which supports that interpretation that the Tibbet Canyon-Smoky Hollow contact is a relatively conformable succession (Peterson, 1969a; Eaton, 1991). Therefore, this study follows the original lithostratigraphic units of Peterson (1969b), and designates the lower bounds of the Smoky Hollow Member as the fine-grained deposits overlying the sandstone cliff of the Tibbet Canyon Member.

The informal designation of the lower Smoky Hollow Member in this study was defined primarily based on the prevalence of floodplain facies. It comprises approximately the lower half of the sub-Calico bed Smoky Hollow Member and is marked by a dominance of facies association 1a with minor occurrences of facies

Figure 8. A and B. Nature of the Tibbet Canyon-Smoky Hollow Member (TCM-SHM) contact showing a channel body erosively overlying shoreface deposits (left), and planar bedded medium-grained sandstone with abundant shell fragments (right) overlain by coastal plain mudstone of the Smoky Hollow Member (not pictured); C and D. Nature of the Calico bed-John Henry Member contact in the south showing a fluvial sandstone erosively overlying the Calico bed (left) and an interbedded heterogeneous estuarine sandstone erosively overlying the Calico bed (right); E&F. Transgressive ravinement surface of the upper Calico bed-John Henry Member (CB-JHM) contact in the north showing abundant quartzite pebble clasts and common shark teeth (right); Note: staff is 1.5 m tall with 0.25 m (red and white) and 0.10 (gray) subdivision

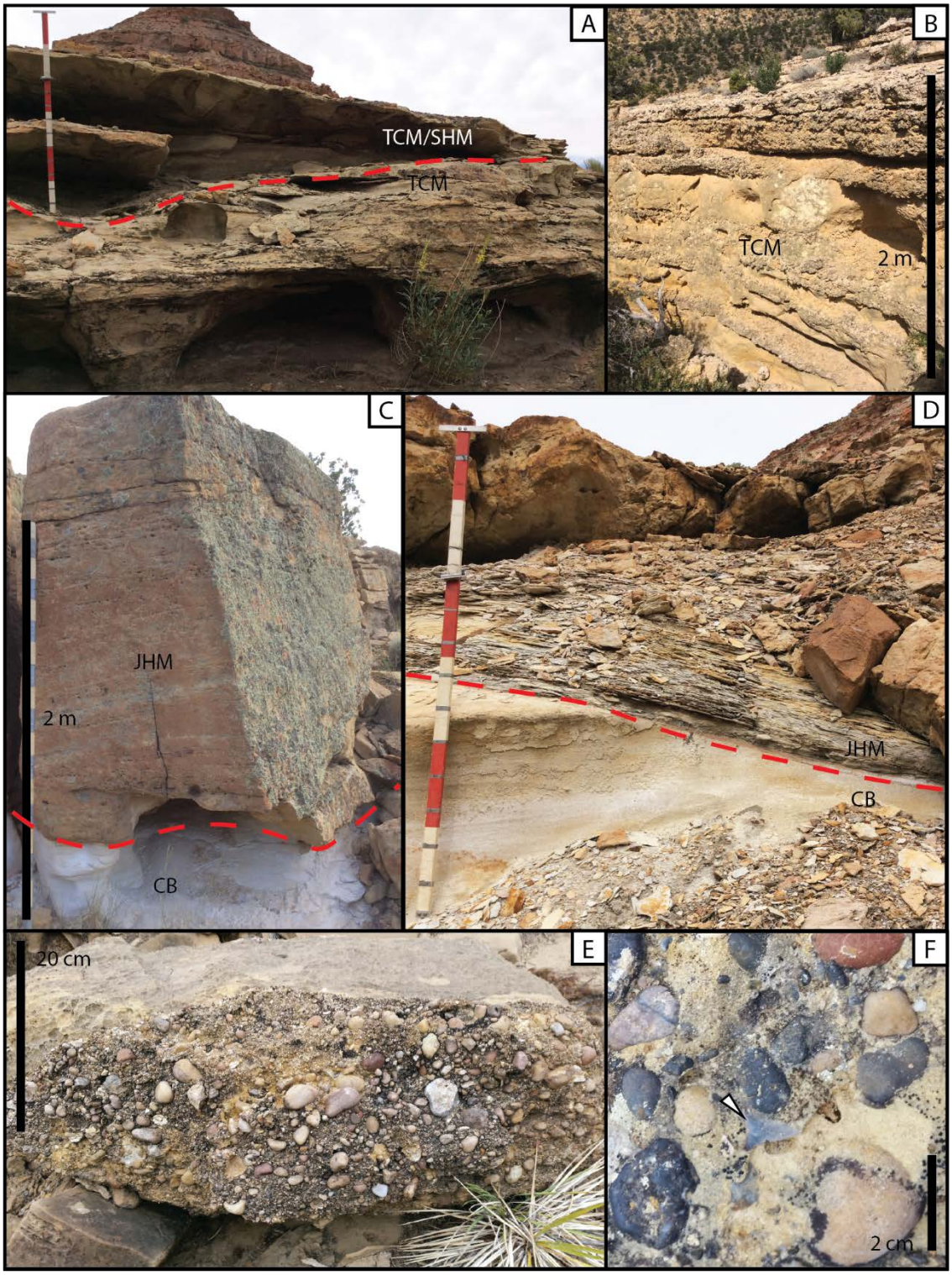
A
TCM/SHM
TCM
B
TCM
2 m
C
JHM
2 m
CB
D
JHM
CB
E
20 cm
F
2 cm

association 1b (Figure 7). Facies association 1a in this unit is recognized by common occurrences of coal and carbonaceous mudstone with thin (<0.5 m) crevasse deposits (Figure 3A). Facies association 1b occurs as isolated, thin (<2 m), fine- to medium-grained fluvial channel bodies.

Facies association 2 is rare in the lower Smoky Hollow Member, observed only at Buck Hollow (Figure 1). It is marked by interbedded thin (<2 m), fine- to medium-grained fluvial channel bodies and carbonaceous mudstone. These channel bodies are typically massive to trough-cross-stratified and have common occurrences soft sediment deformation, sigmoidal bedding, and *Ophiomorpha* and *Thalassinoides* traces. Tibert and Leckie (2004) interpreted the basal 5 m of the Smoky Hollow Member near Shakespeare Mine (Figure 1) as estuarine based upon foraminiferal assemblages within mudstones. This suggests that estuarine deposits might be more prominent in the Smoky Hollow Member than those indicated by facies association alone, particularly where sections are dominantly mudstone.

Spatially, the lower Smoky Hollow Member is marked by a decrease in thickness from 30–40 m in the north to 5–15 m in the south: a product of the decrease in overall thickness of the Smoky Hollow Member (Figure 7). The green siltstone to fine-grained sandstone beds of facies association 1 are only present in the south where they are very common in the lower Smoky Hollow Member. Paleocurrents from this interval also show spatial variation, transitioning from directed to the east-southeast at northern outcrops (mean=103°), and to the east at southern outcrops (mean = 78°; Figure 7; Table 3).

Middle Smoky Hollow Member

The middle Smoky Hollow Member was defined primarily by the increased abundance of fluvial channels. It is gradational with the lower Smoky Hollow Member and is, therefore, approximately the top half of the sub-Calico bed Smoky Hollow Member. Floodplain facies of the middle Smoky Hollow Member are typically composed of massive tan to gray mudstone and carbonaceous mudstone. Coal beds are only present in the middle Smoky Hollow Member at Tibbet Canyon in the south, where one 0.5 m thick, lenticular bed underlies the Calico bed. Channel bodies increase in vertical and horizontal amalgamation upsection, transitioning from thin (<2 m), isolated channel bodies that are 10s of meters laterally, to thick (<10 m) channel bodies that are 10s to 100s of meters laterally (Figure 7). Average grain size increases upsection from fine- to coarse-grained, with gravel lithofacies occurring in some of the stratigraphically highest channel bodies.

Similar to the lower Smoky Hollow Member, the middle Smoky Hollow Member thins from 30–40 m in the north to 5–15 m in the south (Figure 7). Channel bodies in the north are also thicker in the north, ranging from 3 to 10 m in the north and 1 to 8 m in the south. Channel bodies are sometimes rare to absent in the central study area, with only isolated, thin (<2 m) occurrences. At these outcrops, the lower and middle Smoky Hollow Member were each designated as half the stratigraphic thickness below the Calico bed. Furthermore, the middle Smoky Hollow Member shows similar spatial paleocurrent trends to the lower Smoky Hollow Member though paleocurrent indicators are more north-directed in the former. Within the middle Smoky Hollow Member, southern paleocurrent indicators are oriented to the east (mean = 091°) and southern

paleocurrent indicators are oriented east-northeast (mean = 072°; Figure 7; Table 3). Paleocurrents also show a greater standard deviation in the north (1σ = 32°) than the south (1σ = 28°; Table 3).

Lower Calico bed

The Calico bed is a prominent amalgamated ledge-forming sandstone unit throughout the study area. It is separated into a lower and upper unit in this study based on differences in architecture and facies associations. The lower Calico bed is distinguished by its prominent white color and coarse-grained deposits. It is primarily composed of facies association 2 with rare occurrences of facies association 1 in thin (<0.2 m) lenticular beds of laminated mudstone or rip-up clasts. Channel bodies of facies association 2 in the lower Calico bed are typically coarse-grained sandstone to conglomeratic with abundant pebbles throughout.

Spatially, the lower Calico bed decreases in thickness from 8 to 15 m in the north to 0 to 10 m in south (Figure 7), attendant with changes in channel belt architecture. In the north, the lower Calico bed occurs as a regionally continuous, multistory channel complex, whereas in the south, it is more commonly an isolated, single story channel bodies or as a locally continuous, multistory channel complex (Figure 7). The lower Calico bed is locally absent in the south due to both pinching out and erosion from overlying deposits (Figure 8C–D). As such, the nature of the upper bounding surface of the lower Calico bed is variable across the plateau. Additionally, the underlying paleocurrent trends continue into the lower Calico bed, which have increasingly north-directed orientations, particularly in the northern outcrops (mean = 047°; cf. 056° in the south; Figure 7; Table 3), and have increasingly different standard deviations (1σ = 40° in

the north; cf. $1\sigma = 31°$ in the south; Table 3).

The lower Calico bed is topped by a thin (<0.2 m), layer of concentrated iron-oxide minerals that is locally traceable for 100s m at each outcrop in north. In the northeast, there is a 1.2 m thick gradational succession from gray mudstone into mottled, and rooted yellow-orange siltstone and sandstone that is topped by the iron-oxide layer (Figure 6). This succession represents a gradational laterite profile that is topped by a ferricrete layer (Ollier et al., 1990). These profiles are often associated with kaolinized parent rock, a key characteristic of the underlying lower Calico bed (Bourman and Ollier, 2002). Laterite profiles generally form as a result of weathering in tropical to subtropical environments with distinct seasonality, whereas ferricretes can form in tropical to temperate climates (Widdowson, 2007; Bourman and Ollier, 2002). The laterite profile is only present at Buck Hollow in the northeast, but the ferricrete layer is present throughout the northern study area. This layer, however, is absent to the south, where the lower Calico bed equivalent is instead topped by a *Glossifungites* surface (Figure 6). This surface forms the boundary between the lower and upper Calico bed in the north, and forms the Smoky Hollow-John Henry Member contact in the south (Figure 6).

Upper Calico Bed

The upper Calico bed is only present in the northern study area where it is also part of the Calico bed ledge-forming unit, but grades into a slope former upsection at many localities. It is distinguished by its orange-brown color, lithologic heterogeneity, and prevalence of facies association 2 (Figure 7; Figure 8C–D). Generally, the basal 0.5–2 m of upper Calico bed is similar in grain size to the lower Calico bed, ranging from very coarse to pebbly, but typically fines upward. In the northeast, the upper 2–5 m

consists of massive mudstone and carbonaceous mudstone beds separating isolated tidally-influenced channel bodies (Figure 5; Figure 7). The ledge-forming section is regionally continuous in the north where it ranges from 10 to 20 m thick. Based upon aerial photo interpretation, however, the upper Calico bed thins to the south, pinching out approximately 15 km south of Utah Highway 12 (Figure 9D). When compared with stratigraphically lower paleocurrent measurements, the shift to more northern-directed paleocurrent indicators is reversed, showing a transition back to east-northeast (mean = 061°) from more northerly (mean = 047°) lower Calico bed measurements (Figure 7; Table 3). The spatial difference in paleocurrent standard deviations remains, however, being greater in the north ($1\sigma = 42°$) relative to the south ($1\sigma = 26°$; Table 3)

The upper Calico bed is topped in the north by a quartzite pebble lag that is regionally traceable for 1000s of m (Figure 8A–B), previously interpreted to be a transgressive ravinement surface (Hettinger et al., 1993; Chentnik et al., 2015; Mulhern et al., in press). This lag ranges in thickness from a single layer of pebbles to 0.2 m thick, and is generally found underlying tabular, lower shoreface sandstone and offshore mudstone packages of the lower John Henry Member. The lag is absent in the central study area, where the Calico bed is directly overlain by fluvial strata of the lower John Henry Member (Figure 8C), and in the south where fluvial to estuarine strata of the lower John Henry Member directly overlie lower Calico bed equivalent strata (Purcell et al., in press). Furthermore, the Calico bed is altogether absent along the southeastern margin of the study area along Fifty Mile Mountain (Figure 9C). Here, the Smoky Hollow Member thins and appears to be absent, though this interpretation is based on aerial photography.

Figure 9. Isoline maps illustrating the fan-shaped morphology of the Smoky Hollow Member (SHM) distributive fluvial system. A. Thickness map for the entire fluvial Smoky Hollow Member with average paleocurrent orientations shown for the north and south; B. Thickness map for the lower through middle Smoky Hollow Member; C. Thickness map for the lower Calico bed; D. Thickness map for the upper Calico Bed showing the average paleocurrent orientation; E. Average sandstone grain size (in phi) in the fluvial Smoky Hollow Member; F. Net-to-gross, defined as ratio of sand thickness to total thickness, for the fluvial Smoky Hollow Member.

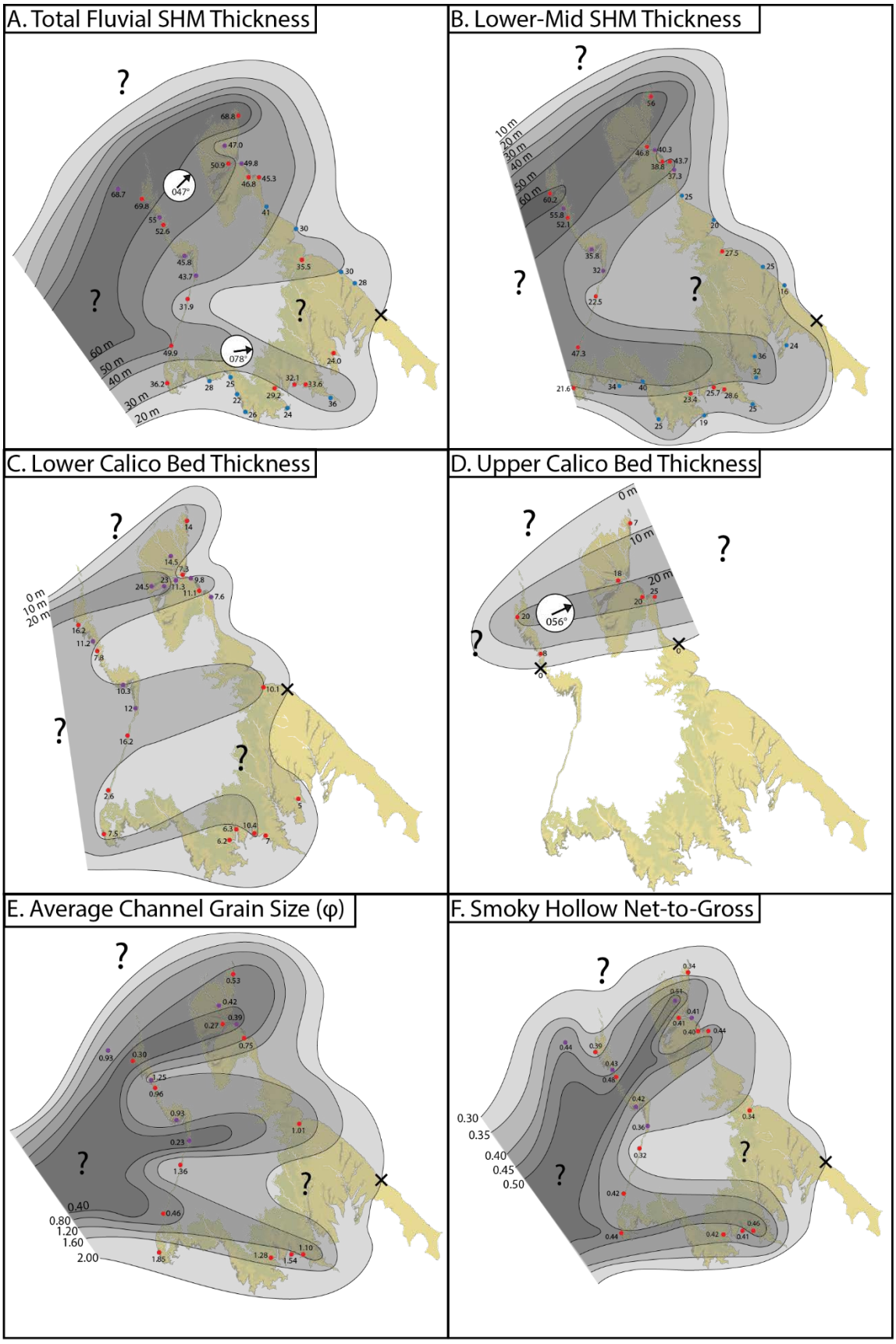
A. Total Fluvial SHM Thickness
B. Lower-Mid SHM Thickness
C. Lower Calico Bed Thickness
D. Upper Calico Bed Thickness
E. Average Channel Grain Size (φ)
F. Smoky Hollow Net-to-Gross
047°
078°
056°
60 m
50 m
40 m
30 m
20 m
10 m
0 m
0.40
0.80
1.20
1.60
2.00
0.30
0.35
0.40
0.45
0.50

Petrography

Detrital Modes

The dominant grain types in sandstone samples of the Smoky Hollow Member through lower John Henry Member (n = 37) include (in order of decreasing relative abundance): monocrystalline quartz (Qm), potassium feldspar (K), polycrystalline quartz (Qp), and sedimentary lithic fragments (Ls; Table 4; Figure 10A–B). Monocrystalline quartz ranges in relative abundance from 29 to 79% (mean = 57%) throughout the section. It is generally subangular and shows sweeping extinction. Potassium feldspar ranges in relative abundance from 1 to 33% (mean = 21%). Plagioclase grains were not observed. Polycrystalline quartz ranges in relative abundance from 0 to 34% (mean = 13%), and generally occurs as elongate, crenulated to sutured grains with common recrystallization observed. Microcrystalline quartz ranges in relative abundance from 0 to 11% (mean = 4%). Sedimentary lithic fragments range in relative abundance from 0 to 19% (mean = 4%), and are primarily detrital carbonate. Volcanic rock fragments are rare, <5% (mean = 1%). Relative abundances of each of these constituent grains vary stratigraphically in a consistent manner across the study area.

Sandstones in the lower Smoky Hollow Member (n = 6) are feldspathic litharenite to lithic arkose, with an average composition of $Qt_{67}F_{20}Lu_{13}$ (Figure 11A). Polycrystalline quartz is relatively low for the section, averaging 9% of relative abundance (Figure 10B). The primary type of lithic fragment observed was detrital calcite, occurring as rounded, medium-sized grains, ranging in relative abundance from 3 to 15%. These calcite grains are characteristic of lower Smoky Hollow Member samples and become increasingly rare upsection.

Table 4

Results from petrographic point counting. Samples are separated into locations and stratigraphic unit (LSHM=lower Smoky Hollow Member, MSHM 1=lower middle Smoky Hollow Member, MSHM 2= upper middle Smoky Hollow Member, LCB=lower Calico bed, UCB=upper Calico bed, LJHM=lower John Henry Member). Values are in percentages. Values under "Grains" sub-headings are normalized to one another (Qm=monocrystalline quartz, F=feldspar, Lt=total lithic fragments, Qt=total quartz, Lu=unstable lithic fragments, Qmu=Qm with undulatory extinction, Qms=Qm with straight extinction, Qp=polycrystalline quartz). Values under "Interstitial Material" subheadings are absolute to total point counts (n=500) for each sample.

		Grains									Interstitial Material						
ID	**Interval**	**Q_m**	**F**	**L_t**	**Q_t**	**F**	**L_u**	**Q_{mu}**	**Q_{ms}**	**Q_p**	**Mat.**	**Cem.**	**φ**	**Kao.**	**Clay**	**Calc.**	**Hem.**
AW-01	UCB	70.8	4.8	24.3	93.7	4.8	1.4	37.6	38.6	23.8	0.0	0.6	16.4	0.0	0.0	0.0	0.6
AW-02	LCB	35.5	29.4	35.0	67.3	29.4	3.3	38.2	17.5	44.2	15.5	0.6	5.4	12.9	2.6	0.0	0.6
AW-03	LSHM	54.0	19.0	27.0	69.3	19.0	11.6	51.9	34.2	13.9	5.0	4.0	15.4	0.4	4.6	0.0	4.0
AW-04	MSHM 1	40.2	26.8	33.0	64.7	26.8	8.5	51.2	17.6	31.2	13.7	2.0	14.3	3.6	10.2	0.0	2.0
AW-05	MSHM 2	41.0	22.9	36.1	75.5	22.9	1.6	45.2	18.4	36.4	13.4	4.0	8.6	1.2	12.2	0.0	4.0
BH-02	UCB	62.4	25.6	12.0	73.3	25.6	1.2	57.9	29.8	12.3	9.3	0.2	5.1	4.1	5.1	0.0	0.2
BH-05	LCB	64.2	25.0	10.8	73.5	25.0	1.5	65.6	26.0	8.4	20.6	3.1	12.7	2.0	18.6	0.0	3.1
BH-06	LJHM	67.5	19.5	13.1	74.7	19.5	5.9	49.6	46.2	4.2	4.9	6.3	15.0	2.4	2.6	0.0	6.3
BH-11	LSHM	67.1	16.3	16.6	72.1	16.3	11.6	65.0	31.6	3.4	8.8	16.2	7.8	0.8	8.0	13.6	2.6
BH-12	MSHM 1	69.2	18.5	12.3	79.9	18.5	1.6	35.3	27.4	37.3	12.0	0.4	11.0	1.6	10.4	0.2	0.2
BH-13	MSHM 2	60.9	28.5	10.6	69.7	28.5	1.8	72.7	16.2	11.1	8.4	2.6	10.0	2.2	6.2	0.0	2.6

Table 4 continued

ID	Interval	Grains									Interstitial Material						
		Q_m	F	L_t	Q_t	F	L_u	Q_{mu}	Q_{ms}	Q_p	Mat	Cem	φ	Kao	Clay	Calc	Hem
COY-01	USHM	60.2	31.9	7.9	65.9	31.9	2.2	66.1	13.4	20.5	4.4	8.7	6.4	0.2	4.2	1.0	7.8
COY-02	LCB	62.8	23.6	13.5	75.0	23.6	1.4	71.6	13.0	15.4	8.3	1.6	3.4	2.4	6.0	1.4	0.2
COY-03	LJHM	51.3	19.7	29.1	59.4	19.7	20.9	36.4	62.8	0.8	4.0	49.3	0.0	0.0	4.0	47.3	2.0
KG-01	LJHM	79.4	0.6	19.9	96.0	0.6	3.4	42.8	40.0	17.2	0.8	1.4	3.2	0.0	0.8	1.0	0.4
KG-03	LCB	41.6	28.7	29.8	68.1	28.7	3.2	40.1	21.4	38.5	20.4	0.4	4.6	17.8	2.6	0.0	0.4
KG-04	LSHM	59.4	20.8	19.8	66.2	20.8	13.0	42.6	50.3	7.1	7.6	28.9	1.8	1.0	6.6	27.3	1.6
KG-05	MSHM 1	41.0	26.9	32.1	68.2	26.9	4.9	60.1	25.6	14.3	14.6	4.0	7.6	3.8	10.8	0.0	4.0
KG-06	MSHM 2	53.7	24.0	22.3	72.1	24.0	3.8	43.8	37.2	19.0	30.1	1.0	0.8	0.0	30.1	0.2	0.8
LHC-01	LCB	64.2	16.4	19.3	80.9	16.4	2.6	32.9	48.8	18.3	0.4	12.2	10.8	0.0	0.4	2.6	9.6
LHC-02	LJHM	59.0	11.3	29.7	85.4	11.3	3.3	47.4	46.8	5.7	0.4	0.6	14.4	0.0	0.4	0.0	0.6
MC-01	LCB	55.4	29.4	15.1	69.0	29.4	1.6	58.7	23.6	17.7	12.2	9.2	3.4	6.2	6.0	0.0	9.2
MC-02	UCB	71.1	15.0	13.9	82.6	15.0	2.3	58.5	28.2	13.3	3.6	0.6	9.2	0.2	3.4	0.0	0.6
MC-05	LJHM	61.8	27.6	10.6	66.4	27.6	6.0	57.7	37.7	4.6	12.6	1.4	12.4	0.8	11.8	1.2	0.2
MC-07	MSHM 1	69.4	11.3	19.4	87.9	11.3	0.8	53.5	32.7	13.9	8.4	11.0	6.2	0.2	8.2	0.0	11.0
MC-11	LSHM	47.7	30.5	21.9	62.6	30.5	7.0	44.6	42.2	13.3	9.8	25.7	3.8	2.8	7.0	23.1	2.6
MC-12	MSHM 2	62.9	26.6	10.5	70.7	26.6	2.7	57.7	24.1	18.2	15.0	3.2	7.2	5.0	10.0	0.0	3.2
MC-13	LJHM	62.4	16.8	20.7	75.6	16.8	7.6	46.9	40.1	12.9	8.7	4.4	5.6	1.2	7.5	1.2	3.2

Table 4 continued

ID	Interval	Grains								Interstitial Material						
		Qm	F	Lt	Qt	F	Lu	Qmu	Qms	Qp	Mat	Cem	φ	Kao	Clay	Calc	Hem
SM-01	LSHM	58.0	12.9	29.2	67.4	12.9	19.7	55.4	36.1	8.4	1.0	33.9	1.4	0.6	0.4	33.9	0.0
SM-02	MSHM	60.8	19.0	20.2	76.9	19.0	4.0	63.8	28.6	7.7	10.8	1.2	18.6	2.4	8.4	0.0	1.2
SM-03	LCB	28.8	33.2	37.9	65.4	33.2	1.4	35.4	10.5	54.1	16.6	0.0	10.6	9.8	6.8	0.0	0.0
SM-04	UCB	48.9	19.9	31.2	75.9	19.9	4.2	51.9	17.4	30.7	0.8	3.0	15.0	0.2	0.6	0.0	3.0
TC-01	LCB	46.7	27.8	25.6	69.3	27.8	2.9	45.5	25.4	29.1	13.6	0.8	4.2	7.6	6.0	0.6	0.2
TC-02	LJHM	69.8	3.0	27.3	95.5	3.0	1.5	52.8	22.8	24.4	2.2	16.2	1.8	0.2	2.0	2.2	14.0
TG-01	LSHM	57.1	20.1	22.8	61.9	20.1	18.0	55.4	40.6	4.0	8.0	32.0	1.2	1.0	7.0	31.4	0.6
TG-02	LCB	52.6	25.9	21.4	69.8	25.9	4.2	55.2	23.0	21.9	14.2	0.6	5.0	1.0	13.2	0.0	0.6
TG-03	UCB	64.3	7.5	28.2	91.1	7.5	1.4	50.4	20.2	29.4	4.4	3.6	6.2	0.8	3.6	0.0	3.6

Figure 10. A. Stratigraphic variations in average relative abundance of total quartz (Qt), feldspar (F) and unstable lithic fragments (Lu) including lower Smoky Hollow Member (LSHM), lower-middle Smoky Hollow Member (MSHM 1), upper middle Smoky Hollow Member (MSHM 2), lower Calico bed (LCB), upper Calico bed (UCB), and the lower John Henry Member (LJHM); B. Stratigraphic variations in average relative abundance of polycrystalline quartz (Qp); C. Stratigraphic variations in average abundance of intergranular clay (total) and kaolinite; D. stratigraphic variations in average abundance of intergranular cement (total), calcite, and hematite.

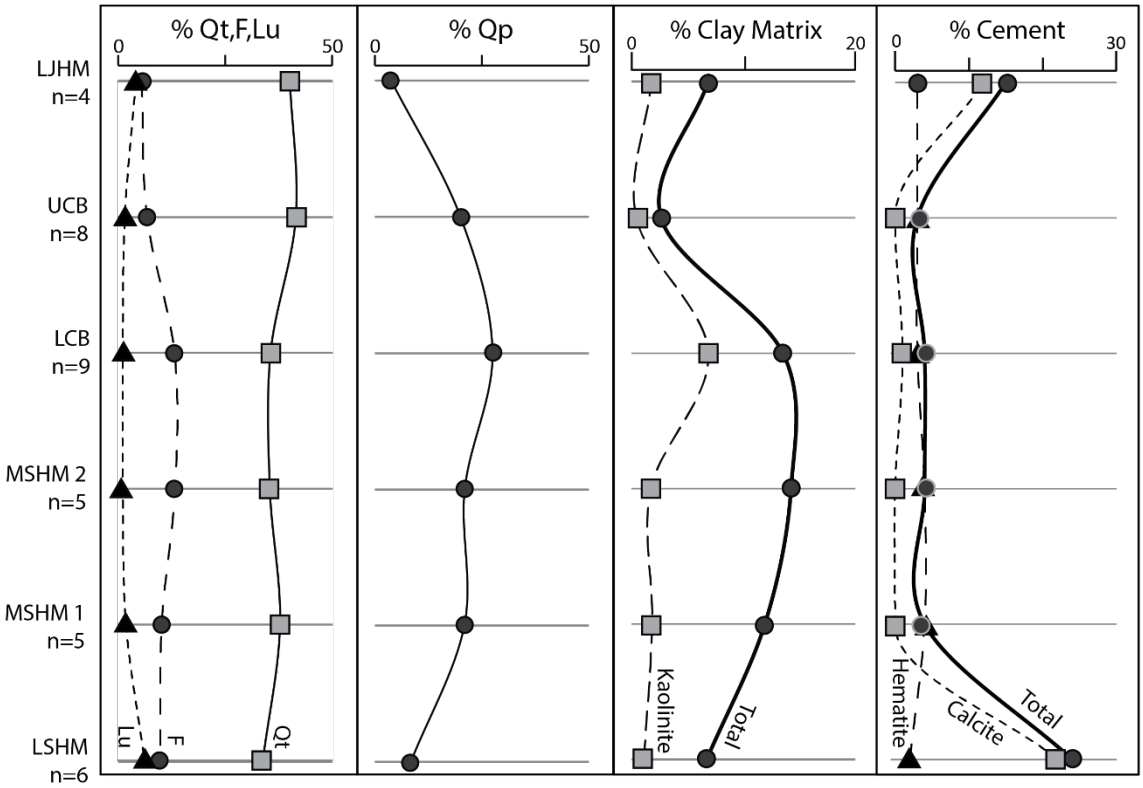
% Qt,F,Lu
0
50
% Qp
0
50
% Clay Matrix
0
20
% Cement
0
30
LJHM
n=4
UCB
n=8
LCB
n=9
MSHM 2
n=5
MSHM 1
n=5
LSHM
n=6
Lu
F
Qt
Kaolinite
Total
Hematite
Calcite
Total

Figure 11. A. Ternary diagrams showing the variation in modal sandstone composition between the lower Smoky Hollow Member (SHM) through lower Calico bed (left) and the upper Calico bed through lower John Henry Member (JHM) (right); B. Ternary diagrams showing the gradational changes in modal sandstone composition above the Calico bed unconformity. C. Photomicrographs showing the compositional variation among the lower Smoky Hollow Member (C1), middle Smoky Hollow Member (C2), lower Calico bed (C3), and the upper Calico bed (C4). Note: upper ternary diagrams range from 0-50% F and Lu, and 50-100% Qt.

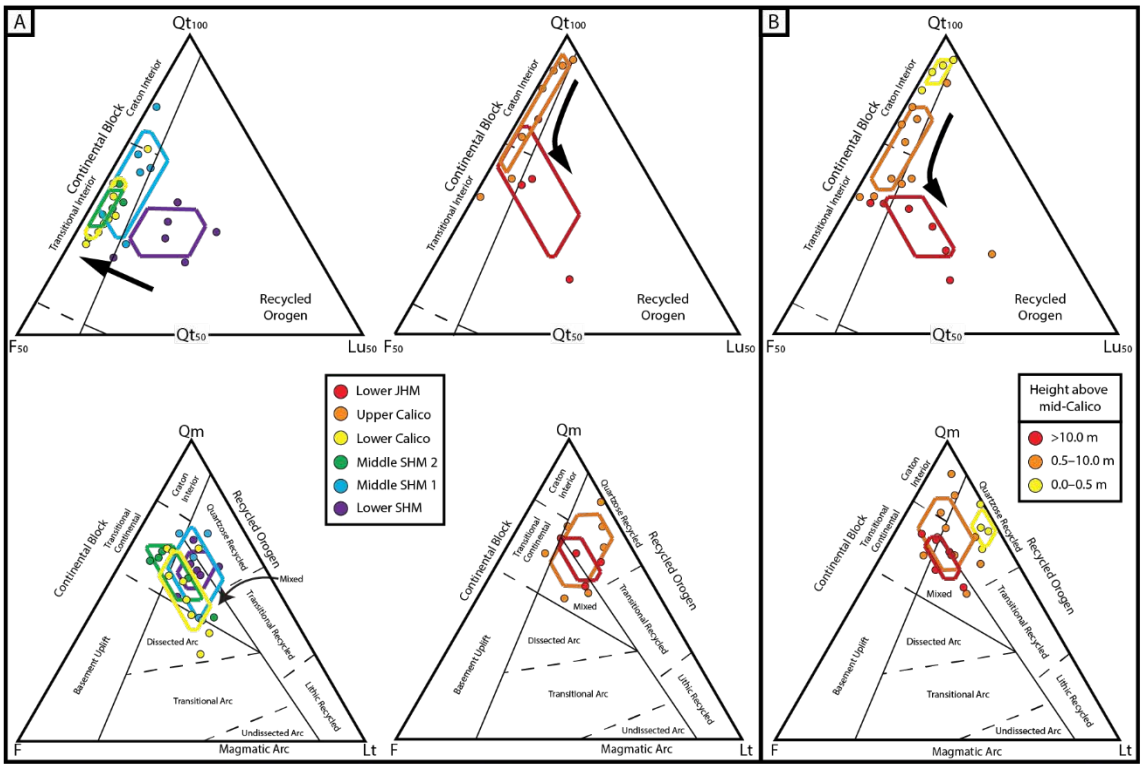
A
B
Qt100
Qt50
F50
Lu50
Continental Block
Craton Interior
Transitional Interior
Recycled Orogen
Lower JHM
Upper Calico
Lower Calico
Middle SHM 2
Middle SHM 1
Lower SHM
Height above mid-Calico
>10.0 m
0.5–10.0 m
0.0–0.5 m
Qm
F
Lt
Transitional Continental
Quartzose Recycled
Transitional Recycled
Lithic Recycled
Mixed
Dissected Arc
Transitional Arc
Undissected Arc
Basement Uplift
Magmatic Arc

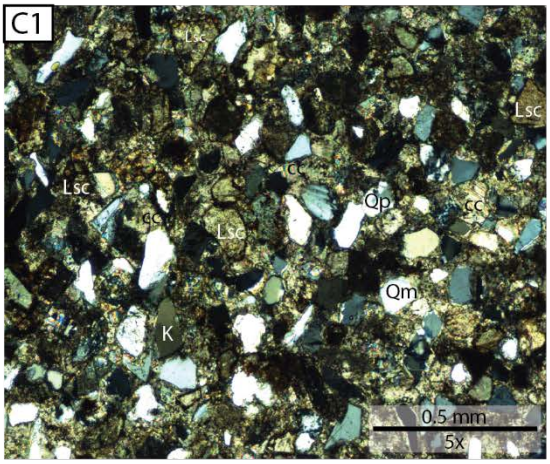
C1
Lsc
cc
Qp
K
Qm
0.5 mm
5x

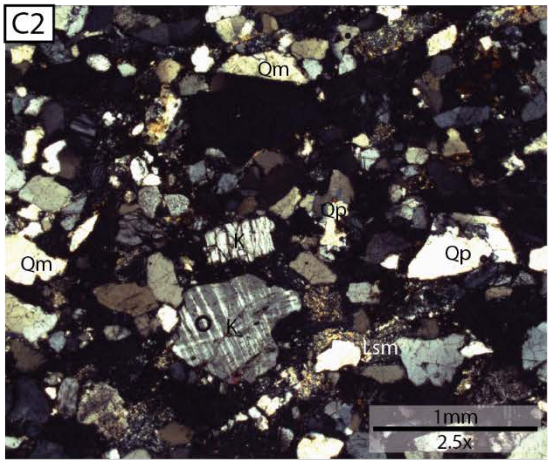
C2
Qm
Qp
K
Lsm
1mm
2.5x

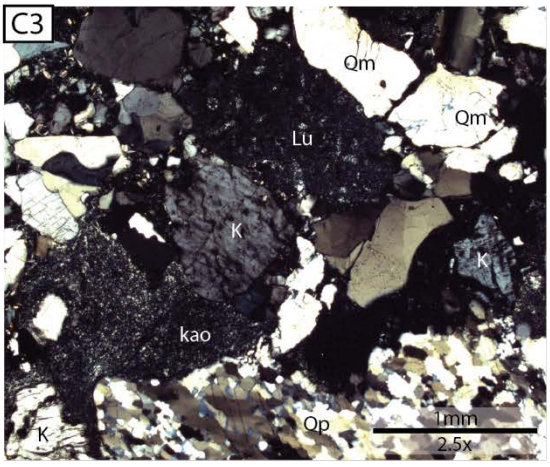
C3
Qm
Lu
K
kao
Qp
1mm
2.5x

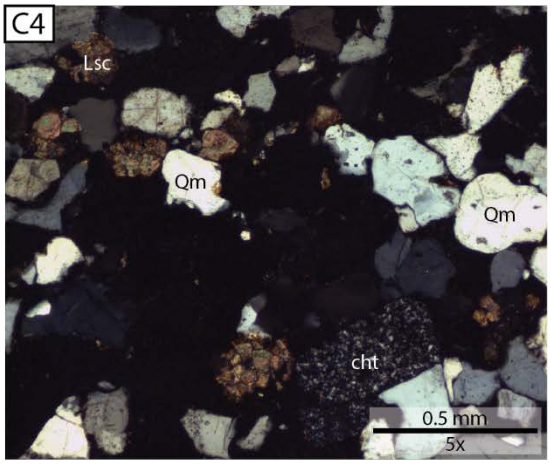
C4
Lsc
Qm
cht
0.5 mm
5x

The middle Smoky Hollow Member records a dramatic decrease in lithic fragments (2%; Figure 10A) compared to the lower Smoky Hollow Member (13%). Middle Smoky Hollow Member sandstones are primarily subarkosic to arkosic, with average compositions of $Qt_{76}F_{21}Lu_3$ and $Qt_{71}F_{27}Lu_2$ for the lower and upper subdivisions respectively (Figure 11A). The relative abundance of polycrystalline quartz is higher in the middle Smoky Hollow Member (19%) than in the lower Smoky Hollow Member (9%; Figure 10B). Detrital carbonate grains are very rare in the middle Smoky Hollow Member, only observed in two samples, each with a relative abundance of 2%.

Lower Calico bed sandstone samples (n = 9) are some of the most lithic fragment-poor sandstones of the section. They are almost entirely arkoses and have an average composition of $Qt_{71}F_{27}Lu_2$ (Figure 11A). They have a roughly equivalent composition to the uppermost middle Smoky Hollow Member samples, but are much more enriched in polycrystalline quartz, which comprises an average relative abundance of 27% **(**Figure 10B).

Upper Calico bed sandstones (n = 9) are the most quartz-rich samples of the section, ranging from subarkose to quartz arenite, with an average composition of $Qt_{87}F_{11}L_2$ (Figure 11A). The high concentration of quartz may be due to sampling bias, however, as the quartz arenite samples are from the lower 0.5 m of the upper Calico bed. These basal deposits quickly transition upsection, however, decreasing in average grain size, and increasing in feldspar and lithic fragment content (Figure 11B). When basal samples (n = 4) are removed from upper Calico bed calculations, the average composition (n = 5) changes to $Qt_{79}F_{17}L_4$, showing a higher relative concentration of feldspar and lithic fragments, including 1–3% detrital carbonate grains.

Three lower John Henry Member samples were collected to compare to previous studies and assess its genetic relationship to the upper Calico bed. The average composition of these sandstones is $Qt_{69}F_{21}L_{10}$, and ranges from lithic arkose to feldspathic litharenite (Figure 11A**)**. These results are similar to the previous studies that found an average composition of $Qt_{67}F_{23}L_{10}$ for basal John Henry Member sandstones (Allen and Johnson, 2010a; Szwarc, et al. 2014; Gooley, et al., 2016). Furthermore, when lower John Henry Member are plotted with upper Calico bed samples by stratigraphic height, they show a continuous upsection compositional trend from predominantly quartz to increasing feldspar content followed by increasing lithic fragments (Figure 10A; Figure 11B). These samples also continue the trend of increasing relative abundance of detrital calcite grains, ranging from 3–13%, showing similar compositions to lower Smoky Hollow Member sandstones (3–15%).

The compositional variations outlined above reveal two distinct trends in source terranes as first defined by Dickinson and Suczek (1979) and later modified by Ingersoll et al. (1984; Figure 11). From the lower Smoky Hollow Member through the basal upper Calico bed, there is a transition in the source terrane signal from being strongly recycled orogenic to transitional interior to craton interior. Above the basal upper Calico bed, this trend reverses, returning to a recycled orogenic source terrane signal upsection. The craton interior source terrane signal of the basal upper Calico bed is likely the product of reworking lower Calico bed sediments, a conclusion first suggested by Peterson (1969b) in his original description of the Calico bed. Recycling is supported by a well-sorted texture, an abundance of stable, very coarse-grained quartz grains, and a lack of clay minerals in the basal 1 m of the upper Calico bed. These characteristics shift upsection

within 5 m of the base of the upper Calico bed, with poorly- to moderately-sorted sandstones containing abundant clays that show a recycled orogenic source signal (Figure 10C; Figure 11B).

Cement

There are three main types of interstitial cement present in the samples: clay, calcite, and iron oxide, the compositional trends of which are illustrated in Figure 10C-D. Clay minerals are primarily authigenic based on the presence of sand grain-sized concentrations of clays, and the common observation of K-feldspar grains partially weathered to clay. Samples show moderate amounts of clay minerals throughout the section, ranging on average from 3–14% total composition, with some samples having as much as 30% clay (Figure 10C; Table 4). Stratigraphically, there is a trend of increasing relative clay abundance from an average of 7% in the lower Smoky Hollow Member to 14% in the lower Calico bed. There is a sharp decrease in clay content apparent across the middle Calico bed contact, with the upper Calico bed having a 3% average relative abundance of clay which slightly increases to 5% in the lower John Henry Member (Figure 10C). Similarly, kaolinite relative abundance increases slightly upsection from 1% to 7% between the lower Smoky Hollow and lower Calico bed, followed by a sharp decrease across the mid-Calico bed contact to 1% in the upper Calico bed (Figure 10C).

In contrast to upsection trends in clay content, there exists a nearly inverse trend in calcite cementation. Calcite cement is most abundant in the lower Smoky Hollow Member with an average relative abundance of 22%, which decreases rapidly upsection into the lower and upper Calico bed to an average relative abundance of 1% for both units (Figure 10D). The lower John Henry Member shows a sharp return in calcite cementation

with an average relative abundance of 16%. The source of this calcite cement is likely a combination of in-situ detrital calcite grains as well as pore fluids rich in calcium carbonate derived from local and regional detrital calcite grains. This interpretation is supported by the presence of partially weathered calcite grains, grain-sized calcite cement accumulations, and thin veneers of calcite cement coating grains.

Detrital Zircon U-Pb Geochronology

Detrital zircon geochronology data (n = 10 samples; n = 530 accepted analyses) are summarized in Table 5. Samples were collected from the northeast at Main Canyon (n = 5), the southwest at Rock House Cove (n = 2), and the south at Kelly Grade (n = 3; Figure 1). Samples primarily targeted the lower Calico bed (n = 3) and upper Calico bed (n = 3). Two samples were also collected from the lower John Henry Member: one from a tidal bar sandstone at Kelly Grade (Purcell et al., in press), and one from a lower shoreface sandstone at Main Canyon (Chentnik et al., 2015). One sample from the middle Smoky Hollow Member, and one sample from the upper Tibbet Canyon Member were also analyzed. Previous analyses by Szwarc et al. (2015) are also included in the discussion.

A significant number of the analyses were discordant, with accepted analyses ranging from 35 to 71% (mean = 54%) per sample, which was likely caused by metamictization of Proterozoic and Archean detrital zircon grains. Zircons exhibit fracture patterns (Corfu et al., 2004), and linear discordance trends consistent with a lead loss event (Schoene, 2014), both hallmarks of metamict zircons. Two distinct linear discordance trends project to a single lower intercept on Concordia at ~92 Ma. Their upper intercepts are approximately 1400 and 1700 Ma, respectively. Several analyses lie

Table 5

Summary of concordant detrital zircon analyses per sample, arranged by location and stratigraphic unit (TCM = Tibbet Canyon Member, SHM = Smoky Hollow Member, LCB = lower Calico bed, UCB = upper Calico bed, LJHM = lower John Henry Member). Summary includes number and percentage of concordant analyses and percent of concordant analyses in each age population (A = 86-260 Ma, B = 260-1250 Ma, C = 1250-1900 Ma, D > 1900 Ma).

Location	**Sample ID**	**Interval**	**Facies**	**Concordant Analyses (n)**	**Concordant Analyses (%)**	**A (%)**	**B (%)**	**C (%)**	**D (%)**
Kelly Grade	KG-01	LJHM	Tidal	56	56	20	9	71	0
	KG-02	UCB	Fluvial/Tidal	49	49	22	16	59	2
	KG-03	LCB	Fluvial	35	35	11	17	71	0
Main Canyon	MC-05	LJHM	Marine	66	71	14	9	77	0
	MC-02	UCB	Tidal	49	49	10	14	73	2
	MC-01	LCB	Fluvial	63	66	6	8	83	3
	MC-07	SHM	Fluvial	58	58	12	36	48	3
	MC-03	TCM	Tidal	55	55	7	18	71	4
Rock House Cove	RHC-02	LJHM	Fluvial	55	55	24	9	65	2
	RHC-01	LCB	Fluvial	41	41	17	12	66	5
Total				527	53	14	15	70	1

between these trends. These zircons likely hold important clues about the source area, but pending further investigation, this study focuses on the concordant analyses.

Dates that are ≤10% discordant are shown on relative probability plots and subdivided into four age populations (Figure 12A). These age populations were primarily based on source terranes exposed near the Cordilleran foreland basin during deposition of the Straight Cliffs Formation (Turonian-early Campanian), and follow the same subdivisions proposed by Szwarc et al. (2015).

Population A: 86-260 Ma

Detrital zircon grains from population A comprise 14% of all concordant grains (Figure 12A). They range in relative abundance from 6 to 24% per sample. There are prominent peaks in population A at 90, 147, and 225 Ma (Figure 12A).

There is an upsection increase in the average relative abundance of population A grains from 3% in the Tibbet Canyon Member to 16% in the upper Calico bed and 9% in the lower John Henry Member (Figure 12B). Geographically, the average relative abundance of population A grains decreases from southwest (Rock House Cove, mean = 20%) to northeast (Main Canyon, mean = 10%). The youngest dates from this study were used to revise previous maximum depositional ages from Szwarc et al. (2015) for each unit using three or more concordant grains that overlap at 2σ, as described by Dickinson and Gehrels (2009). This results in maximum depositional ages of 93.2 ± 1.1 Ma for the top Tibbet Canyon Member (n = 4), 92.8 ± 4.1 Ma for the sub-Calico bed Smoky Hollow Member (n = 3), 89.9 ± 1.9 Ma for the lower Calico bed (n = 4), and 88.0 ± 1.1 Ma for the upper Calico bed (n = 3; Table 6).

Figure 12. A. Relative probability plot containing ages from all concordant detrital zircons in this study (N=10, n=530). Prominent peaks are labeled for each age population (denoted by shaded colors) at 90 Ma, 147 Ma, 225 Ma, 370 Ma, 490 Ma, 1140 Ma, 1425 Ma, and 1710 Ma; B. Relative probability plots for samples grouped by stratigraphic unit (TCM=Tibbet Canyon Member, SHM=Smoky Hollow Member, LCB=lower Calico bed, UCB=upper Calico bed, LJHM=lower John Henry Member) highlighting temporal variations in the average relative abundance of age populations A, B, C. Note: data from Szwarc et al. (2015) included in part B.

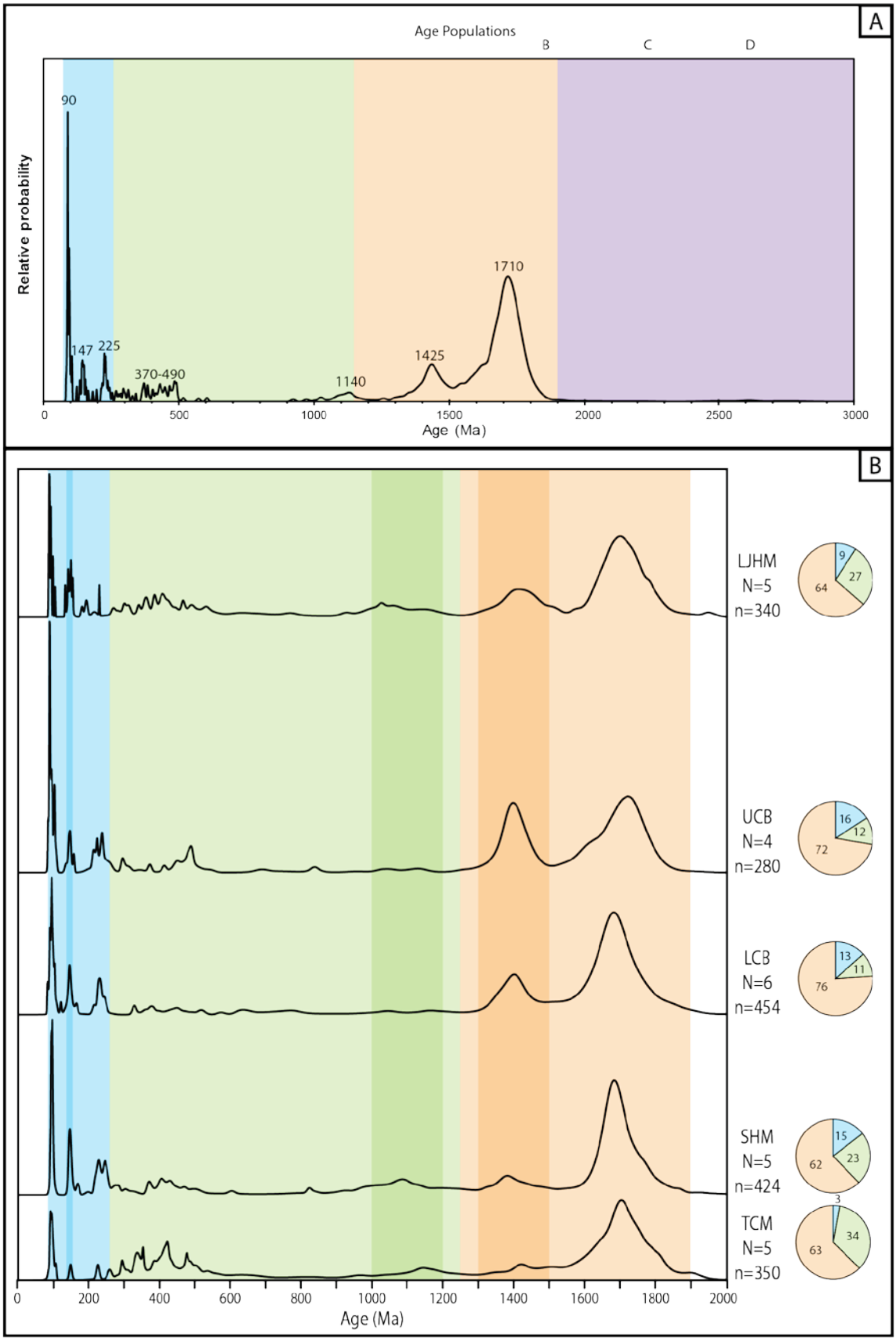
A
Age Populations
B
C
D
Relative probability
90
147
225
370-490
1140
1425
1710
0
500
1000
1500
2000
2500
3000
Age (Ma)
B
LJHM
N=5
n=340
9
27
64
UCB
N=4
n=280
16
12
72
LCB
N=6
n=454
13
11
76
SHM
N=5
n=424
15
23
62
TCM
N=5
n=350
3
34
63
0
200
400
600
800
1000
1200
1400
1600
1800
2000
Age (Ma)

Table 6

Calculated maximum depositional ages for Tibbet Canyon and Smoky Hollow Members, including the lower and upper Calico Bed. Ages were calculated based on youngest concordant ages that overlapped at 2-sigma uncertainty (after Dickinson and Gehrels, 2009).

Unit	Youngest Grains	Maximum Depositional Age
Upper Calico Bed	87.0 ± 3.0 88.2 ± 1.6 88.1 ± 1.3	88.0 ± 1.1 Ma
Lower Calico Bed	87.5 ± 3.5 89.0 ± 1.7 90.4 ± 1.7 90.8 ± 1.6	89.9 ± 1.9 Ma
Smoky Hollow Member	90.9 ± 3.3 91.8 ± 1.8 94.2 ± 1.7	92.8 ± 4.1 Ma
Tibbet Canyon Member	92.0 ± 10.0 92.7 ± 1.6 93.3 ± 2.2 94.4 ± 2.5	93.2 ± 1.1 Ma

Detrital zircon grains of population A were primarily sourced from volcanic and plutonic origins of the Cordilleran magmatic arc in southern California, southern Nevada, and southwestern Arizona (Szwarc et al., 2015). Magmatism was active along the arc between approximately 80 and 260 Ma (Chen and Moore, 1982; Miller et al., 1994; Barth and Wooden, 2006) and these dates, along with the youngest detrital zircon age from this study (86 Ma) define the age range of this population.

Some Jurassic-Triassic detrital zircons within population A may have been transported directly from the Cordilleran magmatic arc sources through airfall, or perhaps were deposited in the retroarc foreland basin and later reworked in transverse drainages during active thrusting along the Sevier fold-thrust belt. Airfall is inferred to be a relatively minor transport mechanism, however, as the Smoky Hollow Member is generally ash-poor, population A detrital zircons are generally abraded, and volcanism was active throughout deposition despite trends in population A relative abundance. Sevier-sourced grains in population A are also expected to be minor in influence, as Triassic-Jurassic strata involved in Sevier thrusting were typically overlain by Paleozoic strata during middle to Late Cretaceous thrusting (Miller, 1966; Goldstrand, 1994; DeCelles and Coogan, 2009).

Population B: 260—1250 Ma

Detrital zircons of population B span the Paleozoic through the Mesoproterozoic. They comprise 15% of all concordant grains and range in relative abundance from 8 to 36% per sample. Prominent age peaks population B include 370, 490, and 1140 Ma (Figure 12A).

There is an upsection decrease in the average relative abundance of population B

from 36% in the Tibbet Canyon Member to 14% in the lower Calico bed (Figure 12B**)**. This trend changes above the lower Calico bed to a slight increase in relative population B abundance (16% in the upper Calico bed), continuing into the lower John Henry Member (17%). There are no significant spatial trends in the relative abundance of population B (Figure 13).

The primary source area for population B detrital zircons was the Sevier fold-thrust belt of central Utah (Szwarc et al., 2015). Sevier thrust sheets during this time involved Proterozoic through Mesozoic sedimentary and metasedimentary strata that contained multicycle detrital zircons of Proterozoic through Paleozoic age (Miller, 1963, 1966; Fleck & Carr, 1990; Goldstrand, 1994; Walker et al., 1995; Dickinson and Gehrels, 2009; Lawton et al., 2010). In particular, these strata contain prominent Grenville-aged detrital zircons (900-1250 Ma) and lesser amounts of Neoproterozoic and Paleozoic detrital zircons (Dickinson and Gehrels, 2008a, 2008b, 2009; Lawton et al., 2010; Lawton and Bradford, 2011).

A secondary source for population B detrital zircons may be the Mogollon Highlands of central Arizona. Paleozoic through Lower Cretaceous sedimentary strata were exposed prior to Early Cretaceous rifting of the Bisbee Basin in southern Arizona and New Mexico (Bilodeau, 1986). Similar to strata of the Sevier fold-thrust belt, sedimentary strata of the Mogollon Highlands contained Mesoproterozoic through Paleozoic detrital zircons derived from eastern Laurentia (Bilodeau, 1986; Dickinson and Gehrels, 2008a, 2008b). Uplift of the Bisbee rift shoulder led to erosion of these deposits, but it is possible that these strata persisted into the Late Cretaceous in isolated areas.

Figure 13. Relative probability plots for each sample from the lower Straight Cliffs Formation (TCM=Tibbet Canyon Member, SHM=Smoky Hollow Member, LCB=lower Calico bed, UCB=upper Calico bed, LJHM= lower John Henry Member) at northern outcrops (A) and southern outcrops (B). Samples are grouped vertically according to location (approximately proximal-to-distal to the prominent sources south of the study area) and horizontally by stratigraphic interval. The name, facies, and number of grains corresponding to each sample are labeled. Note: data from Szwarc et al., 2015 included where noted.

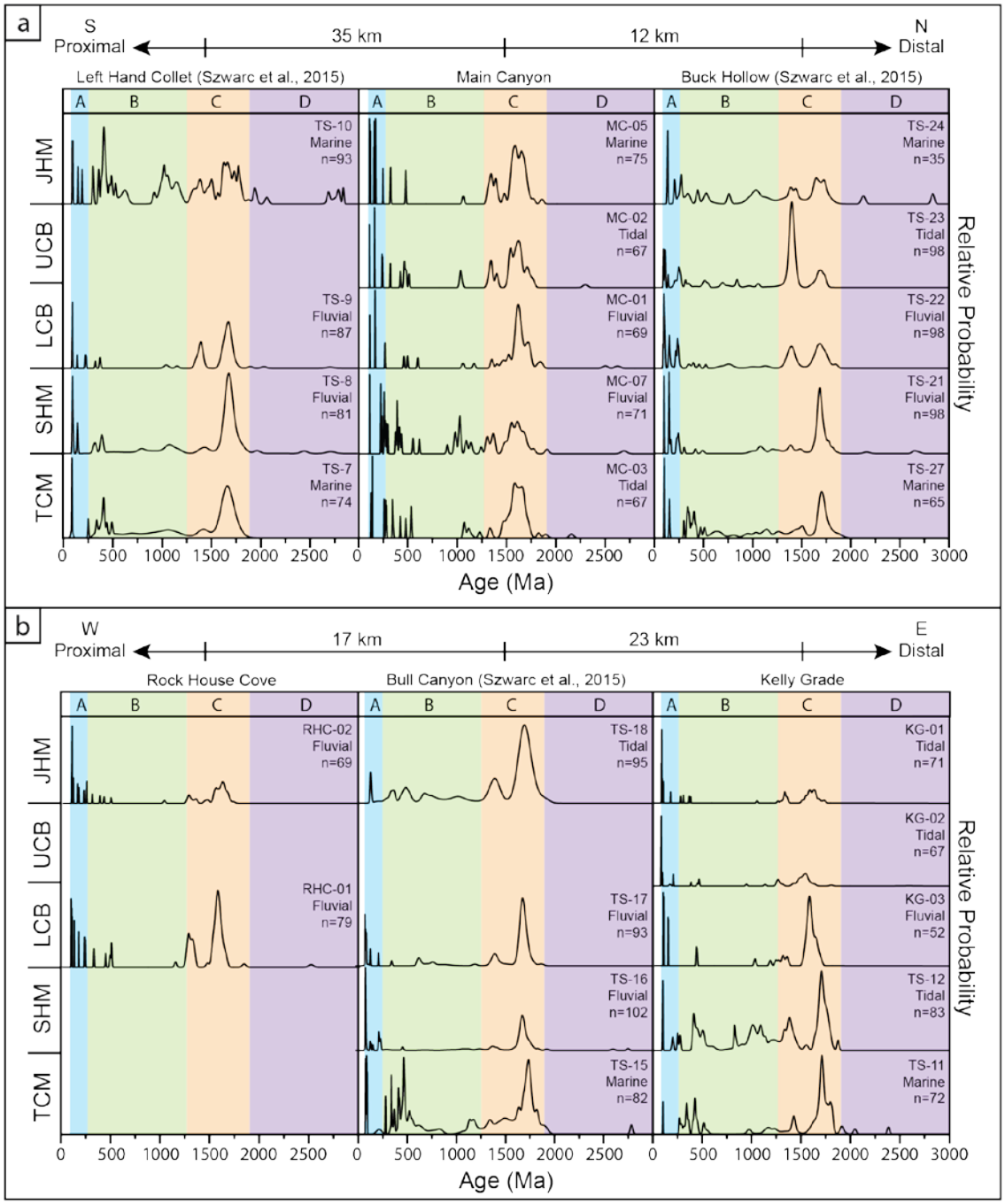
a
S
Proximal
35 km
12 km
N
Distal
Left Hand Collet (Szwarc et al., 2015)
Main Canyon
Buck Hollow (Szwarc et al., 2015)
A
B
C
D
JHM
UCB
LCB
SHM
TCM
TS-10 Marine n=93
MC-05 Marine n=75
TS-24 Marine n=35
MC-02 Tidal n=67
TS-23 Tidal n=98
TS-9 Fluvial n=87
MC-01 Fluvial n=69
TS-22 Fluvial n=98
TS-8 Fluvial n=81
MC-07 Fluvial n=71
TS-21 Fluvial n=98
TS-7 Marine n=74
MC-03 Tidal n=67
TS-27 Marine n=65
0 500 1000 1500 2000 2500 0 500 1000 1500 2000 2500 0 500 1000 1500 2000 2500 3000
Age (Ma)
Relative Probability
b
W
Proximal
17 km
23 km
E
Distal
Rock House Cove
Bull Canyon (Szwarc et al., 2015)
Kelly Grade
RHC-02 Fluvial n=69
TS-18 Tidal n=95
KG-01 Tidal n=71
KG-02 Tidal n=67
RHC-01 Fluvial n=79
TS-17 Fluvial n=93
KG-03 Fluvial n=52
TS-16 Fluvial n=102
TS-12 Tidal n=83
TS-15 Marine n=82
TS-11 Marine n=72
0 500 1000 1500 2000 2500 0 500 1000 1500 2000 2500 0 500 1000 1500 2000 2500 3000
Age (Ma)
Relative Probability

Population C: 1250—1900 Ma

Mesoproterozoic to Paleoproterozoic detrital zircons of population C are the most abundant in Tibbet Canyon through lower John Henry Member strata, comprising 69% of all concordant grains analyzed, and ranging in relative abundance from 48% to 83% per sample. Prominent age peaks in this population occur at 1425 and 1710 Ma and a minor peak at 1840 Ma (Figure 12A). Although not included in this analysis, the discordant analyses associated with metamict grains also likely reflect population C input, based on upper concordia intercepts in the same age ranges.

Temporally, there is an increase in the relative amount of population C from the Tibbet Canyon Member through the lower Calico bed, increasing in average abundance from 58% to 72% (Figure 12B). There is a slight decrease in relative abundance into the upper Calico bed and lower John Henry Member, showing an average relative abundance of 69%, however this trend is not evident in every sample. There are no strong spatial trends in population C detrital zircon abundance.

Detrital zircons of population C were derived primarily from the Mogollon Highlands in central Arizona (Szwarc et al., 2015). Yavapai-Mazatzal basement rocks in this area are primarily metamorphosed magmatic bodies that contain ca. 1.8-1.6 Ga crust that developed during the ca. 1.7 Ga Yavapai and ca. 1.6 Ga Mazatzal orogenies (Whitmeyer and Karlstrom, 2007). Population C detrital zircons are also present in Mesozoic sedimentary strata of the Sevier fold-thrust belt to various amounts (Dickinson and Gehrels, 2008a, 2008b, 2009; Lawton and Bradford, 2011; Laskowski et al., 2013), although this is interpreted to be a less likely source of population C zircons for reasons discussed below.

Population D: 1900—3000 Ma

Detrital zircons of population D include Paleoproterozoic through Mesoarchean ages. They are the least abundant grains in all samples, averaging 2% of all concordant grains analyzed. Among individual samples, relative abundance ranges from 0% to 5%, and they show no temporal or spatial trends. There is no significant age peak in this population. These grains are likely multicycle grains from Mesozoic through Proterozoic strata in the Sevier fold-thrust belt (Dickinson and Gehrels, 2009; Lawton et al., 2010).

DISCUSSION

Depositional Model

The spatial and stratigraphic trends apparent in Smoky Hollow Member strata are consistent with the model of a prograding distributive fluvial system (DFS) within the Kaiparowits Basin (Figure 14). This DFS represents the distal reaches of a major axial drainage system that flowed from southwest to northeast, subparallel to the Sevier fold-thrust belt, with secondary input from Sevier-sourced transverse drainages. Competing drainage systems have identified for younger Cretaceous sections in this area (Peterson and Ryder, 1975; Peterson and Kirk, 1977; Lawton et al., 2003, 2014; Szwarc et al., 2015; Chentnik et al., 2015), and a similar northeast-southwest trending drainage system was proposed for as early as the Late Jurassic Morrison Formation in this area (Owen et al., 2015a, 2015b). The Smoky Hollow Member, however, records the renewed establishment of an axial system in the basin following the regression of the Western Interior Seaway in early Turonian time (Cobban, 1994).

Distributive Fluvial System Model

Previous studies of the Smoky Hollow Member, and the Calico bed in particular, interpreted these strata to be mainly valley-confined, degradational to aggradational deposits formed during a cycle of relative sea level fall then rise (Bobb, 1991; Shanley and McCabe, 1991, 1993). An alternative depositional model presented here stems from recent research on large DFSs, which are a dominant geomorphic feature in modern

Figure 14. Map showing the three primary source regions for detrital zircons during the deposition of the Smoky Hollow Member in the late Turonian and the representative ages of these zircons in relation to the Kaiparowits Plateau (KP), Henry Mountains region (HM), and Black Mesa (BM). Black lines with triangles represent modern day expressions of thrust faults that were active (solid) and inactive (dashed) during Smoky Hollow Member deposition (from DeCelles, 2004). Also shown is the estimated location of the Paleogene California paleoriver (from Davis et al., 2010), an estimate course for the late Turonian axial fluvial system that deposited the Smoky Hollow Member, and the estimated paleodrainage divides during this time (red dashed lines)(from Wernicke, 2011).

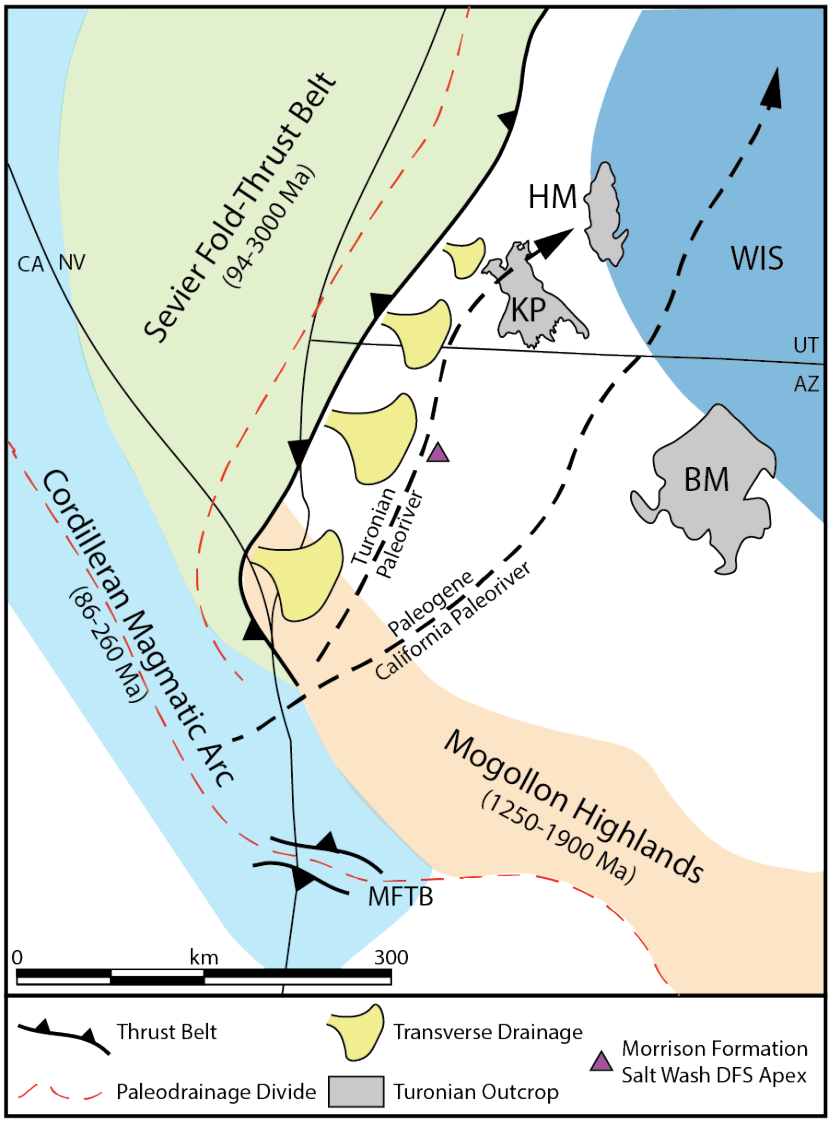
Sevier Fold-Thrust Belt
(94-3000 Ma)
CA
NV
HM
KP
WIS
UT
AZ
BM
Turonian
Paleoriver
Paleogene
California Paleoriver
Cordilleran Magmatic Arc
(86-260 Ma)
Mogollon Highlands
(1250-1900 Ma)
MFTB
0
km
300
Thrust Belt
Transverse Drainage
Morrison Formation
Salt Wash DFS Apex
Paleodrainage Divide
Turonian Outcrop

continental basins and were likely common in the ancient as well (Hartley et al., 2010; Weissann et al., 2010, 2015). In addition to their typically radial planform geometries, modern large DFSs share similar downstream trends including: decreasing discharge, sediment bedload, channel size (width and depth), and channel density, as well as a transition from well- to poorly-drained soils (Davidson et al., 2013; Hartley et al., 2010, 2013, 2015; Weissmann et al., 2010, 2013). If preserved, these deposits should display spatial and stratigraphic trends reflecting these modern characteristics. For progradational DFSs, these trends include proximal-to-distal decreases in the following: overall thickness, average grain size, sand:mud ratio, channel size, channel amalgamation, channel sinuosity, and abundance of well-drained paleosols. Upsection variations should also reflect progradation of the system (Hartley et al., 2013; Weissmann et al., 2013, Owen et al., 2015b).

Proximal to distal trends in the facies, thickness, paleocurrent, and provenance data presented here are consistent with a DFS model. Smoky Hollow Member strata display proximal to distal thinning (SW to NE), and radial distributions (Figure 9A-C). The radial geometry is also evident when mapping average grain size and net-to-gross (total sandstone thickness to total thickness) (Figure 9E-F). At least two primary fan lobes are apparent: one in the south directed approximately east, and one in the north directed approximately northeast (Figure 9A-C). Lastly, paleocurrent measurements increase in spread (standard deviation) distally from an average of 28° to 36°. This increase perhaps reflects increased sinuosity downstream (Table 3). One criticism of the DFS model is that many rivers, including tributive systems, share similar downstream trends, such as decreases in channel size and average grain size. If the Smoky Hollow

Member was a tributive system, however, a radial geometry and diverging paleocurrent indicators would likely absent.

These spatial trends correspond to temporal trends that are also consistent with a prograding DFS. All outcrop locations of the Smoky Hollow Member record upsection increases in fluvial channels (FA 1b) relative to floodplain deposits (FA 1a; Figure 7). Within the floodplain deposits, crevasse deposits decrease in abundance upsection, and most occur in the lower Smoky Hollow Member. Where crevasse deposits are preserved, they record a series of coarsening- and thickening-upward packages below fluvial channel bodies (Figure 3A**)**. These types of crevasse deposits are indicative of a progradational or aggradational avulsion style rather than a degradational style (Jones and Hajek, 2007).

Within channel bodies across the study area, there is an upsection increase in amalgamation, average grain size, and channel size **(**Figure 7**)**. Previous studies have attributed the increase in amalgamation and grain size to changes in fluvial style from meandering in the lower Smoky Hollow Member to braided in the lower Calico bed, due to a variety of allogenic mechanisms (Bobb, 1991; Shanley and McCabe, 1993, 1995). Identification of meandering fluvial style requires recognition of lateral accretion sets which may not be readily identified based on outcrop exposure, especially in channel bodies with limited grain size variation (Hartley et al., 2015). Lateral accretion sets are present in fluvial channels of the Smoky Hollow Member, but they become increasingly downstream-oriented upsection, which may be a function of decreased dispersion, or increased difficulty recognizing these lateral modes in the coarse-grained Calico bed. Furthermore, many modern DFS rivers can be primarily braided (14% of modern

examples) or sinuous (26%) from apex to toe (Hartley et al., 2010). Therefore, the upsection changes observed in the Smoky Hollow Member do not require a change of fluvial style, but could reflect progradation of coarser, proximal DFS facies within increasingly larger channels of similar planform type.

Another key characteristic of prograding DFSs is the upsection transition from poorly- to well-drained paleosols in floodplain deposits. The progradation of coarse-grained channel deposits characteristic of proximal facies allows greater infiltration of groundwater and a deepening of the water table (Hartley et al., 2013). Floodplain deposits are characterized by carbonaceous mudstone throughout the Smoky Hollow Member, though there is a decrease in abundance of coals upsection. These carbonaceous mudstones likely reflect the humid/wet climate conditions during this time (Orlansky, 1971; Slingerland et al., 1996; Akyuz et al., 2015) but may also record the relative proximity of these deposits to paleoshoreline, estimated to be located <50 km to the east of the study area (Cobban et al., 1994; Gardner and Cross, 1994; Roberts and Kirschbaum, 1995). Few modern examples of DFSs span the continental-marine transition due to global Holocene transgression. The Zambezi River of Mozambique is one modern analogue that spans this transition, however. The Zambezi drainage system, which terminates in the Indian Ocean, is marked by high amounts of preserved organic matter and perennial groundwater inundation as far as 120 km upstream despite a seasonal monsoonal climate (Moore et al., 2007). This suggests that DFSs within a paludal-type setting, like the Smoky Hollow Member, may not display a strong spatiotemporal trends in paleosol drainage as suggested for purely continental settings (Hartley et al., 2013).

In addition to providing an improved depositional framework, the DFS model provides an alternate mechanism for the progradation of the Smoky Hollow Member. Progradation of more proximal DFS facies does not necessarily require changes in accommodation and/or sediment supply; it may result from periodic incision in the more proximal area of the fan due to autogenic processes (Davidson et al., 2013, Weissmann et al., 2013). This contrasts previous models of the Smoky Hollow Member that relied on purely allogenic processes.

Calico Bed Unconformity

Previous depositional models for the Smoky Hollow Member largely focused on a regional Late Turonian unconformity associated with the Calico bed. Biostratigraphic ages suggest this unconformity spans the Late Turonian through middle to Late Coniacian, approximately 3 My (Eaton, 1991; Titus, et al., 2005). Shanley and McCabe (1993, 1995) placed a sequence boundary at the base of the Calico bed, stating that its coarse-grained, fluvial facies record a major basinward shift in facies compared to the less amalgamated fluvial strata below. The results of the present study indicate that this unconformity was misplaced, agreeing with earlier interpretations that the Calico bed is gradational with the underlying Smoky Hollow Member (Peterson, 1969b; Bobb, 1991; Eaton, 1991). Thus, the unconformity occurs at the boundary between the lower and upper Calico bed in the north, which translates to the top of the Calico bed in the south (Figure 6; Figure 15).

Architectural Evidence

Whereas the lower Smoky Hollow Member through lower Calico bed show a gradational increase in sandstone amalgamation and average grain size, these trends

Figure 15. Schematic cross section from south to north (A-A') along the eastern edge of the study area, showing the angular unconformity between the Smoky Hollow Member (SHM) and the overlying John Henry Member (JHM). Also labelled: TCM=Tibbet Canyon Member, LCB= lower Calico bed, UCB= upper Calico bed, and "A" and "B" shorefaces of the JHM.

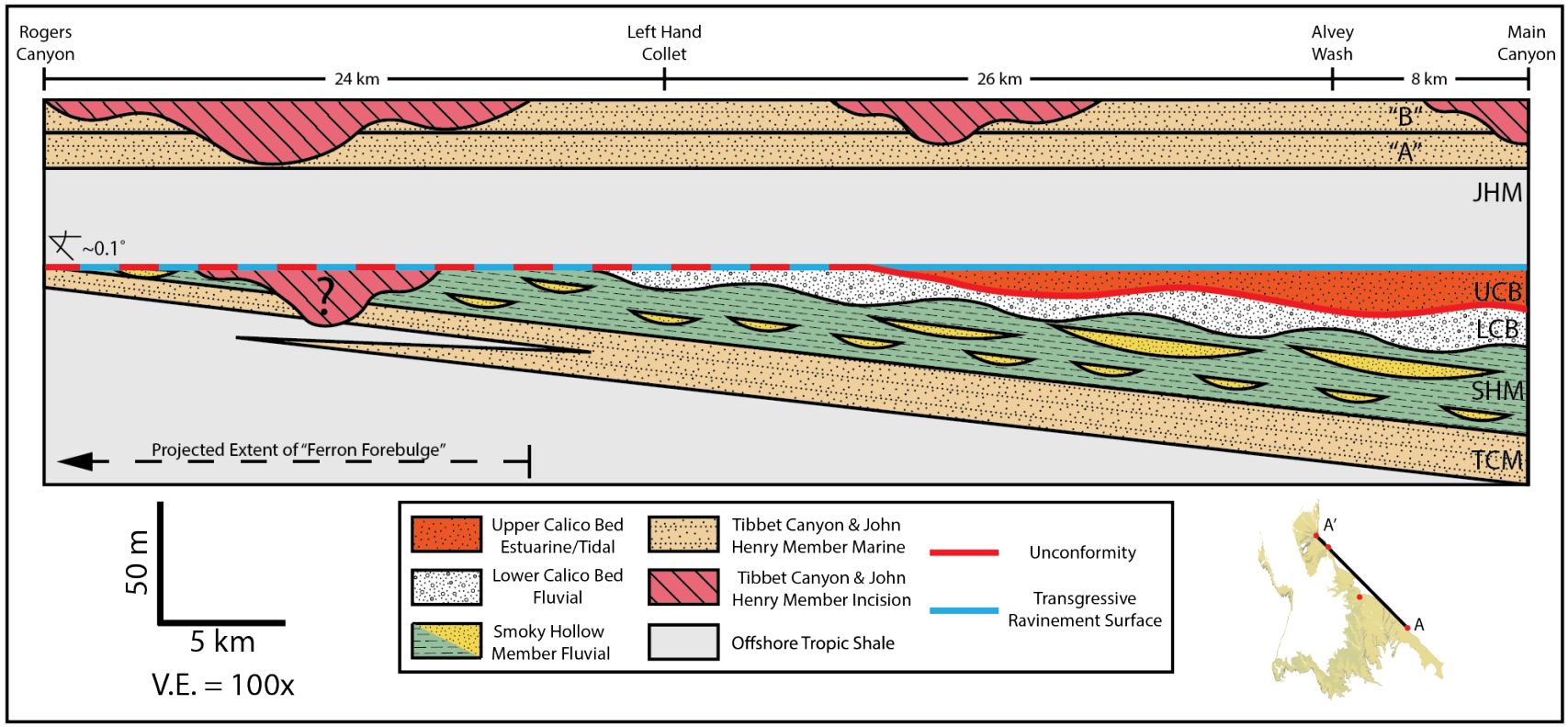
Rogers Canyon
Left Hand Collet
Alvey Wash
Main Canyon
24 km
26 km
8 km
"B"
"A"
JHM
~0.1°
?
UCB
LCB
SHM
TCM
Projected Extent of "Ferron Forebulge"
50 m
5 km
V.E. = 100x
Upper Calico Bed Estuarine/Tidal
Lower Calico Bed Fluvial
Smoky Hollow Member Fluvial
Tibbet Canyon & John Henry Member Marine
Tibbet Canyon & John Henry Member Incision
Offshore Tropic Shale
Unconformity
Transgressive Ravinement Surface
A'
A

reverse in the upper Calico bed. The basal upper Calico bed is typically very coarse-grained but these lithofacies are commonly tidally-influenced and quickly transition upsection to more heterolithic, finer-grained units with even more tidal influence (Figure 3; Figure 4). Tidal indicators diminish to the west, where the upper Calico bed is more fluvial-dominated. These trends support the interpretation that the upper Calico bed is estuarine in nature (Hettinger et al., 1993), and that the regressive lower and transgressive upper Calico bed units are genetically distinct.

Spatially, the Upper Calico bed is only present in the north and is thickest along the west-east transect from Shakespeare Mine to Alvey Wash, ranging from 20 to 25 m, respectively (Figure 9D). This axis of thickest deposits aligns with average paleocurrent orientations to the east for these strata. A pinch-out of upper Calico bed strata is observed on aerial photos to south of this axis approximately 10 km along the western margin of the study area and 20 km along the western margin (Figure 9D; Figure 15). This suggests the upper Calico bed represents incised valley-fill with an axis oriented west to east, and a width of approximately 20 km in the west that increases to 40 km seaward. These dimensions are within the range of previously studied modern and ancient incised valleys (Schumm and Ethridge, 2012). The presence of the upper Calico bed only in the north is likely due to confinement by this incised valley during subsequent transgression. Valley-confinement also helps explain the highly amalgamated nature of these deposits, the thickness variations, and the incisional contact between the lower and upper Calico bed. The lack of upper Calico bed strata in the south may be due to an absence of a significant incised valley system there, or removal during a subsequent lower John Henry Member unconformity (Chentnik, et al., 2015; Mulhern et al., in press; Purcell et al., in press),

which may also help explain the dramatically reduced thickness of the Smoky Hollow Member in the south.

The Smoky Hollow Member thins significantly from approximately 70 m thick to 0 m over approximately 60 km along 50 Mile Mountain (Figure 1). Aerial photo mapping indicates a slight angular unconformity between the upper part of the Smoky Hollow Member and the John Henry Member of 0 to 1° (Figure 15), further supporting the placement of a major unconformity at the middle/top Calico bed, rather than the base. Peterson (1969b) was the first to document a regional low-angle unconformity which was later measured as less than 1° regionally by a US Department of Energy resource evaluation for the area (Bureau of Land Management, 1990).

Compositional Evidence

Variations in sandstone composition support the gradational relationship between the middle Smoky Hollow Member and lower Calico bed, and the unconformable distinction between the lower and upper Calico bed. The upsection enrichment in subangular quartz and feldspar is transitional rather than abrupt (Figure 10A), and the average composition of middle Smoky Hollow Member and lower Calico bed sandstones are statistically very similar within 1σ uncertainty (Figure 11A). Across the mid-Calico boundary, however, upper Calico bed sandstones are abruptly the most quartz-rich samples. Furthermore, compositional trends reverse starting in the upper Calico bed, and show a gradational relationship with the overlying John Henry Member (Figure 11A–B), suggesting that the upper Calico bed is more conformable with overlying strata than underlying. Similarly, the abundance of detrital zircons within populations A and C transitionally increase upsection into the lower Calico bed with relative to the abundance

of population B detrital zircons. Across the mid-Calico boundary there is a reversal in these trends that continues into the lower to middle John Henry Member (Figure 12C) (Szwarc et al., 2015).

Trends in intergranular composition are perhaps even more compelling for defining the mid-Calico bed unconformity. The lower Calico bed's distinctive white color is due to the abundance of authigenic kaolinite within the matrix. Similar high concentrations of authigenic kaolinite within sandstones are commonly attributed to periods of subaerial exposure, and therefore, tied to unconformities (Macaulay et al., 1993; McCarthy and Plint, 1998; Ketzer et al., 2003). The abundance of kaolinite in lower Calico bed sandstones (0-18%, 7% average) supports the interpretation of an unconformity, especially given the negligible amounts of kaolinite found in underlying and overlying strata, despite their similar detrital compositions (Figure 10C).

These compositional trends are inconsistent with previously discussed depositional models, in which the lower Calico bed represents fluvial deposits that were deposited during active valley incision as terrace deposits, or following subsequent base level rise (Shanley and McCabe, 1993, 1995). In these and other models of incised valley formation, the low accommodation setting of the valley floor leads to multiple episodes of aggradation and incision leaving behind coarse-grained sand and gravel deposits (Zaitlin et al., 1994). Clay-sized sediment would likely be winnowed out during reworking of valley-confined deposits, and a mid-Calico unconformity would therefore best explain why the lower Calico bed has the highest average concentration of clay (14%), versus the basal upper Calico bed, which has the lowest average of the section (2%; Figure 10C). A previous interpretation by Peterson (1969b) also suggested that

coarse-grained deposits immediately overlying the lower Calico bed were likely reworked from it.

Finally, the surface at the top of the lower Calico bed is supportive of an unconformity. In the north, the regionally extensive ferruginous horizon is indicative of ferricrete development. Ferricrete preferentially forms in areas of groundwater discharge, such as valley floors and walls, and estuaries (Widdowson, 2007), so the presence of this regionally extensive horizon in the northern study area suggests that primary incision occurred after deposition of the lower Calico bed, not before. In the south, a *Glossifungites* surface caps the Calico bed, which is interpreted as a combined unconformity with subaerial exposure and a transgressive surface formed during marine transgression of lowermost John Henry Member strata. Transgressive ravinement along this surface is suggested by the presence of estuarine tidal bars of the John Henry Member that locally remove the Calico bed in Tibbet Canyon (Purcell et al., in press; Figure 1).

Axial Versus Transverse Drainages

Paleocurrent measurements and provenance data suggest the Smoky Hollow Member DFS was generally oriented from southwest to northeast. This northeast orientation is subparallel to the trend of the Sevier fold-thrust belt at this latitude (Figure 14), pointing to the interactions between a primary basin-axial drainage system and fluvial systems running transverse to the fold-thrust belt (Lawton et al., 2003, 2014; Szwarc et al., 2015).

Sediment dispersal patterns in fluvial strata throughout the Straight Cliffs Formation across the Kaiparowits Plateau generally vary from 000° to 132° (1σ) with an

average of 065° based on more than 8000 measurements (Gallin et al., 2010; Szwarc et al., 2015; Gooley et al., 2016). Smoky Hollow Member data are consistent with the overall dataset, with paleoflow indicators (n > 1700) that generally vary between 025° to 110° (1σ) with an average direction of 068° (Figure 7). The data also suggest waning influence of transverse drainages (relative to axial) upsection based on a transition from more easterly and southeasterly trends in the lower Smoky Hollow Member to more northeasterly for overlying strata (Figure 7).

Modal sandstone compositions record a similar upsection increase in the influence of an axial system. Rounded to subrounded sedimentary lithic grains are relatively common in the lower Smoky Hollow Member ($Qt_{66}F_{20}Lu_{14}$), as opposed to a greater proportion of angular to subangular quartz and potassium feldspar in the lower Calico bed ($Qt_{71}F_{27}Lu_{3}$; Table 4, Figure 10A). These trends are interpreted to reflect decreasing sediment input from the Sevier fold-thrust belt via transverse drainage systems, as this is the most likely source for rounded, multicycle sedimentary and meta-sedimentary grains (Miller, 1966; Armstrong, 1969; Uygur and Picard, 1980; DeCelles and Coogan, 2006; Trendell et al., 2012). Mogollon Highlands basement rock is mainly composed of metamorphosed granodioritic volcanic rocks and associated metasedimentary quartzites (Eisele and Isachsen, 2001), and intrusive bodies of the Cordilleran magmatic arc largely consisted of granitic plutons (Barth and Wooden, 2006; Cecil et al., 2012), both of which help explain the shift to more angular quartz and feldspar grains. The dataset does not preclude sediment input from the Sevier fold-thrust belt or any Paleozoic or Mesozoic sedimentary cover that might have existed in these source areas during the time, but it does point to decreased relative input from these sources during Calico bed deposition.

Temporally, there are simultaneous increases in both population A (86-260 Ma) and population C (1250-3000 Ma) detrital zircons relative to population B (260-1250 Ma) upsection (Figure 12C; Figure 13). Although these populations are not unique to a specific source area, there are trends within each population that support increased sediment delivery from the south/southwest via the axial fluvial system. Within population A, there is an upsection increase in the relative abundance of ca. 147 Ma detrital zircons, which are unique to the Independence dike swarm of southern California and Nevada (Coleman et al., 2000). Within population B, there is an upsection decrease in the relative abundance of ca. 1100 Ma age detrital zircons, and increase in the relative abundance of ca. 1400 Ma detrital zircons, which is attributed to increasing input from the Mogollon Highlands relative to the Sevier fold-thrust belt. Strata exposed in both of these source regions are expected to have ca. 1400 Ma zircons, however, the Sevier source region is strongly associated with a prominent ca. 1100 Ma peak, which should be absent from the Mogollon source area (Whitmeyer and Karlstrom, 2007; Dickinson and Gehrels, 2009; Lawton et al., 2010). The negligible amount of ca. 1100 in much of Smoky Hollow Member strata highlights how limited sediment input from the Sevier fold-thrust is inferred to be during this time.

Multiple lines of evidence suggest the major sediment sources for the Smoky Hollow Member were the Mogollon Highlands and Cordilleran magmatic arc. These source areas lie south/southwest of the Kaiparowits Basin and sediment was likely transported into the basin by an axial fluvial system that interacted with secondary transverse drainages along the Sevier thrust front (Figure 14; Lawton et al., 2003, 2014; Roberts, 2007; Szwarc et al., 2015; Chentnik et al., 2015; Gooley et al., 2016). Studies of

adjacent basins in northern Arizona and central and northern Utah have documented similar south-to-north flowing axial systems (collectively termed the California paleoriver) that show evidence of being sourced from southern California in Paleogene time (Young and McKee, 1978; Elston and Young, 1991; Goldstrand, 1994; Davis et al., 2010; Dickinson et al., 2012); Figure 14). Similar foredeep-axial drainages have been documented as early as the mid-Cretaceous (Dickinson and Gehrels, 2008) and possibly the Late Jurassic (Owen, 2015a, 2015b), but the Smoky Hollow Member represents the initial progradation of this iteration of the California paleoriver following the middle Turonian regression of the Western Interior Seaway in southern Utah, which possibly persisted in some form for at least another 30 My.

Initial progradation during Smoky Hollow Member time may have been driven by the peak in magmatic activity in the Cordilleran magmatic arc in southern California and along the margin of the Mogollon Highlands (Figure 14), leading to increased exhumation, as first suggested by Peterson and Kirk (1977). Furthermore, the initiation of the Maria fold-thrust belt in the Mogollon Highlands ca. 90 Ma (Knapp and Heizler, 1990; Barth et al., 2004; Salem, 2009) may have also contributed to this increased sediment supply (Szwarc et al., 2015). We speculate that the ca. 92 Ma Pb loss event signaled by the discordant metamict zircons may also reflect this source, and if so would imply rapid (<5 my) exhumation and deposition at least 250 km from source.

The demonstrated importance of this basin-axial drainage system is in contrast to many previous studies of other regions the Cordilleran foreland basin, which stress the importance of transverse sediment dispersal (Heller at al., 1988; Fillmore, 1991; Horton et al., 2004; Lawton et al., 2010). Furthermore, this decrease in Sevier signal contradicts

previous models (Bobb, 1991; Little, 1997) that suggested the progradation of the coarse-grained Calico bed was a signal of tectonic quiescence in the thrust front leading to the redistribution of proximal, wedge-top deposits into the basin. This current study and similar studies underscore the potential for decoupling of accommodation controls (i.e., load-driven subsidence in the fold-thrust belt) from extrabasinal sediment input controls (Goldstrand, 1994; Dickinson and Gehrels, 2008; Dickinson et al., 2012; Szwarc et al., 2015).

All of this is not to say, however, that transverse drainages did not influence deposition in the basin during this time. The lower Smoky Hollow and lower John Henry Members show more easterly and south-easterly paleoflow trends concordant with increased provenance signals from the Sevier fold-thrust belt, and there is sediment ultimately derived from the fold-thrust belt throughout the section. However, these data do suggest a dominant axial drainage system throughout Smoky Hollow Member deposition, without episodic incursions of transverse fans as has been suggested for younger parts of the Cretaceous section in the Kaiparowits basin (Lawton et al., 2014; Szwarc et al., 2014).

Regional Correlation

Previous studies correlate the lower Straight Cliffs Formation with part of the Ferron Sandstone Member of the Mancos Shale in central Utah (Ryer, 1981, 2004; Bobb, 1991; Gardner, 1995; Shanley and McCabe, 1995). More specifically, correlation with the Notom delta of the Ferron Sandstone near the Henry Mountains is considered here based on its location down-depositional dip (to the northeast), overlapping depositional ages, and similar progradational stacking patterns (Figure 16A).

Figure 16. A. Location of the Notom Ferron Sandstone in the Henry Mountains region in relation to the Kaiparowits Plateau, highlighting the forebulge interpreted by Fielding (2011) extended parallel to the trend of the active thrust belt at the time; B. Correlation between Kaiparowits Plateau strata (TCM=Tibbet Canyon Member, SHM=Smoky Hollow Member, LCB= lower Calico bed, UCB=upper Calico bed, LJHM=lower John Henry Member) and Ferron Sandstone strata with boxed numbers referring to part C; C. Paleogeographic reconstructions showing Smoky Hollow Member prograding as Notom delta in Henry basin (1), fed further by development of bypass surface in Kaiparowits basin (2), followed by subsequent transgression and deposition of upper Calico bed (3) and lower John Henry Member offshore deposits (4)

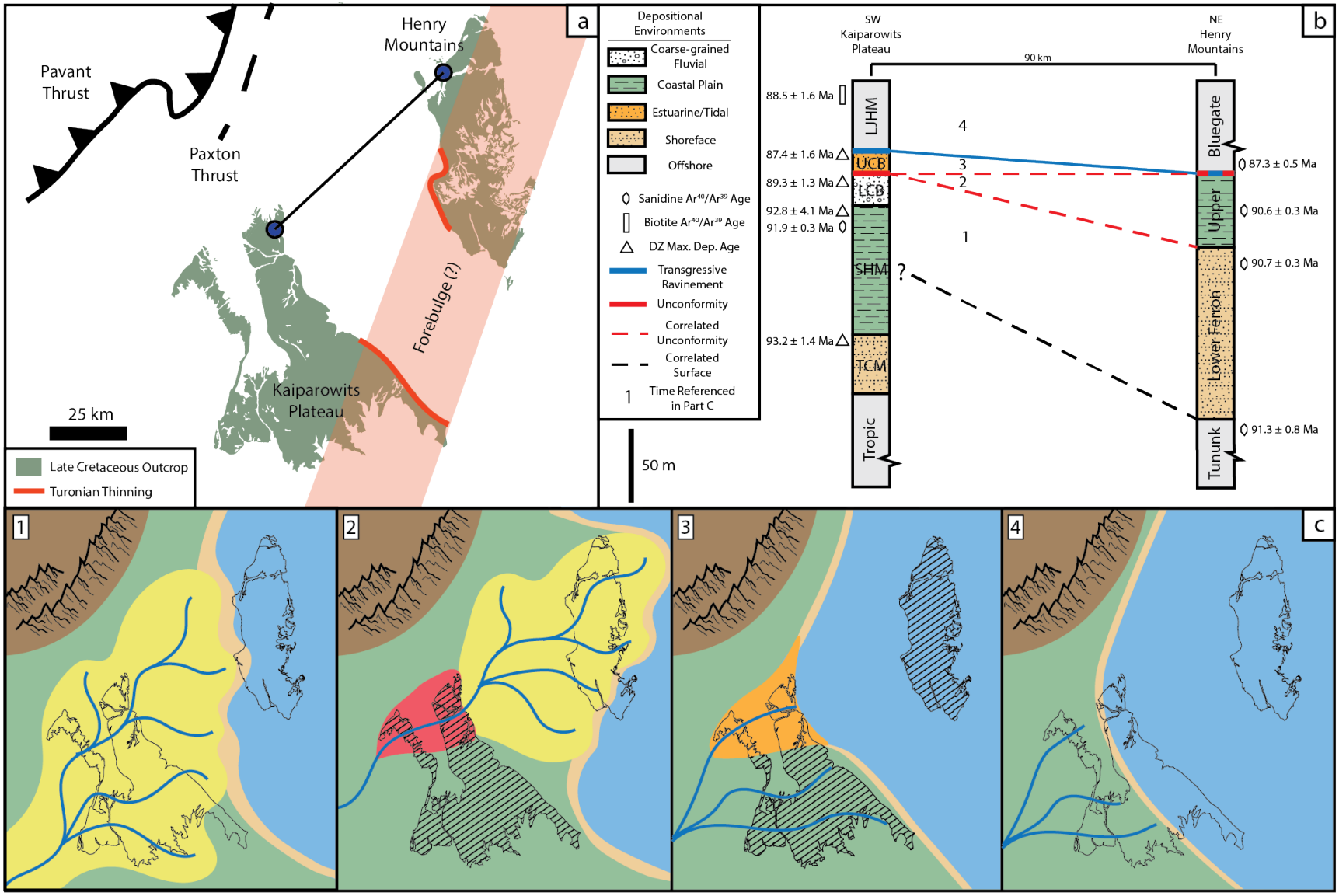
a
Pavant Thrust
Paxton Thrust
Henry Mountains
Kaiparowits Plateau
Forebulge (?)
25 km
Late Cretaceous Outcrop
Turonian Thinning
Depositional Environments
Coarse-grained Fluvial
Coastal Plain
Estuarine/Tidal
Shoreface
Offshore
Sanidine Ar40/Ar39 Age
Biotite Ar40/Ar39 Age
DZ Max. Dep. Age
Transgressive Ravinement
Unconformity
Correlated Unconformity
Correlated Surface
1 Time Referenced in Part C
50 m
b
SW Kaiparowits Plateau
NE Henry Mountains
90 km
88.5 ± 1.6 Ma
87.4 ± 1.6 Ma
89.3 ± 1.3 Ma
92.8 ± 4.1 Ma
91.9 ± 0.3 Ma
93.2 ± 1.4 Ma
LHM
UCB
LCB
SHM
TCM
Tropic
Bluegate
Upper
Lower Ferron
Tununk
87.3 ± 0.5 Ma
90.6 ± 0.3 Ma
90.7 ± 0.3 Ma
91.3 ± 0.8 Ma
1
2
3
4
?
c
1
2
3
4

The Notom delta of the Ferron Sandstone Member is informally separated into a lower unit comprised mainly of marine facies, interpreted as forced-regressive deltaic units (Li et al., 2011; Fielding, 2015), and an upper unit of mainly fluvial to floodplain facies, interpreted as basin-stepping, stacked incised valley-fill deposits (Fielding, 2010; Li et al., 2010; Li and Bhattacharya, 2013). The overall regressive nature of these units contrasts with the younger Last Chance delta of the Ferron Sandstone Member along the Wasatch Plateau further to north (Gardner, 1995), where the unit is regressive in the lower member and transgressive in the upper member (Anderson and Ryer, 2004). Shanley and McCabe (1995) correlated Straight Cliffs Formation strata to these younger Last Chance delta strata, interpreting the lower Ferron Sandstone as time-equivalent to the regressive highstand of their Tibbet sequence, and the upper Ferron Sandstone as the distal equivalent of their transgressive Calico sequence. Due to age relations and proximity, however, correlation is more reasonable between the Smoky Hollow Member and the Notom delta of the Ferron Sandstone Member in the Henry Basin, which is henceforth referred to simply as the Notom Ferron delta.

Based on radiometric dates, the Notom Ferron delta is time-equivalent only to the upper Smoky Hollow Member (Zhu et al., 2012; Figure 16B), and is likely the downstream equivalent to some portion of this prograding fluvial system based on paleocurrent measurements. These ages further suggest that the abrupt basinward shift in facies seen between the lower and upper Notom Ferron delta is the downstream equivalent of the mid-Calico unconformity and bypass surface (Figure 16C). Incision during the mid-Calico bed unconformity could have redistributed lower Calico bed deposits to the north, forming the upper Ferron Notom delta. The upper Calico bed

represents transgressive fill of the incised valley in the Kaiparowits basin during subsequent sea-level rise, and the offshore equivalent is the Blue Gate Shale in the Henry Basin. Correlation between the transgressive upper Calico bed and regressive upper Notom delta, therefore is unlikely (Li and Bhattacharya, 2013). Lastly, a combined unconformity/transgressive lag overlying the upper Ferron Sandstone (Li et al., 2010) is similar to the transgressive lag that commonly overlies the Calico bed near the base of the John Henry Member (Hettinger et al., 1993; Chentnik et al., 2015; Mulhern et al., in press). Radiometric ages indicate that the major unconformity in the Notom Ferron delta occurred at this combined unconformity-transgressive lag (Zhu et al., 2012), and has a similar duration (~3.5 Ma) to the mid-Calico unconformity (Figure 16B).

This alternative correlation between the Smoky Hollow Member and the Notom delta in the Henry basin questions the main mechanism driving the regional unconformity. Shanley and McCabe (1995) tied the sequence boundary to eustatic sea-level drops at 90 and 88.5 Ma based on sea-level curves from Haq (1988). The unconformity has also been tied to late Turonian unconformities within the Toreva Sandstone of Black Mesa in northeastern Arizona (Francyzk, 1988), and within the Gallup Sandstone of the San Juan basin in southwestern Colorado/northwestern New Mexico (Peterson and Kirk, 1977; Nummedal and Riley, 1991). These examples also cite eustatic controls, however, updated sea-level curves have shown that eustatic sea-level remained relatively static during the late Turonian and early Coniacian, with punctuated drops not occurring until approximately 88 and 86 Ma (Miller, 2009). Furthermore, recent modeling studies have shown that eustatic regression, while an important control on shoreline progradation, is expected to have minimal control on the progradation of

gravels (Armitage et al., 2016a, b). Therefore, the presence of the gravel-rich lower Calico bed cannot be attributed to a eustatic-driven unconformity. Although smaller-scale fluctuations in stratal architecture may well reflect eustatic and/or climatic signals, such as monsoons (Zhu et al., 2012; Li and Bhattacharya, 2013; Famubode and Bhattacharya, 2016), this study agrees with previous arguments that this major unconformity primarily reflects regional tectonics.

Fielding (2011) documented thinned Notom Ferron delta strata that were folded into an anticline, and interpreted it as a structural arch. He attributed this deformation to the migration of the forebulge, which contrasts with previous interpretations that place the location of the forebulge to the east of the Henry Basin during the Turonian (DeCelles and Currie, 1996; White et al., 2002; DeCelles, 2004). In the Kaiparowits basin, tilting and erosion related to the previously-described angular unconformity between the Smoky Hollow and John Henry Members was calculated at 0.1° along Fifty Mile Mountain, which is consistent with the expected angular unconformity associated with forebulges of <<1° (DeCelles and Giles, 1997; Figure 15). Based on the timing of events constrained by radiometric dates, deformation caused by the hypothesized forebulge preceded John Henry Member deposition, but coincided with or followed deposition of the lower Calico bed, and is perhaps the main cause of the mid-Calico bed unconformity and the thinning of strata in general to south. This unconformity is most apparent along Fifty Mile Mountain and coincides with the trend of the forebulge interpreted by Fielding (2011), as extended parallel to the trend of Sevier thrust front, approximately 120 km to the east during this time (Figure 15; Figure 16A). The position of the thrust front was relatively static at this time, although thrusts in southwestern Utah were active, and duplexing was

occurring in central Utah (DeCelles, 2004; DeCelles and Coogan, 2006), which may help explain this signal.

CONCLUSIONS

The Smoky Hollow Member of the Straight Cliffs Formation primarily records progradation of a basin-axial distributive fluvial system into the Kaiparowits basin during the Turonian. The Smoky Hollow Member is interpreted as a DFS based on spatial and temporal variations in stratigraphic architecture, thickness, average grain size distributions, and paleocurrent indicators that are consistent with conceptual model predictions for analogous systems. Paleocurrent indicators, modal sandstone composition and detrital zircon age population trends indicate that this fluvial system was sourced primarily from the Mogollon Highlands and Cordilleran magmatic arc to the south and southwest, with more episodic influx from the Sevier fold-thrust belt via transverse drainage systems.

Although previously linked to tectonic activity in the Sevier fold-thrust belt or eustatic regression in the Western Interior Seaway, progradation was likely driven by high sediment supply rates. The timing of shortening in the Sevier thrust-front does not correspond with depositional architecture of the Smoky Hollow Member, and these strata record a distinct decrease in detritus from the Sevier fold-thrust belt upsection. Similarly, eustatic sea-level curves reveal no major regressions during this time and the effects of sea-level fluctuations are believed to be negligible in the regional progradation of gravels. Thus, eustatic sea-level fluctuations could not have been responsible for the progradational architecture of the Smoky Hollow Member. Alternatively, increased in

sediment supply from the south was possibly due to increased magmatic and orogenic activity in the source areas to the southwest or a climate-induced increase in discharge in these areas could have increased sediment supply from the south.

Progradation of the Smoky Hollow Member eventually led to a maximum regression recorded by the lower Calico bed in the Kaiparowits basin and its distal equivalent, the Notom Ferron Delta in the Henry basin. Following this progradation, there was a significant regional unconformity that lasted approximately 2-3 Myr. Based on architectural and thickness variations, this unconformity was likely driven by uplift related to tectonic activity in the Sevier fold-thrust belt.

These results show that the relationship between accommodation and sediment supply may be complex and somewhat counterintuitive. Despite that the Kaiparowits Basin was proximal to both tectonic (Sevier) and eustatic (Western Interior Seaway) controls on accommodation, Smoky Hollow Member strata show dramatic temporal changes that are not necessarily linked to either. Instead, depositional architecture was controlled by the sediment supply from extrabasinal sources. Autogenic processes associated with DFS progradation were also likely important. The primary role of sediment supply identified in this study stands in stark contrast to numerous previous accommodation-driven models, widely cited to explain the stratigraphic architecture of Cordilleran foreland basin fill.

APPENDIX

DETRITAL ZIRCON ISOTOPIC DATA

Raw isotopic data from all detrital zircon geochronologic analyses. Samples are organized by location, and analyses are arranged according to analysis number, Analyses that have been corrected for common Pb are presented with corrected isotope ratios, and raw ratios are not included. Discarded analyses are not presented in this appendix.

Table 7

Detrital Zircon Isotopic Data

Sample	Analysis	238/206	Uncertainty (abs.)	207/206	Uncertainty (abs.)	206/238 Age (Ma)	Uncertainty (Ma)	207/206 Age (Ma)	Uncertainty (Ma)	Best Age (Ma)	Uncertainty (Ma)	Discordance (%)
KG-01	1	4.28817	0.07956	0.09183	0.00451	1351.2	25.1	1463.9	71.9	1351.2	25.1	8%
KG-01	2	3.70370	0.06247	0.10620	0.00534	1540.8	26.0	1735.2	87.3	1540.8	26.0	11%
KG-01	3	6.07533	0.09619	0.10838	0.00532	982.3	15.6	1772.4	87.0	940.8	15.6	45%
KG-01	4	68.51192	0.89998	0.05834	0.00301	93.4	1.2	542.6	28.0	92.2	1.3	83%
KG-01	5	3.43171	0.05744	0.10490	0.00523	1648.5	27.6	1712.6	85.4	1648.5	27.6	4%
KG-01	6	3.63769	0.06174	0.10772	0.00532	1565.6	26.6	1761.2	87.0	1565.6	26.6	11%
KG-01	7	3.55745	0.05097	0.10719	0.00527	1596.9	22.9	1752.2	86.2	1596.9	22.9	9%
KG-01	8	3.24570	0.04886	0.10726	0.00531	1731.4	26.1	1753.4	86.8	1731.4	26.1	1%
KG-01	9	67.59954	0.89743	0.05107	0.00261	94.7	1.3	244.0	12.5	94.3	1.3	61%
KG-01	10	3.46141	0.04626	0.10671	0.00524	1636.0	21.9	1744.0	85.7	1636.0	21.9	6%
KG-01	11	5.05306	0.07039	0.11647	0.00573	1164.0	16.2	1902.7	93.6	1164.0	16.2	39%
KG-01	12	17.56543	0.22553	0.16208	0.00794	356.9	4.6	2477.5	121.4	309.6	5.3	86%
KG-01	13	3.54484	0.04705	0.10603	0.00523	1601.9	21.3	1732.2	85.4	1601.9	21.3	8%
KG-01	14	4.14594	0.07940	0.11020	0.00542	1392.9	26.7	1802.7	88.7	1392.9	26.7	23%
KG-01	15	4.34028	0.05605	0.09277	0.00455	1336.6	17.3	1483.2	72.7	1336.6	17.3	10%
KG-01	16	70.62147	1.09805	0.04940	0.00275	90.6	1.4	166.9	9.3	90.5	1.4	46%
KG-01	17	73.71370	1.00813	0.05053	0.00260	86.9	1.2	219.4	11.3	86.6	1.2	60%
KG-01	18	3.22685	0.04258	0.10690	0.00525	1740.2	23.0	1747.2	85.8	1740.2	23.0	0%
KG-01	19	3.29164	0.04271	0.10679	0.00525	1710.1	22.2	1745.3	85.7	1710.1	22.2	2%
KG-01	20	3.42349	0.04730	0.10697	0.00526	1652.0	22.8	1748.4	86.0	1652.0	22.8	6%
KG-01	21	3.36474	0.04425	0.10581	0.00521	1677.4	22.1	1728.4	85.0	1677.4	22.1	3%
KG-01	22	3.48311	0.04773	0.10551	0.00521	1627.0	22.3	1723.2	85.2	1627.0	22.3	6%
KG-01	23	3.57526	0.05670	0.10660	0.00532	1589.9	25.2	1742.1	86.9	1589.9	25.2	9%
KG-01	24	4.49640	0.06743	0.09255	0.00455	1294.5	19.4	1478.7	72.7	1294.5	19.4	12%
KG-01	25	3.66300	0.06145	0.10887	0.00534	1556.0	26.1	1780.6	87.4	1556.0	26.1	13%
KG-01	26	20.26342	0.34324	0.13121	0.00646	310.5	5.3	2114.2	104.1	280.6	5.3	85%
KG-01	27	71.17438	1.01980	0.04991	0.00261	89.9	1.3	190.8	10.0	89.7	1.3	53%
KG-01	28	3.55114	0.04662	0.10701	0.00526	1599.4	21.0	1749.1	86.0	1599.4	21.0	9%
KG-01	29	3.55366	0.05460	0.13150	0.00655	1598.4	24.6	2118.1	105.6	1598.4	24.6	25%
KG-01	30	3.44234	0.04762	0.11103	0.00545	1644.0	22.7	1816.3	89.2	1644.0	22.7	9%
KG-01	31	3.99521	0.05289	0.10864	0.00533	1440.0	19.1	1776.7	87.1	1440.0	19.1	19%
KG-01	32	3.90625	0.05216	0.11022	0.00541	1469.3	19.6	1803.0	88.5	1469.3	19.6	19%

Table 7 continued

Sample	Analysis	238/206	Uncertainty (abs.)	207/206	Uncertainty (abs.)	206/238 Age (Ma)	Uncertainty (Ma)	207/206 Age (Ma)	Uncertainty (Ma)	Best Age (Ma)	Uncertainty (Ma)	Discordance (%)
KG-01	33	3.46380	0.04483	0.10733	0.00527	1635.0	21.2	1754.6	86.1	1635.0	21.2	7%
KG-01	34	3.50385	0.04590	0.11117	0.00546	1618.5	21.2	1818.6	89.3	1618.5	21.2	11%
KG-01	35	6.51508	0.08816	0.09180	0.00450	920.5	12.5	1463.3	71.8	896.9	12.7	37%
KG-01	36	3.69686	0.04887	0.10886	0.00534	1543.3	20.4	1780.4	87.3	1543.3	20.4	13%
KG-01	37	30.16591	0.45893	0.16163	0.00796	210.2	3.2	2472.8	121.8	181.2	3.5	91%
KG-01	38	3.44471	0.04953	0.10789	0.00530	1643.0	23.6	1764.1	86.7	1643.0	23.6	7%
KG-01	39	4.28082	0.05588	0.09297	0.00456	1353.3	17.7	1487.3	73.0	1353.3	17.7	9%
KG-01	40	5.79039	0.07867	0.11088	0.00544	1027.0	14.0	1813.9	88.9	1027.0	14.0	43%
KG-01	41	4.81464	0.07862	0.10995	0.00541	1216.6	19.9	1798.6	88.4	1216.6	19.9	32%
KG-01	42	3.58038	0.04707	0.10740	0.00527	1587.8	20.9	1755.8	86.2	1587.8	20.9	10%
KG-01	43	5.19211	0.08418	0.09261	0.00455	1135.4	18.4	1479.9	72.6	1135.4	18.4	23%
KG-01	44	3.78788	0.05703	0.10732	0.00527	1510.3	22.7	1754.4	86.2	1510.3	22.7	14%
KG-01	45	70.35812	0.90711	0.05142	0.00265	91.0	1.2	259.7	13.4	90.6	1.2	65%
KG-01	46	71.87006	0.93517	0.04964	0.00248	89.1	1.2	178.2	8.9	88.9	1.2	50%
KG-01	47	4.42321	0.05568	0.09290	0.00456	1313.9	16.5	1485.8	72.9	1313.9	16.5	12%
KG-01	48	3.52485	0.04785	0.10879	0.00535	1610.0	21.9	1779.3	87.5	1610.0	21.9	10%
KG-01	49	3.76648	0.04782	0.10709	0.00526	1517.9	19.3	1750.5	86.0	1517.9	19.3	13%
KG-01	50	7.18907	0.10625	0.12197	0.00601	839.6	12.4	1985.2	97.8	785.7	12.7	58%
KG-01	51	71.72572	0.95405	0.05010	0.00256	89.3	1.2	199.6	10.2	89.0	1.2	55%
KG-01	52	3.36248	0.04519	0.10621	0.00522	1678.4	22.6	1735.4	85.3	1678.4	22.6	3%
KG-01	53	4.23908	0.05457	0.09122	0.00448	1365.3	17.6	1451.2	71.3	1365.3	17.6	6%
KG-01	54	5.45256	0.07755	0.10834	0.00531	1085.5	15.4	1771.7	86.9	1085.5	15.4	39%
KG-01	55	3.42936	0.04628	0.10772	0.00529	1649.5	22.3	1761.2	86.4	1649.5	22.3	6%
KG-01	56	4.21941	0.07756	0.11042	0.00543	1371.1	25.2	1806.3	88.8	1371.1	25.2	24%
KG-01	57	4.52694	0.06345	0.11394	0.00559	1286.6	18.0	1863.2	91.4	1286.6	18.0	31%
KG-01	58	3.48554	0.04665	0.10510	0.00519	1626.0	21.8	1716.1	84.8	1626.0	21.8	5%
KG-01	59	7.39481	0.09559	0.10439	0.00512	817.6	10.6	1703.6	83.6	781.2	11.0	52%
KG-01	60	3.62188	0.04827	0.10791	0.00530	1571.7	20.9	1764.4	86.6	1571.7	20.9	11%
KG-01	61	4.33651	0.05600	0.09257	0.00454	1337.6	17.3	1479.1	72.6	1337.6	17.3	10%
KG-01	62	3.68732	0.05056	0.10654	0.00523	1546.9	21.2	1741.0	85.5	1546.9	21.2	11%
KG-01	63	15.59089	0.20453	0.09480	0.00465	400.8	5.3	1524.1	74.7	381.2	5.4	74%
KG-01	64	3.45782	0.04674	0.10816	0.00531	1637.5	22.1	1768.7	86.8	1637.5	22.1	7%

Table 7 continued

Sample	Analysis	238/206	Uncertainty (abs.)	207/206	Uncertainty (abs.)	206/238 Age (Ma)	Uncertainty (Ma)	207/206 Age (Ma)	Uncertainty (Ma)	Best Age (Ma)	Uncertainty (Ma)	Discordance (%)
KG-01	65	4.33651	0.05600	0.09251	0.00454	1337.6	17.3	1477.9	72.6	1337.6	17.3	9%
KG-01	66	4.60830	0.06181	0.09162	0.00451	1266.0	17.0	1459.5	71.8	1266.0	17.0	13%
KG-01	67	3.41181	0.04365	0.10749	0.00528	1657.0	21.2	1757.3	86.3	1657.0	21.2	6%
KG-01	68	15.42258	0.19835	0.13137	0.00646	405.0	5.2	2116.4	104.0	367.3	5.6	81%
KG-01	69	3.34113	0.04345	0.11008	0.00543	1687.8	21.9	1800.7	88.8	1687.8	21.9	6%
KG-01	70	7.71605	0.13285	0.11104	0.00545	785.6	13.5	1816.5	89.1	743.4	13.4	57%
KG-01	71	4.33840	0.06771	0.10795	0.00530	1337.1	20.9	1765.1	86.7	1337.1	20.9	24%
KG-01	72	3.58038	0.04707	0.10775	0.00529	1587.8	20.9	1761.7	86.4	1587.8	20.9	10%
KG-01	73	3.63769	0.04795	0.10883	0.00534	1565.6	20.6	1779.9	87.4	1565.6	20.6	12%
KG-01	74	6.46705	0.08776	0.11495	0.00564	926.9	12.6	1879.1	92.2	878.4	13.0	51%
KG-01	75	4.38212	0.07251	0.10603	0.00520	1325.1	21.9	1732.2	85.0	1325.1	21.9	24%
KG-01	76	73.44301	0.99096	0.04854	0.00245	87.2	1.2	125.7	6.3	87.1	1.2	31%
KG-01	77	3.59583	0.04731	0.10621	0.00522	1581.8	20.8	1735.4	85.2	1581.8	20.8	9%
KG-01	78	9.16590	0.11804	0.10685	0.00524	667.5	8.6	1746.4	85.7	631.9	8.9	62%
KG-01	79	7.16332	0.10011	0.11303	0.00555	842.4	11.8	1848.7	90.7	797.2	12.1	54%
KG-01	80	7.60746	0.09874	0.11188	0.00548	796.1	10.3	1830.2	89.7	753.0	10.8	56%
KG-01	81	8.94534	0.12108	0.12680	0.00622	683.1	9.2	2054.1	100.7	630.9	9.7	67%
KG-01	82	59.25224	0.76449	0.04946	0.00244	107.9	1.4	169.7	8.4	107.7	1.4	36%
KG-01	83	4.25532	0.05481	0.09150	0.00450	1360.7	17.5	1457.0	71.6	1360.7	17.5	7%
KG-01	84	7.51315	0.11989	0.10743	0.00529	805.5	12.9	1756.3	86.5	766.4	12.9	54%
KG-01	85	3.47947	0.04506	0.10664	0.00523	1628.5	21.1	1742.8	85.5	1628.5	21.1	7%
KG-01	86	3.56379	0.04584	0.10758	0.00528	1594.4	20.5	1758.8	86.3	1594.4	20.5	9%
KG-01	87	5.62746	0.07909	0.07728	0.00386	1054.4	14.8	1128.4	56.4	1054.4	14.8	7%
KG-01	88	10.41341	0.14565	0.10213	0.00505	591.1	8.3	1663.2	82.2	561.1	8.5	64%
KG-01	89	3.57910	0.04520	0.10810	0.00531	1588.3	20.1	1767.6	86.8	1588.3	20.1	10%
KG-01	90	4.37637	0.05733	0.09271	0.00456	1326.6	17.4	1482.0	72.8	1326.6	17.4	10%
KG-01	91	3.60750	0.04602	0.10805	0.00530	1577.2	20.1	1766.8	86.7	1577.2	20.1	11%
KG-01	92	6.55351	0.08744	0.10678	0.00524	915.5	12.2	1745.2	85.7	875.9	12.6	48%
KG-01	93	6.45203	0.08601	0.10700	0.00524	928.9	12.4	1748.9	85.7	889.0	12.8	47%
KG-01	94	3.50631	0.04501	0.10830	0.00531	1617.5	20.8	1771.0	86.9	1617.5	20.8	9%
KG-01	95	8.32501	0.11326	0.11384	0.00559	731.3	9.9	1861.6	91.4	688.0	10.3	61%
KG-01	96	4.35540	0.05779	0.09268	0.00455	1332.4	17.7	1481.4	72.7	1332.4	17.7	10%

Table 7 continued

Sample	Analysis	238/206	Uncertainty (abs.)	207/206	Uncertainty (abs.)	206/238 Age (Ma)	Uncertainty (Ma)	207/206 Age (Ma)	Uncertainty (Ma)	Best Age (Ma)	Uncertainty (Ma)	Discordance (%)
KG-01	97	4.33840	0.05603	0.09204	0.00452	1337.1	17.3	1468.2	72.1	1337.1	17.3	9%
KG-01	98	3.67647	0.04855	0.10912	0.00535	1550.9	20.5	1784.8	87.5	1550.9	20.5	13%
KG-01	99	3.50263	0.04496	0.10614	0.00522	1619.0	20.8	1734.1	85.2	1619.0	20.8	7%
KG-01	100	3.82702	0.04867	0.10998	0.00539	1496.5	19.0	1799.1	88.2	1496.5	19.0	17%
KG-02	1	3.49406	0.09380	0.11840	0.00353	1622.5	43.6	1932.2	57.5	1622.5	43.6	16%
KG-02	2	4.34216	0.08448	0.08925	0.00253	1336.1	26.0	1409.5	39.9	1336.1	26.0	5%
KG-02	3	8.43313	0.15910	0.20660	0.00587	722.4	13.6	2879.1	81.8	599.9	12.2	75%
KG-02	4	3.42701	0.07046	0.11930	0.00339	1650.5	33.9	1945.8	55.2	1650.5	33.9	15%
KG-02	5	3.76506	0.07402	0.10404	0.00295	1518.4	29.9	1697.4	48.1	1518.4	29.9	11%
KG-02	6	4.32152	0.08629	0.09037	0.00254	1341.8	26.8	1433.4	40.3	1341.8	26.8	6%
KG-02	7	3.52734	0.06914	0.10481	0.00295	1609.0	31.5	1711.0	48.2	1609.0	31.5	6%
KG-02	8	4.28449	0.08073	0.08978	0.00253	1352.3	25.5	1420.9	40.0	1352.3	25.5	5%
KG-02	9	3.83730	0.10533	0.10842	0.00311	1492.9	41.0	1773.0	50.9	1492.9	41.0	16%
KG-02	10	3.67242	0.08202	0.10776	0.00305	1552.5	34.7	1761.9	49.8	1552.5	34.7	12%
KG-02	11	3.61272	0.07109	0.10656	0.00300	1575.2	31.0	1741.4	49.1	1575.2	31.0	10%
KG-02	12	70.42254	1.34063	0.05018	0.00166	90.9	1.7	203.3	6.7	90.6	1.7	55%
KG-02	13	4.19639	0.08192	0.09290	0.00263	1377.9	26.9	1485.8	42.1	1377.9	26.9	7%
KG-02	14	72.88630	1.43621	0.05724	0.00180	87.8	1.7	500.8	15.8	86.8	1.7	82%
KG-02	15	3.42349	0.06408	0.10972	0.00309	1652.0	30.9	1794.8	50.6	1652.0	30.9	8%
KG-02	16	3.49895	0.06950	0.11129	0.00313	1620.5	32.2	1820.6	51.2	1620.5	32.2	11%
KG-02	17	3.34336	0.06501	0.10964	0.00310	1686.8	32.8	1793.4	50.8	1686.8	32.8	6%
KG-02	18	3.47222	0.06577	0.11069	0.00312	1631.5	30.9	1810.8	51.0	1631.5	30.9	10%
KG-02	19	3.51617	0.06990	0.11121	0.00314	1613.5	32.1	1819.3	51.3	1613.5	32.1	11%
KG-02	20	7.35294	0.15247	0.10618	0.00299	822.0	17.0	1734.8	48.9	783.8	16.0	53%
KG-02	21	3.24675	0.06327	0.09916	0.00290	1730.9	33.7	1608.4	47.1	1730.9	33.7	8%
KG-02	22	3.44709	0.06644	0.10126	0.00284	1642.0	31.7	1647.3	46.2	1642.0	31.7	0%
KG-02	23	3.54233	0.06807	0.09378	0.00265	1602.9	30.8	1503.7	42.4	1602.9	30.8	7%
KG-02	24	3.55492	0.06791	0.09061	0.00255	1597.9	30.5	1438.4	40.5	1597.9	30.5	11%
KG-02	25	3.39443	0.06805	0.09061	0.00257	1664.5	33.4	1438.4	40.8	1664.5	33.4	16%
KG-02	26	62.15040	1.42856	0.03630	0.00207	102.9	2.4	-608.3	-34.6	104.4	2.4	117%
KG-02	27	3.45423	0.06578	0.08406	0.00237	1639.0	31.2	1293.9	36.5	1639.0	31.2	27%
KG-02	28	3.42114	0.06630	0.08004	0.00231	1653.0	32.0	1198.0	34.6	1653.0	32.0	38%

Table 7 continued

Sample	Analysis	238/206	Uncertainty (abs.)	207/206	Uncertainty (abs.)	206/238 Age (Ma)	Uncertainty (Ma)	207/206 Age (Ma)	Uncertainty (Ma)	Best Age (Ma)	Uncertainty (Ma)	Discordance (%)
KG-02	29	3.64034	0.07172	0.08051	0.00229	1564.6	30.8	1209.5	34.3	1564.6	30.8	29%
KG-02	30	3.39789	0.06498	0.07864	0.00224	1663.0	31.8	1163.1	33.2	1663.0	31.8	43%
KG-02	31	2.97265	0.06563	0.15130	0.00482	1869.3	41.3	2360.7	75.2	1869.3	41.3	21%
KG-02	32	3.42701	0.06560	0.08013	0.00228	1650.5	31.6	1200.2	34.2	1650.5	31.6	38%
KG-02	33	4.41891	0.09333	0.06748	0.00199	1315.1	27.8	852.6	25.1	1315.1	27.8	54%
KG-02	34	3.49773	0.07350	0.08428	0.00237	1621.0	34.1	1299.0	36.5	1621.0	34.1	25%
KG-02	35	4.27899	0.15905	0.08910	0.00286	1353.9	50.3	1406.3	45.2	1353.9	50.3	4%
KG-02	36	11.83292	0.22745	0.09835	0.00283	523.0	10.1	1593.1	45.8	497.5	9.5	67%
KG-02	37	4.48632	0.08770	0.07680	0.00216	1297.2	25.4	1116.0	31.3	1297.2	25.4	16%
KG-02	38	4.84262	0.09160	0.07894	0.00222	1210.1	22.9	1170.6	32.9	1210.1	22.9	3%
KG-02	39	3.23311	0.06468	0.09115	0.00261	1737.3	34.8	1449.7	41.5	1737.3	34.8	20%
KG-02	40	4.85909	0.09940	0.10109	0.00287	1206.4	24.7	1644.2	46.6	1206.4	24.7	27%
KG-02	41	68.44627	1.37435	0.04940	0.00177	93.5	1.9	166.9	6.0	93.3	1.9	44%
KG-02	42	3.35121	0.07022	0.11095	0.00313	1683.4	35.3	1815.0	51.2	1683.4	35.3	7%
KG-02	43	9.60615	0.27376	0.10819	0.00314	638.4	18.2	1769.2	51.4	602.6	16.9	64%
KG-02	44	26.67378	0.55454	0.10366	0.00298	237.3	4.9	1690.7	48.6	221.8	4.6	86%
KG-02	45	1.87266	0.12391	0.16720	0.00722	2758.3	182.5	2529.8	109.3	2758.3	182.5	9%
KG-02	46	3.47222	0.06657	0.11035	0.00310	1631.5	31.3	1805.2	50.8	1631.5	31.3	10%
KG-02	47	3.40948	0.06563	0.10965	0.00309	1658.0	31.9	1793.6	50.5	1658.0	31.9	8%
KG-02	48	3.55872	0.07145	0.10928	0.00307	1596.4	32.1	1787.4	50.2	1596.4	32.1	11%
KG-02	49	69.78367	1.40662	0.05029	0.00170	91.7	1.8	208.4	7.1	91.4	1.8	56%
KG-02	50	3.38181	0.06725	0.10692	0.00301	1670.0	33.2	1747.6	49.2	1670.0	33.2	4%
KG-02	51	13.86963	0.29634	0.12345	0.00354	448.8	9.6	2006.7	57.6	412.1	8.9	78%
KG-02	52	68.54010	1.35641	0.04782	0.00149	93.4	1.8	90.4	2.8	93.4	1.8	3%
KG-02	53	3.65097	0.07493	0.11008	0.00309	1560.6	32.0	1800.7	50.5	1560.6	32.0	13%
KG-02	54	8.83392	0.17713	0.08652	0.00246	691.3	13.9	1349.8	38.4	671.7	13.2	49%
KG-02	55	4.11353	0.07944	0.08983	0.00257	1402.8	27.1	1421.9	40.6	1402.8	27.1	1%
KG-02	56	3.43761	0.06758	0.10584	0.00300	1646.0	32.4	1729.0	49.1	1646.0	32.4	5%
KG-02	57	5.59597	0.10751	0.09083	0.00255	1059.9	20.4	1443.0	40.6	1059.9	20.4	27%
KG-02	58	3.43171	0.06493	0.10767	0.00302	1648.5	31.2	1760.4	49.4	1648.5	31.2	6%
KG-02	59	3.41064	0.06793	0.10204	0.00300	1657.5	33.0	1661.6	48.8	1657.5	33.0	0%
KG-02	60	64.98570	1.22609	0.04845	0.00150	98.4	1.9	121.3	3.7	98.4	1.9	19%

Table 7 continued

Sample	Analysis	238/206	Uncertainty (abs.)	207/206	Uncertainty (abs.)	206/238 Age (Ma)	Uncertainty (Ma)	207/206 Age (Ma)	Uncertainty (Ma)	Best Age (Ma)	Uncertainty (Ma)	Discordance (%)
KG-02	61	3.39559	0.06859	0.10384	0.00296	1664.0	33.6	1693.9	48.2	1664.0	33.6	2%
KG-02	62	11.83432	0.28022	0.12660	0.00381	522.9	12.4	2051.3	61.8	479.7	11.4	75%
KG-02	63	3.41297	0.06656	0.10367	0.00299	1656.5	32.3	1690.8	48.8	1656.5	32.3	2%
KG-02	64	18.24152	0.38428	0.34446	0.00968	344.0	7.2	3682.7	103.5	221.0	6.4	91%
KG-02	65	17.69912	1.69056	0.43800	0.03149	354.3	33.8	4045.0	290.8	186.8	22.5	91%
KG-02	66	70.22472	1.54459	0.05210	0.00307	91.1	2.0	289.8	17.1	90.7	2.0	69%
KG-02	67	6.10128	0.17040	0.10159	0.00289	978.4	27.3	1653.4	47.1	944.6	25.7	41%
KG-02	68	3.28084	0.06535	0.10488	0.00299	1715.1	34.2	1712.2	48.7	1715.1	34.2	0%
KG-02	69	2.88101	0.05789	0.10485	0.00297	1920.7	38.6	1711.7	48.5	1920.7	38.6	12%
KG-02	70	3.74252	0.11213	0.10825	0.00306	1526.6	45.7	1770.2	50.1	1526.6	45.7	14%
KG-02	71	3.32447	0.07125	0.10798	0.00312	1695.3	36.3	1765.6	50.9	1695.3	36.3	4%
KG-02	72	4.29738	0.08348	0.09749	0.00275	1348.6	26.2	1576.7	44.4	1348.6	26.2	14%
KG-02	73	70.87172	1.59315	0.05769	0.00189	90.3	2.0	518.0	17.0	89.2	2.0	83%
KG-02	74	4.26258	0.08490	0.09848	0.00280	1358.6	27.1	1595.5	45.3	1358.6	27.1	15%
KG-02	75	3.45543	0.06848	0.11956	0.00336	1638.5	32.5	1949.7	54.8	1638.5	32.5	16%
KG-02	76	3.42818	0.06939	0.11708	0.00333	1650.0	33.4	1912.1	54.4	1650.0	33.4	14%
KG-02	77	3.79795	0.08762	0.10418	0.00304	1506.7	34.8	1699.9	49.7	1506.7	34.8	11%
KG-02	78	3.48675	0.07027	0.11648	0.00334	1625.5	32.8	1902.9	54.5	1625.5	32.8	15%
KG-02	79	3.57143	0.16601	0.11990	0.00478	1591.4	74.0	1954.7	77.9	1591.4	74.0	19%
KG-02	80	3.47826	0.06901	0.11659	0.00331	1629.0	32.3	1904.6	54.1	1629.0	32.3	14%
KG-02	81	3.61272	0.07524	0.09694	0.00273	1575.2	32.8	1566.1	44.1	1575.2	32.8	1%
KG-02	82	3.47222	0.07345	0.09333	0.00263	1631.5	34.5	1494.6	42.0	1631.5	34.5	9%
KG-02	83	3.58552	0.07519	0.08793	0.00247	1585.8	33.3	1381.0	38.8	1585.8	33.3	15%
KG-02	84	3.53232	0.08239	0.08409	0.00238	1607.0	37.5	1294.6	36.6	1607.0	37.5	24%
KG-02	85	4.02577	0.09303	0.08099	0.00231	1430.2	33.1	1221.2	34.8	1430.2	33.1	17%
KG-02	86	3.51247	0.07035	0.07589	0.00214	1615.0	32.3	1092.2	30.9	1615.0	32.3	48%
KG-02	87	11.88919	0.24139	0.09079	0.00261	520.6	10.6	1442.2	41.4	499.9	10.1	64%
KG-02	88	5.89623	0.11535	0.06934	0.00195	1009.9	19.8	908.9	25.5	1009.9	19.8	11%
KG-02	89	3.52734	0.07183	0.06801	0.00194	1609.0	32.8	868.9	24.8	1609.0	32.8	85%
KG-02	90	6.05327	0.16277	0.06746	0.00200	985.6	26.5	852.0	25.3	990.8	25.8	16%
KG-02	91	4.33463	0.08919	0.05985	0.00169	1338.2	27.5	598.2	16.9	1338.2	27.5	124%
KG-02	92	3.57782	0.06930	0.07245	0.00203	1588.8	30.8	998.6	28.0	1588.8	30.8	59%

Table 7 continued

Sample	Analysis	238/206	Uncertainty (abs.)	207/206	Uncertainty (abs.)	206/238 Age (Ma)	Uncertainty (Ma)	207/206 Age (Ma)	Uncertainty (Ma)	Best Age (Ma)	Uncertainty (Ma)	Discordance (%)
KG-02	93	3.62450	0.07083	0.07035	0.00199	1570.7	30.7	938.6	26.5	1570.7	30.7	67%
KG-02	94	70.07708	1.37219	0.03310	0.00101	91.3	1.8	-866.6	-26.5	93.0	1.8	111%
KG-02	95	3.86250	0.08189	0.07602	0.00215	1484.2	31.5	1095.6	30.9	1484.2	31.5	35%
KG-02	96	70.57163	1.44907	0.03700	0.00166	90.7	1.9	-556.5	-25.0	91.9	1.9	116%
KG-02	97	3.72578	0.07894	0.08140	0.00230	1532.7	32.5	1231.1	34.8	1532.7	32.5	24%
KG-02	98	6.59196	0.16087	0.10167	0.00292	910.5	22.2	1654.8	47.6	876.3	20.9	45%
KG-02	99	3.59195	0.07225	0.09281	0.00261	1583.3	31.8	1484.0	41.8	1583.3	31.8	7%
KG-02	100	3.20924	0.06864	0.09935	0.00280	1748.6	37.4	1611.9	45.4	1748.6	37.4	8%
KG-03	1	3.63636	0.14149	0.08238	0.00397	1566.1	60.9	1254.6	60.4	1566.1	60.9	-25%
KG-03	2	3.55999	0.13838	0.07736	0.00373	1595.9	62.0	1130.5	54.5	1595.9	62.0	-41%
KG-03	3	5.03778	0.19624	0.07670	0.00371	1167.3	45.5	1113.4	53.8	1167.3	45.5	-5%
KG-03	4	5.87579	0.22470	0.07213	0.00347	1013.2	38.7	989.6	47.6	1013.2	38.7	-2%
KG-03	5	5.46150	0.21060	0.06871	0.00331	1083.9	41.8	890.0	42.8	1083.9	41.8	-22%
KG-03	6	9.89120	0.38334	0.06683	0.00322	620.9	24.1	832.5	40.1	616.2	23.4	25%
KG-03	7	3.98089	0.15456	0.06315	0.00304	1444.7	56.1	713.3	34.4	1444.7	56.1	-103%
KG-03	8	3.92773	0.15104	0.06114	0.00295	1462.2	56.2	644.2	31.1	1462.2	56.2	-127%
KG-03	9	5.87199	0.22634	0.06676	0.00322	1013.8	39.1	830.3	40.0	1013.8	39.1	-22%
KG-03	10	4.30663	0.16666	0.06009	0.00291	1346.0	52.1	606.8	29.4	1346.0	52.1	-122%
KG-03	11	3.60101	0.13927	0.06196	0.00300	1579.8	61.1	672.7	32.6	1579.8	61.1	-135%
KG-03	12	45.59964	1.76847	0.03515	0.00186	139.8	5.4	-696.8	-36.8	142.2	5.5	120%
KG-03	13	4.76872	0.18578	0.05850	0.00282	1227.2	47.8	548.5	26.4	1227.2	47.8	-124%
KG-03	14	47.43833	1.81665	0.03775	0.00190	134.5	5.1	-502.8	-25.3	136.3	5.2	127%
KG-03	15	3.87147	0.15145	0.07524	0.00362	1481.1	57.9	1074.9	51.7	1481.1	57.9	-38%
KG-03	16	3.90168	0.15001	0.07969	0.00384	1470.9	56.6	1189.3	57.3	1470.9	56.6	-24%
KG-03	17	8.34794	0.32323	0.07972	0.00384	729.4	28.2	1190.1	57.3	715.5	27.1	39%
KG-03	18	4.65983	0.17898	0.07782	0.00374	1253.3	48.1	1142.3	54.9	1253.3	48.1	-10%
KG-03	19	5.63158	0.21581	0.09565	0.00460	1053.7	40.4	1540.9	74.0	1053.7	40.4	32%
KG-03	20	8.74126	0.34264	0.10244	0.00497	698.3	27.4	1668.8	81.0	665.4	25.7	58%
KG-03	21	3.45782	0.13449	0.11585	0.00558	1637.5	63.7	1893.1	91.2	1637.5	63.7	14%
KG-03	22	3.37952	0.13006	0.11832	0.00569	1670.9	64.3	1931.0	92.9	1670.9	64.3	13%
KG-03	23	6.41437	0.24791	0.11926	0.00574	934.0	36.1	1945.2	93.6	880.8	33.5	52%
KG-03	24	4.63392	0.17901	0.12640	0.00627	1259.6	48.7	2048.5	101.7	1259.6	48.7	39%

Table 7 continued

Sample	Analysis	238/206	Uncertainty (abs.)	207/206	Uncertainty (abs.)	206/238 Age (Ma)	Uncertainty (Ma)	207/206 Age (Ma)	Uncertainty (Ma)	Best Age (Ma)	Uncertainty (Ma)	Discordance (%)
KG-03	25	4.26439	0.16464	0.12435	0.00598	1358.0	52.4	2019.6	97.1	1358.0	52.4	33%
KG-03	26	3.85505	0.15010	0.12121	0.00583	1486.8	57.9	1974.1	95.0	1486.8	57.9	25%
KG-03	27	3.63636	0.14069	0.11850	0.00572	1566.1	60.6	1933.7	93.4	1566.1	60.6	19%
KG-03	28	4.51060	0.17286	0.09953	0.00478	1290.9	49.5	1615.3	77.6	1290.9	49.5	20%
KG-03	29	3.63901	0.13952	0.11357	0.00546	1565.1	60.0	1857.3	89.4	1565.1	60.0	16%
KG-03	30	3.69959	0.14349	0.11229	0.00540	1542.3	59.8	1836.8	88.3	1542.3	59.8	16%
KG-03	31	3.72578	0.14514	0.10658	0.00513	1532.7	59.7	1741.7	83.8	1532.7	59.7	12%
KG-03	32	3.67918	0.14323	0.10775	0.00521	1549.9	60.3	1761.7	85.2	1549.9	60.3	12%
KG-03	33	4.51467	0.17426	0.10679	0.00513	1289.8	49.8	1745.3	83.9	1289.8	49.8	26%
KG-03	34	4.38982	0.16964	0.10334	0.00499	1323.0	51.1	1685.0	81.3	1323.0	51.1	21%
KG-03	35	3.66032	0.14094	0.10430	0.00502	1557.0	60.0	1702.0	82.0	1557.0	60.0	9%
KG-03	36	3.60620	0.13973	0.10288	0.00496	1577.7	61.1	1676.7	80.8	1577.7	61.1	6%
KG-03	37	3.43879	0.13347	0.10180	0.00495	1645.5	63.9	1657.2	80.6	1645.5	63.9	1%
KG-03	38	4.36491	0.16864	0.08867	0.00427	1329.8	51.4	1397.0	67.3	1329.8	51.4	5%
KG-03	39	10.97333	0.42131	0.09670	0.00465	562.2	21.6	1561.4	75.0	536.8	20.4	64%
KG-03	40	3.56888	0.13776	0.10548	0.00509	1592.4	61.5	1722.7	83.1	1592.4	61.5	8%
KG-03	41	5.07099	0.20083	0.10527	0.00507	1160.3	46.0	1719.0	82.7	1160.3	46.0	33%
KG-03	42	3.50263	0.13454	0.10698	0.00515	1619.0	62.2	1748.6	84.1	1619.0	62.2	7%
KG-03	43	3.55872	0.13807	0.10850	0.00523	1596.4	61.9	1774.4	85.6	1596.4	61.9	10%
KG-03	44	3.77359	0.14678	0.10863	0.00523	1515.4	58.9	1776.6	85.5	1515.4	58.9	15%
KG-03	45	4.59137	0.18000	0.10600	0.00521	1270.2	49.8	1731.7	85.0	1270.2	49.8	27%
KG-03	46	6.48929	0.26650	0.10995	0.00533	923.9	37.9	1798.6	87.2	880.9	35.4	49%
KG-03	47	3.63901	0.14055	0.10960	0.00529	1565.1	60.5	1792.8	86.5	1565.1	60.5	13%
KG-03	48	3.63901	0.14105	0.10858	0.00526	1565.1	60.7	1775.7	86.0	1565.1	60.7	12%
KG-03	49	3.80518	0.14776	0.10958	0.00527	1504.2	58.4	1792.4	86.2	1504.2	58.4	16%
KG-03	50	5.80720	0.22887	0.12895	0.00620	1024.2	40.4	2083.7	100.2	1024.2	40.4	51%
KG-03	51	3.61925	0.13954	0.10902	0.00524	1572.7	60.6	1783.1	85.8	1572.7	60.6	12%
KG-03	52	4.49843	0.17664	0.09104	0.00441	1294.0	50.8	1447.4	70.0	1294.0	50.8	11%
KG-03	53	5.23835	0.20509	0.11317	0.00544	1126.2	44.1	1850.9	89.1	1126.2	44.1	39%
KG-03	54	3.77786	0.14584	0.10949	0.00527	1513.8	58.4	1790.9	86.1	1513.8	58.4	15%
KG-03	55	3.66032	0.14035	0.10836	0.00521	1557.0	59.7	1772.0	85.2	1557.0	59.7	12%
KG-03	56	3.38066	0.13389	0.10669	0.00519	1670.4	66.2	1743.6	84.9	1670.4	66.2	4%

Table 7 continued

Sample	Analysis	238/206	Uncertainty (abs.)	207/206	Uncertainty (abs.)	206/238 Age (Ma)	Uncertainty (Ma)	207/206 Age (Ma)	Uncertainty (Ma)	Best Age (Ma)	Uncertainty (Ma)	Discordance (%)
KG-03	57	4.91884	0.19041	0.10613	0.00514	1193.0	46.2	1734.0	84.0	1193.0	46.2	31%
KG-03	58	3.59066	0.13863	0.10461	0.00505	1583.8	61.1	1707.5	82.5	1583.8	61.1	7%
KG-03	59	4.32339	0.16699	0.08997	0.00440	1341.3	51.8	1424.9	69.7	1341.3	51.8	6%
KG-03	60	3.48311	0.13435	0.10905	0.00527	1627.0	62.8	1783.6	86.2	1627.0	62.8	9%
KG-03	61	3.53232	0.13676	0.10623	0.00514	1607.0	62.2	1735.7	83.9	1607.0	62.2	7%
KG-03	62	3.61533	0.14010	0.10574	0.00513	1574.2	61.0	1727.2	83.8	1574.2	61.0	9%
KG-03	63	3.60360	0.13814	0.10675	0.00514	1578.8	60.5	1744.7	84.0	1578.8	60.5	10%
KG-03	64	3.65764	0.14154	0.10656	0.00514	1558.0	60.3	1741.4	84.0	1558.0	60.3	11%
KG-03	65	3.65898	0.14013	0.10718	0.00516	1557.5	59.6	1752.0	84.3	1557.5	59.6	11%
KG-03	66	65.52651	2.52531	0.05180	0.00268	97.6	3.8	276.6	14.3	97.2	3.7	65%
KG-03	67	3.74252	0.14376	0.10772	0.00518	1526.6	58.6	1761.2	84.7	1526.6	58.6	13%
KG-03	68	3.51370	0.14152	0.10370	0.00510	1614.5	65.0	1691.4	83.1	1614.5	65.0	5%
KG-03	69	3.47415	0.13250	0.10968	0.00528	1630.7	62.2	1794.1	86.4	1630.7	62.2	9%
KG-03	70	3.64166	0.14000	0.10946	0.00526	1564.1	60.1	1790.4	86.1	1564.1	60.1	13%
KG-03	71	3.98883	0.15488	0.10994	0.00531	1442.1	56.0	1798.4	86.8	1442.1	56.0	20%
KG-03	72	11.18318	0.42851	0.08714	0.00419	552.1	21.2	1363.6	65.5	533.2	20.1	60%
KG-03	73	4.58842	0.17555	0.09414	0.00453	1271.0	48.6	1510.9	72.7	1271.0	48.6	16%
KG-03	74	5.60853	0.21591	0.09638	0.00463	1057.7	40.7	1555.2	74.7	1057.7	40.7	32%
KG-03	75	3.71195	0.14322	0.10843	0.00522	1537.8	59.3	1773.2	85.3	1537.8	59.3	13%
KG-03	76	5.63063	0.22144	0.10774	0.00520	1053.8	41.4	1761.5	85.1	1053.8	41.4	40%
KG-03	77	6.64717	0.25412	0.10785	0.00518	903.4	34.5	1763.4	84.7	862.8	32.3	49%
KG-03	78	4.49640	0.17319	0.09385	0.00452	1294.5	49.9	1505.1	72.4	1294.5	49.9	14%
KG-03	79	6.69792	0.26015	0.12380	0.00700	897.0	34.8	2011.7	113.7	839.8	32.4	55%
KG-03	80	13.79310	0.53767	0.09535	0.00458	451.2	17.6	1535.0	73.8	429.7	16.6	71%
KG-03	81	14.03115	0.53623	0.09871	0.00475	443.8	17.0	1599.9	76.9	420.7	16.0	72%
KG-03	82	3.61402	0.14058	0.10385	0.00502	1574.7	61.3	1694.0	81.8	1574.7	61.3	7%
KG-03	83	10.58537	0.40982	0.10445	0.00504	581.9	22.5	1704.7	82.2	550.6	21.1	66%
KG-03	84	3.96511	0.15361	0.11098	0.00534	1449.8	56.2	1815.5	87.3	1449.8	56.2	20%
KG-03	85	73.26007	2.83515	0.04640	0.00244	87.4	3.4	18.5	1.0	87.5	3.4	-374%
KG-03	86	3.80084	0.14888	0.10214	0.00496	1505.7	59.0	1663.4	80.8	1505.7	59.0	9%
KG-03	87	3.75235	0.14721	0.10133	0.00493	1523.0	59.8	1648.6	80.3	1523.0	59.8	8%
KG-03	88	3.66300	0.14127	0.10180	0.00503	1556.0	60.0	1657.2	81.9	1556.0	60.0	6%

Table 7 continued

Sample	Analysis	238/206	Uncertainty (abs.)	207/206	Uncertainty (abs.)	206/238 Age (Ma)	Uncertainty (Ma)	207/206 Age (Ma)	Uncertainty (Ma)	Best Age (Ma)	Uncertainty (Ma)	Discordance (%)
KG-03	89	8.00192	0.30836	0.10398	0.00500	759.1	29.3	1696.3	81.6	723.9	27.4	55%
KG-03	90	4.78698	0.18471	0.08688	0.00419	1223.0	47.2	1357.8	65.4	1223.0	47.2	10%
KG-03	91	3.69686	0.14178	0.10403	0.00500	1543.3	59.2	1697.2	81.6	1543.3	59.2	9%
KG-03	92	8.57559	0.33027	0.08742	0.00420	711.0	27.4	1369.8	65.8	690.6	26.1	48%
KG-03	93	4.30663	0.16600	0.10307	0.00496	1346.0	51.9	1680.1	80.9	1346.0	51.9	20%
KG-03	94	3.69549	0.14306	0.10574	0.00509	1543.8	59.8	1727.2	83.1	1543.8	59.8	11%
KG-03	95	3.64166	0.14021	0.10194	0.00492	1564.1	60.2	1659.7	80.0	1564.1	60.2	6%
KG-03	96	4.85909	0.18646	0.10656	0.00512	1206.4	46.3	1741.4	83.7	1206.4	46.3	31%
KG-03	97	3.66838	0.14126	0.10375	0.00501	1554.0	59.8	1692.3	81.7	1554.0	59.8	8%
KG-03	98	3.46741	0.13394	0.10480	0.00509	1633.5	63.1	1710.8	83.1	1633.5	63.1	5%
KG-03	99	3.56506	0.13739	0.10456	0.00509	1593.9	61.4	1706.6	83.0	1593.9	61.4	7%
MC-01	1	3.59971	0.05882	0.10109	0.00247	1580.3	25.8	1644.2	40.1	1580.3	25.8	4%
MC-01	2	25.66076	0.40275	0.04781	0.00123	246.4	3.9	89.9	2.3	247.5	3.9	-174%
MC-01	3	3.42349	0.05912	0.10135	0.00261	1652.0	28.5	1649.0	42.4	1652.0	28.5	0%
MC-01	4	3.51865	0.06751	0.10429	0.00262	1612.5	30.9	1701.8	42.7	1612.5	30.9	5%
MC-01	5	7.91578	0.12938	0.11230	0.00275	766.9	12.5	1837.0	45.0	724.0	11.8	58%
MC-01	6	3.54610	0.06595	0.10399	0.00255	1601.4	29.8	1696.5	41.6	1601.4	29.8	6%
MC-01	7	4.02091	0.08161	0.08580	0.00229	1431.8	29.1	1333.7	35.6	1431.8	29.1	-7%
MC-01	8	3.05998	0.09026	0.11350	0.00391	1822.9	53.8	1856.2	63.9	1822.9	53.8	2%
MC-01	9	3.30142	0.05327	0.10688	0.00265	1705.7	27.5	1746.9	43.4	1705.7	27.5	2%
MC-01	10	3.37268	0.05695	0.10181	0.00249	1673.9	28.3	1657.4	40.5	1673.9	28.3	-1%
MC-01	11	3.58552	0.06018	0.10182	0.00248	1585.8	26.6	1657.6	40.4	1585.8	26.6	4%
MC-01	12	4.56413	0.08477	0.10749	0.00264	1277.1	23.7	1757.3	43.2	1277.1	23.7	27%
MC-01	13	3.79219	0.07139	0.09988	0.00248	1508.7	28.4	1621.8	40.3	1508.7	28.4	7%
MC-01	14	5.10491	0.07993	0.10710	0.00258	1153.2	18.1	1750.6	42.1	1153.2	18.1	34%
MC-01	15	3.59195	0.07114	0.09940	0.00263	1583.3	31.4	1612.9	42.6	1583.3	31.4	2%
MC-01	16	3.33111	0.09143	0.11310	0.00349	1692.3	46.4	1849.8	57.1	1692.3	46.4	9%
MC-01	17	3.45304	0.05917	0.10550	0.00271	1639.5	28.1	1723.0	44.2	1639.5	28.1	5%
MC-01	18	3.52361	0.06008	0.10945	0.00267	1610.5	27.5	1790.3	43.6	1610.5	27.5	10%
MC-01	19	6.02955	0.09489	0.10900	0.00263	989.2	15.6	1782.8	42.9	947.0	14.7	45%
MC-01	20	3.43289	0.05992	0.10850	0.00271	1648.0	28.8	1774.4	44.3	1648.0	28.8	7%
MC-01	21	12.12709	0.21825	0.17370	0.00659	510.8	9.2	2593.6	98.4	439.3	8.8	80%

Table 7 continued

Sample	Analysis	238/206	Uncertainty (abs.)	207/206	Uncertainty (abs.)	206/238 Age (Ma)	Uncertainty (Ma)	207/206 Age (Ma)	Uncertainty (Ma)	Best Age (Ma)	Uncertainty (Ma)	Discordance (%)
MC-01	22	3.27654	0.05139	0.10668	0.00259	1717.0	26.9	1743.4	42.4	1717.0	26.9	2%
MC-01	23	1.99960	0.03605	0.17470	0.00433	2614.2	47.1	2603.2	64.6	2614.2	47.1	0%
MC-01	24	3.34672	0.06369	0.10670	0.00287	1685.4	32.1	1743.8	46.9	1685.4	32.1	3%
MC-01	25	4.45633	0.07580	0.11206	0.00273	1305.1	22.2	1833.1	44.7	1305.1	22.2	29%
MC-01	26	3.57654	0.06000	0.10839	0.00264	1589.3	26.7	1772.5	43.1	1589.3	26.7	10%
MC-01	27	3.63504	0.06242	0.10981	0.00266	1566.6	26.9	1796.3	43.5	1566.6	26.9	13%
MC-01	28	3.56761	0.06360	0.10810	0.00265	1592.9	28.4	1767.6	43.3	1592.9	28.4	10%
MC-01	29	3.58938	0.07106	0.10523	0.00262	1584.3	31.4	1718.3	42.8	1584.3	31.4	8%
MC-01	30	3.75375	0.06875	0.11165	0.00276	1522.5	27.9	1826.4	45.2	1522.5	27.9	17%
MC-01	31	43.23390	0.74854	0.05160	0.00180	147.4	2.6	267.7	9.3	146.9	2.5	45%
MC-01	32	3.61141	0.06323	0.10438	0.00257	1575.7	27.6	1703.4	41.9	1575.7	27.6	7%
MC-01	33	3.82995	0.06263	0.10495	0.00256	1495.5	24.5	1713.4	41.8	1495.5	24.5	13%
MC-01	34	5.44366	0.08906	0.10893	0.00264	1087.2	17.8	1781.6	43.1	1087.2	17.8	39%
MC-01	35	3.43997	0.06471	0.10658	0.00263	1645.0	30.9	1741.7	43.0	1645.0	30.9	6%
MC-01	36	3.57271	0.07143	0.10160	0.00254	1590.9	31.8	1653.6	41.3	1590.9	31.8	4%
MC-01	37	43.30879	0.76961	0.04718	0.00148	147.2	2.6	58.3	1.8	147.5	2.6	-152%
MC-01	38	4.59559	0.07210	0.10578	0.00255	1269.2	19.9	1727.9	41.6	1269.2	19.9	27%
MC-01	39	3.54988	0.05838	0.10189	0.00247	1599.9	26.3	1658.8	40.2	1599.9	26.3	4%
MC-01	40	8.86368	0.14986	0.10251	0.00248	689.1	11.7	1670.1	40.4	656.4	11.0	59%
MC-01	41	3.54359	0.06238	0.10322	0.00266	1602.4	28.2	1682.8	43.4	1602.4	28.2	5%
MC-01	42	3.51000	0.06363	0.09884	0.00247	1616.0	29.3	1602.3	40.1	1616.0	29.3	-1%
MC-01	43	3.91389	0.07181	0.10375	0.00253	1466.8	26.9	1692.3	41.3	1466.8	26.9	13%
MC-01	44	3.52361	0.06326	0.10923	0.00269	1610.5	28.9	1786.6	44.0	1610.5	28.9	10%
MC-01	45	3.35233	0.05873	0.10100	0.00270	1682.9	29.5	1642.6	44.0	1682.9	29.5	-2%
MC-01	46	3.27332	0.05754	0.10402	0.00266	1718.5	30.2	1697.1	43.5	1718.5	30.2	-1%
MC-01	47	3.02847	0.05218	0.10346	0.00257	1839.4	31.7	1687.1	41.9	1839.4	31.7	-9%
MC-01	48	3.53857	0.06227	0.10451	0.00257	1604.4	28.2	1705.7	41.9	1604.4	28.2	6%
MC-01	49	6.01685	0.10351	0.14716	0.00358	991.1	17.1	2313.2	56.3	905.2	15.6	57%
MC-01	50	3.29815	0.06378	0.11890	0.00373	1707.2	33.0	1939.8	60.8	1707.2	33.0	12%
MC-01	51	4.89476	0.08767	0.10742	0.00260	1198.4	21.5	1756.1	42.4	1198.4	21.5	32%
MC-01	52	3.48068	0.06576	0.10762	0.00261	1628.0	30.8	1759.5	42.7	1628.0	30.8	7%
MC-01	53	3.72995	0.06445	0.11018	0.00267	1531.2	26.5	1802.4	43.7	1531.2	26.5	15%

Table 7 continued

Sample	Analysis	238/206	Uncertainty (abs.)	207/206	Uncertainty (abs.)	206/238 Age (Ma)	Uncertainty (Ma)	207/206 Age (Ma)	Uncertainty (Ma)	Best Age (Ma)	Uncertainty (Ma)	Discordance (%)
MC-01	54	2.12224	0.03552	0.16540	0.00401	2488.8	41.7	2511.6	60.9	2488.8	41.7	1%
MC-01	55	4.46429	0.07333	0.10917	0.00264	1303.0	21.4	1785.6	43.2	1303.0	21.4	27%
MC-01	56	5.70776	0.11378	0.07660	0.00225	1040.7	20.7	1110.8	32.7	1040.7	20.7	6%
MC-01	57	5.10204	0.08840	0.08316	0.00206	1153.8	20.0	1273.0	31.5	1153.8	20.0	9%
MC-01	58	5.96303	0.11883	0.12940	0.00364	999.4	19.9	2089.8	58.8	933.7	18.5	52%
MC-01	59	3.48918	0.06453	0.10839	0.00273	1624.5	30.0	1772.5	44.7	1624.5	30.0	8%
MC-01	60	12.16101	0.21122	0.10911	0.00267	509.4	8.8	1784.6	43.7	477.8	8.3	71%
MC-01	61	3.96511	0.07893	0.09620	0.00270	1449.8	28.9	1551.7	43.6	1449.8	28.9	7%
MC-01	62	3.74112	0.07449	0.11030	0.00378	1527.1	30.4	1804.4	61.9	1527.1	30.4	15%
MC-01	63	4.34972	0.07639	0.09464	0.00236	1334.0	23.4	1520.9	37.9	1334.0	23.4	12%
MC-01	64	3.51494	0.05932	0.10836	0.00262	1614.0	27.2	1772.0	42.9	1614.0	27.2	9%
MC-01	65	3.47222	0.06079	0.10561	0.00263	1631.5	28.6	1725.0	42.9	1631.5	28.6	5%
MC-01	66	4.18060	0.08403	0.10973	0.00265	1382.5	27.8	1794.9	43.3	1382.5	27.8	23%
MC-01	67	3.26052	0.06276	0.10904	0.00279	1724.4	33.2	1783.4	45.6	1724.4	33.2	3%
MC-01	68	10.58425	0.17609	0.06097	0.00151	582.0	9.7	638.2	15.8	580.9	9.5	9%
MC-01	69	3.09119	0.06324	0.10860	0.00291	1806.8	37.0	1776.1	47.6	1806.8	37.0	-2%
MC-01	70	6.12370	0.12099	0.11677	0.00287	975.1	19.3	1907.4	46.9	924.2	17.9	49%
MC-01	71	3.65097	0.06276	0.10189	0.00250	1560.6	26.8	1658.8	40.7	1560.6	26.8	6%
MC-01	72	5.48546	0.13129	0.09150	0.00555	1079.5	25.8	1457.0	88.4	1079.5	25.8	26%
MC-01	73	3.85505	0.07582	0.10827	0.00267	1486.8	29.2	1770.5	43.6	1486.8	29.2	16%
MC-01	74	3.79507	0.07235	0.09968	0.00254	1507.7	28.7	1618.1	41.2	1507.7	28.7	7%
MC-01	75	4.77555	0.08617	0.10798	0.00266	1225.6	22.1	1765.6	43.5	1225.6	22.1	31%
MC-01	76	3.76364	0.06590	0.09928	0.00254	1518.9	26.6	1610.6	41.3	1518.9	26.6	6%
MC-01	77	67.93478	1.40631	0.04890	0.00294	94.2	2.0	143.0	8.6	94.1	2.0	34%
MC-01	78	3.61011	0.06458	0.10096	0.00256	1576.2	28.2	1641.8	41.7	1576.2	28.2	4%
MC-01	79	3.50877	0.05977	0.10640	0.00291	1616.5	27.5	1738.6	47.6	1616.5	27.5	7%
MC-01	80	7.46826	0.12772	0.10706	0.00262	810.1	13.9	1750.0	42.8	771.2	13.0	54%
MC-01	81	9.87167	0.18280	0.14779	0.00359	622.0	11.5	2320.5	56.4	557.3	10.4	73%
MC-01	82	3.52983	0.06939	0.10217	0.00249	1608.0	31.6	1663.9	40.6	1608.0	31.6	3%
MC-01	83	4.34405	0.07104	0.09044	0.00220	1335.5	21.8	1434.8	34.9	1335.5	21.8	7%
MC-01	84	5.52792	0.08837	0.11760	0.00289	1071.9	17.1	1920.1	47.1	1071.9	17.1	44%
MC-01	85	3.55872	0.05855	0.10451	0.00256	1596.4	26.3	1705.7	41.8	1596.4	26.3	6%

Table 7 continued

Sample	Analysis	238/206	Uncertainty (abs.)	207/206	Uncertainty (abs.)	206/238 Age (Ma)	Uncertainty (Ma)	207/206 Age (Ma)	Uncertainty (Ma)	Best Age (Ma)	Uncertainty (Ma)	Discordance (%)
MC-01	86	3.48918	0.05825	0.10409	0.00258	1624.5	27.1	1698.3	42.2	1624.5	27.1	4%
MC-01	87	3.24465	0.06041	0.10383	0.00261	1731.8	32.2	1693.7	42.5	1731.8	32.2	-2%
MC-01	88	5.17866	0.09440	0.11292	0.00281	1138.1	20.7	1846.9	45.9	1138.1	20.7	38%
MC-01	89	3.30688	0.07302	0.10290	0.00284	1703.2	37.6	1677.1	46.3	1703.2	37.6	-2%
MC-01	90	3.43997	0.05834	0.10770	0.00277	1645.0	27.9	1760.9	45.3	1645.0	27.9	7%
MC-01	91	4.16667	0.06988	0.09562	0.00243	1386.7	23.3	1540.3	39.1	1386.7	23.3	10%
MC-01	92	4.45832	0.07780	0.12820	0.00384	1304.6	22.8	2073.4	62.1	1304.6	22.8	37%
MC-01	93	3.35008	0.05375	0.10510	0.00259	1683.9	27.0	1716.1	42.2	1683.9	27.0	2%
MC-01	94	3.77074	0.06533	0.11416	0.00287	1516.4	26.3	1866.7	47.0	1516.4	26.3	19%
MC-01	95	3.66703	0.06591	0.10662	0.00261	1554.5	27.9	1742.4	42.7	1554.5	27.9	11%
MC-02	1	3.48554	0.08561	0.10571	0.00188	1626.0	39.9	1726.7	30.7	1626.0	39.9	6%
MC-02	2	5.44662	0.14355	0.10737	0.00178	1086.6	28.6	1755.3	29.0	1086.6	28.6	38%
MC-02	3	3.37041	0.08611	0.10447	0.00193	1674.9	42.8	1705.0	31.5	1674.9	42.8	2%
MC-02	4	3.35008	0.08348	0.10526	0.00178	1683.9	42.0	1718.9	29.0	1683.9	42.0	2%
MC-02	5	3.57910	0.09123	0.10534	0.00179	1588.3	40.5	1720.3	29.2	1588.3	40.5	8%
MC-02	6	3.41414	0.08820	0.10808	0.00179	1656.0	42.8	1767.3	29.3	1656.0	42.8	6%
MC-02	7	13.29964	0.36238	0.10205	0.00175	467.3	12.7	1661.7	28.6	441.6	11.8	72%
MC-02	8	3.74532	0.09649	0.10690	0.00178	1525.6	39.3	1747.2	29.2	1525.6	39.3	13%
MC-02	9	4.95540	0.12253	0.14730	0.00322	1185.0	29.3	2314.8	50.7	1185.0	29.3	49%
MC-02	10	3.49284	0.08766	0.10789	0.00179	1623.0	40.7	1764.1	29.3	1623.0	40.7	8%
MC-02	11	3.51865	0.09082	0.10493	0.00186	1612.5	41.6	1713.1	30.4	1612.5	41.6	6%
MC-02	12	3.50385	0.08911	0.10462	0.00187	1618.5	41.2	1707.6	30.5	1618.5	41.2	5%
MC-02	13	5.88235	0.14536	0.07802	0.00135	1012.1	25.0	1147.4	19.9	1012.1	25.0	12%
MC-02	14	20.66970	0.50744	0.05368	0.00100	304.6	7.5	357.6	6.7	304.1	7.4	15%
MC-02	15	12.33350	0.31406	0.14967	0.00249	502.6	12.8	2342.2	38.9	446.6	11.3	79%
MC-02	16	3.64166	0.09134	0.10687	0.00180	1564.1	39.2	1746.7	29.4	1564.1	39.2	10%
MC-02	17	3.37041	0.08692	0.10780	0.00186	1674.9	43.2	1762.6	30.4	1674.9	43.2	5%
MC-02	18	66.97924	1.69525	0.04933	0.00109	95.5	2.4	163.5	3.6	95.4	2.4	42%
MC-02	19	4.22476	0.10749	0.09129	0.00156	1369.5	34.8	1452.7	24.9	1369.5	34.8	6%
MC-02	20	4.40917	0.11990	0.08850	0.00186	1317.7	35.8	1393.4	29.2	1317.7	35.8	5%
MC-02	21	8.17795	0.20033	0.10623	0.00172	743.7	18.2	1735.7	28.0	706.7	16.9	57%
MC-02	22	11.90051	0.31219	0.10114	0.00179	520.1	13.6	1645.1	29.2	493.0	12.7	68%

Table 7 continued

Sample	Analysis	238/206	Uncertainty (abs.)	207/206	Uncertainty (abs.)	206/238 Age (Ma)	Uncertainty (Ma)	207/206 Age (Ma)	Uncertainty (Ma)	Best Age (Ma)	Uncertainty (Ma)	Discordance (%)
MC-02	23	5.91716	0.15141	0.07715	0.00153	1006.6	25.8	1125.1	22.3	1006.6	25.8	11%
MC-02	24	28.71088	0.71690	0.05103	0.00100	220.7	5.5	242.2	4.8	220.6	5.5	9%
MC-02	25	7.03680	0.17405	0.09480	0.00154	856.6	21.2	1524.1	24.7	829.4	19.9	44%
MC-02	26	4.21230	0.10714	0.10896	0.00180	1373.2	34.9	1782.1	29.4	1373.2	34.9	23%
MC-02	27	3.85803	0.10154	0.10667	0.00184	1485.7	39.1	1743.3	30.1	1485.7	39.1	15%
MC-02	28	12.61034	0.31830	0.11578	0.00189	491.9	12.4	1892.1	30.8	457.1	11.4	74%
MC-02	29	4.85909	0.12672	0.11167	0.00190	1206.4	31.5	1826.8	31.1	1206.4	31.5	34%
MC-02	30	4.99501	0.13185	0.09085	0.00154	1176.4	31.1	1443.5	24.5	1176.4	31.1	19%
MC-02	31	5.11692	0.12530	0.10701	0.00174	1150.7	28.2	1749.1	28.4	1150.7	28.2	34%
MC-02	32	13.58696	0.35284	0.14912	0.00250	457.8	11.9	2335.9	39.1	406.3	10.5	80%
MC-02	33	5.06586	0.13197	0.10946	0.00180	1161.3	30.3	1790.4	29.5	1161.3	30.3	35%
MC-02	34	2.37473	0.06031	0.17925	0.00290	2265.5	57.5	2645.9	42.8	2265.5	57.5	14%
MC-02	35	3.75235	0.09619	0.10698	0.00176	1523.0	39.0	1748.6	28.8	1523.0	39.0	13%
MC-02	36	4.88043	0.14377	0.10928	0.00178	1201.6	35.4	1787.4	29.2	1201.6	35.4	33%
MC-02	37	4.38789	0.11087	0.09066	0.00164	1323.5	33.4	1439.5	26.0	1323.5	33.4	8%
MC-02	38	4.52694	0.11612	0.09155	0.00151	1286.6	33.0	1458.1	24.0	1286.6	33.0	12%
MC-02	39	4.71032	0.11917	0.10473	0.00191	1241.1	31.4	1709.6	31.2	1241.1	31.4	27%
MC-02	40	3.53607	0.09383	0.10398	0.00179	1605.4	42.6	1696.3	29.3	1605.4	42.6	5%
MC-02	41	3.78501	0.10049	0.10510	0.00182	1511.3	40.1	1716.1	29.7	1511.3	40.1	12%
MC-02	42	9.98702	0.25491	0.11042	0.00185	615.2	15.7	1806.3	30.3	578.4	14.5	66%
MC-02	43	4.45236	0.11864	0.08810	0.00173	1306.1	34.8	1384.7	27.2	1306.1	34.8	6%
MC-02	44	4.88759	0.12198	0.11291	0.00185	1200.0	29.9	1846.8	30.3	1200.0	29.9	35%
MC-02	45	3.89712	0.10611	0.10950	0.00180	1472.4	40.1	1791.1	29.5	1472.4	40.1	18%
MC-02	46	3.49773	0.08934	0.10673	0.00176	1621.0	41.4	1744.3	28.8	1621.0	41.4	7%
MC-02	47	4.89716	0.12521	0.11295	0.00185	1197.8	30.6	1847.4	30.2	1197.8	30.6	35%
MC-02	48	3.65097	0.09577	0.10158	0.00171	1560.6	40.9	1653.2	27.8	1560.6	40.9	6%
MC-02	49	3.79795	0.09605	0.10677	0.00176	1506.7	38.1	1745.0	28.8	1506.7	38.1	14%
MC-02	50	3.57271	0.09610	0.10808	0.00176	1590.9	42.8	1767.3	28.7	1590.9	42.8	10%
MC-02	51	3.80373	0.10236	0.10422	0.00177	1504.7	40.5	1700.6	28.9	1504.7	40.5	12%
MC-02	52	3.50877	0.09099	0.10801	0.00174	1616.5	41.9	1766.1	28.5	1616.5	41.9	8%
MC-02	53	7.99361	0.21739	0.09070	0.00151	759.9	20.7	1440.3	24.0	736.5	19.5	47%
MC-02	54	3.54736	0.09313	0.10232	0.00176	1600.9	42.0	1666.6	28.7	1600.9	42.0	4%

Table 7 continued

Sample	Analysis	238/206	Uncertainty (abs.)	207/206	Uncertainty (abs.)	206/238 Age (Ma)	Uncertainty (Ma)	207/206 Age (Ma)	Uncertainty (Ma)	Best Age (Ma)	Uncertainty (Ma)	Discordance (%)
MC-02	55	6.15385	0.16266	0.12698	0.00206	970.7	25.7	2056.6	33.3	908.3	23.3	53%
MC-02	56	3.63372	0.09634	0.10877	0.00178	1567.1	41.5	1778.9	29.1	1567.1	41.5	12%
MC-02	57	4.26439	0.10989	0.10854	0.00176	1358.0	35.0	1775.1	28.8	1358.0	35.0	23%
MC-02	58	3.22269	0.08300	0.11675	0.00191	1742.2	44.9	1907.1	31.2	1742.2	44.9	9%
MC-02	59	4.61894	0.11664	0.10838	0.00179	1263.4	31.9	1772.4	29.2	1263.4	31.9	29%
MC-02	60	4.20521	0.11321	0.08912	0.00158	1375.2	37.0	1406.7	24.9	1375.2	37.0	2%
MC-02	61	10.54741	0.26266	0.10537	0.00193	583.9	14.5	1720.8	31.5	551.9	13.5	66%
MC-02	62	40.53506	1.03222	0.11120	0.00349	157.1	4.0	1819.1	57.1	145.0	3.7	91%
MC-02	63	5.23560	0.14058	0.13100	0.00237	1126.8	30.3	2111.4	38.2	1126.8	30.3	47%
MC-02	64	4.22833	0.11316	0.10758	0.00184	1368.5	36.6	1758.8	30.0	1368.5	36.6	22%
MC-02	65	3.38066	0.09731	0.10530	0.00195	1670.4	48.1	1719.6	31.8	1670.4	48.1	3%
MC-02	66	4.38212	0.11642	0.08993	0.00156	1325.1	35.2	1424.0	24.7	1325.1	35.2	7%
MC-02	67	3.97141	0.11015	0.10555	0.00174	1447.8	40.2	1723.9	28.5	1447.8	40.2	16%
MC-02	68	3.75799	0.09738	0.10515	0.00183	1521.0	39.4	1716.9	29.8	1521.0	39.4	11%
MC-02	69	5.29661	0.13390	0.10712	0.00174	1114.9	28.2	1751.0	28.4	1114.9	28.2	36%
MC-02	70	4.87092	0.12366	0.10571	0.00175	1203.7	30.6	1726.7	28.6	1203.7	30.6	30%
MC-02	71	3.78645	0.09447	0.10664	0.00178	1510.8	37.7	1742.8	29.1	1510.8	37.7	13%
MC-02	72	3.56506	0.09127	0.10676	0.00182	1593.9	40.8	1744.8	29.8	1593.9	40.8	9%
MC-02	73	5.81734	0.15985	0.08000	0.00149	1022.6	28.1	1197.0	22.3	1022.6	28.1	15%
MC-02	74	5.38793	0.13740	0.10894	0.00179	1097.5	28.0	1781.8	29.3	1097.5	28.0	38%
MC-02	75	4.44444	0.11673	0.08900	0.00174	1308.2	34.4	1404.2	27.5	1308.2	34.4	7%
MC-02	76	3.77501	0.09587	0.10305	0.00169	1514.9	38.5	1679.8	27.5	1514.9	38.5	10%
MC-02	77	4.18936	0.10709	0.09128	0.00154	1379.9	35.3	1452.5	24.5	1379.9	35.3	5%
MC-02	78	3.67512	0.09307	0.10524	0.00173	1551.5	39.3	1718.5	28.3	1551.5	39.3	10%
MC-02	79	3.58423	0.08875	0.10756	0.00175	1586.3	39.3	1758.5	28.7	1586.3	39.3	10%
MC-02	80	6.03865	0.15491	0.08947	0.00151	987.8	25.3	1414.2	23.9	968.0	24.0	30%
MC-02	81	3.78645	0.09667	0.10825	0.00185	1510.8	38.6	1770.2	30.3	1510.8	38.6	15%
MC-02	82	3.66032	0.09402	0.10681	0.00176	1557.0	40.0	1745.7	28.7	1557.0	40.0	11%
MC-02	83	3.56379	0.08853	0.11133	0.00185	1594.4	39.6	1821.2	30.3	1594.4	39.6	12%
MC-02	84	3.66703	0.09572	0.10547	0.00189	1554.5	40.6	1722.5	30.9	1554.5	40.6	10%
MC-02	85	3.24465	0.08364	0.10413	0.00194	1731.8	44.6	1699.0	31.6	1731.8	44.6	-2%
MC-02	86	4.10172	0.10640	0.10784	0.00184	1406.4	36.5	1763.2	30.0	1406.4	36.5	20%

Table 7 continued

Sample	Analysis	238/206	Uncertainty (abs.)	207/206	Uncertainty (abs.)	206/238 Age (Ma)	Uncertainty (Ma)	207/206 Age (Ma)	Uncertainty (Ma)	Best Age (Ma)	Uncertainty (Ma)	Discordance (%)
MC-02	87	4.39947	0.11314	0.09113	0.00151	1320.3	34.0	1449.3	24.0	1320.3	34.0	9%
MC-02	88	12.42699	0.31620	0.11015	0.00181	498.9	12.7	1801.9	29.6	467.1	11.7	72%
MC-02	89	3.67647	0.09311	0.10705	0.00177	1550.9	39.3	1749.8	28.9	1550.9	39.3	11%
MC-02	90	3.59325	0.09121	0.10604	0.00174	1582.8	40.2	1732.4	28.4	1582.8	40.2	9%
MC-02	91	5.28541	0.14095	0.10691	0.00182	1117.0	29.8	1747.4	29.8	1117.0	29.8	36%
MC-02	92	3.29381	0.08227	0.10600	0.00179	1709.1	42.7	1731.7	29.2	1709.1	42.7	1%
MC-02	93	4.94805	0.13143	0.10621	0.00174	1186.6	31.5	1735.4	28.3	1186.6	31.5	32%
MC-02	94	3.32005	0.08267	0.10363	0.00175	1697.3	42.3	1690.1	28.5	1697.3	42.3	0%
MC-02	95	27.87068	0.71633	0.05100	0.00102	227.2	5.8	240.8	4.8	227.2	5.8	6%
MC-02	96	4.76644	0.12484	0.11563	0.00197	1227.8	32.2	1889.7	32.2	1227.8	32.2	35%
MC-02	97	3.59712	0.09051	0.10605	0.00178	1581.3	39.8	1732.6	29.1	1581.3	39.8	9%
MC-02	98	3.87447	0.09819	0.10817	0.00180	1480.1	37.5	1768.8	29.4	1480.1	37.5	16%
MC-02	99	5.81395	0.15973	0.12891	0.00212	1023.1	28.1	2083.2	34.3	1023.1	28.1	51%
MC-02	100	43.42162	1.15981	0.05090	0.00114	146.8	3.9	236.3	5.3	146.4	3.9	38%
MC-03	1	6.01395	0.22532	0.05801	0.00443	991.6	37.2	530.1	40.5	1007.8	36.8	-87%
MC-03	2	3.46260	0.13214	0.08540	0.00658	1635.5	62.4	1324.6	102.1	1635.5	62.4	-23%
MC-03	3	4.50451	0.17107	0.08951	0.00682	1292.4	49.1	1415.1	107.8	1292.4	49.1	9%
MC-03	4	4.03877	0.15261	0.08559	0.00651	1426.1	53.9	1328.9	101.1	1426.1	53.9	-7%
MC-03	5	3.57271	0.13629	0.08510	0.00651	1590.9	60.7	1317.8	100.8	1590.9	60.7	-21%
MC-03	6	5.26870	0.20195	0.09283	0.00707	1120.3	42.9	1484.4	113.0	1120.3	42.9	25%
MC-03	7	3.66973	0.14166	0.08923	0.00679	1553.5	60.0	1409.1	107.2	1553.5	60.0	-10%
MC-03	8	3.57398	0.13666	0.09012	0.00687	1590.4	60.8	1428.1	108.9	1590.4	60.8	-11%
MC-03	9	3.58938	0.13697	0.09449	0.00721	1584.3	60.5	1517.9	115.8	1584.3	60.5	-4%
MC-03	10	3.77216	0.15073	0.09581	0.00729	1515.9	60.6	1544.0	117.5	1515.9	60.6	2%
MC-03	11	6.48508	0.24610	0.21824	0.01660	924.5	35.1	2967.8	225.7	764.7	33.4	69%
MC-03	12	2.98063	0.12249	0.11920	0.00935	1865.0	76.6	1944.3	152.5	1865.0	76.6	4%
MC-03	13	2.55624	0.09716	0.14246	0.01084	2128.4	80.9	2257.3	171.8	2128.4	80.9	6%
MC-03	14	6.66667	0.25552	0.09867	0.00751	901.0	34.5	1599.1	121.8	870.0	33.2	44%
MC-03	15	4.91642	0.19863	0.07860	0.00618	1193.6	48.2	1162.1	91.4	1193.6	48.2	-3%
MC-03	16	9.65251	0.38351	0.11341	0.00863	635.5	25.2	1854.8	141.1	595.8	24.0	66%
MC-03	17	5.42005	0.22404	0.11066	0.00842	1091.5	45.1	1810.3	137.7	1091.5	45.1	40%
MC-03	18	10.89443	0.41181	0.16063	0.01221	566.1	21.4	2462.3	187.2	497.1	20.2	77%

Table 7 continued

Sample	Analysis	238/206	Uncertainty (abs.)	207/206	Uncertainty (abs.)	206/238 Age (Ma)	Uncertainty (Ma)	207/206 Age (Ma)	Uncertainty (Ma)	Best Age (Ma)	Uncertainty (Ma)	Discordance (%)
MC-03	19	3.67512	0.16409	0.10515	0.00802	1551.5	69.3	1716.9	130.9	1551.5	69.3	10%
MC-03	20	3.59842	0.13983	0.10541	0.00805	1580.8	61.4	1721.5	131.4	1580.8	61.4	8%
MC-03	21	5.95238	0.32382	0.08013	0.00610	1001.1	54.5	1200.2	91.3	1001.1	54.5	17%
MC-03	22	3.52113	0.14592	0.10663	0.00813	1611.5	66.8	1742.6	132.8	1611.5	66.8	8%
MC-03	23	3.66435	0.15636	0.10444	0.00797	1555.5	66.4	1704.5	130.1	1555.5	66.4	9%
MC-03	24	3.69276	0.14224	0.10742	0.00817	1544.9	59.5	1756.1	133.6	1544.9	59.5	12%
MC-03	25	3.82995	0.14638	0.08871	0.00677	1495.5	57.2	1397.9	106.6	1495.5	57.2	-7%
MC-03	26	3.43997	0.13123	0.10353	0.00790	1645.0	62.8	1688.3	128.8	1645.0	62.8	3%
MC-03	27	5.74383	0.21618	0.07885	0.00601	1034.7	38.9	1168.4	89.1	1034.7	38.9	11%
MC-03	28	19.78239	0.75567	0.08795	0.00670	317.9	12.1	1381.4	105.2	304.2	11.7	77%
MC-03	29	16.21008	0.62220	0.05518	0.00421	385.9	14.8	419.5	32.0	385.5	14.7	8%
MC-03	30	3.72301	0.14699	0.10596	0.00806	1533.7	60.6	1731.0	131.7	1533.7	60.6	11%
MC-03	31	4.43066	0.18011	0.08884	0.00676	1311.9	53.3	1400.7	106.6	1311.9	53.3	6%
MC-03	32	3.67918	0.16283	0.10288	0.00784	1549.9	68.6	1676.7	127.8	1549.9	68.6	8%
MC-03	33	3.59712	0.18562	0.10513	0.00800	1581.3	81.6	1716.6	130.6	1581.3	81.6	8%
MC-03	34	3.72301	0.16691	0.10516	0.00800	1533.7	68.8	1717.1	130.6	1533.7	68.8	11%
MC-03	35	3.30360	0.13093	0.09960	0.00765	1704.7	67.6	1616.6	124.2	1704.7	67.6	-5%
MC-03	36	27.10027	1.02213	0.05000	0.00383	233.6	8.8	195.0	15.0	233.8	8.8	-20%
MC-03	37	3.60750	0.14234	0.10532	0.00802	1577.2	62.2	1719.9	130.9	1577.2	62.2	8%
MC-03	38	12.61989	0.47969	0.05560	0.00431	491.6	18.7	436.4	33.8	492.4	18.5	-13%
MC-03	39	3.48189	0.13853	0.10571	0.00808	1627.5	64.8	1726.7	132.0	1627.5	64.8	6%
MC-03	40	3.52734	0.13839	0.10431	0.00798	1609.0	63.1	1702.2	130.2	1609.0	63.1	5%
MC-03	41	4.10004	0.15538	0.11683	0.00889	1406.9	53.3	1908.3	145.1	1406.9	53.3	26%
MC-03	42	7.41290	0.32287	0.11708	0.00891	815.8	35.5	1912.1	145.5	767.2	33.5	57%
MC-03	43	4.10341	0.16001	0.11218	0.00853	1405.9	54.8	1835.0	139.6	1405.9	54.8	23%
MC-03	44	4.39560	0.20548	0.11392	0.00866	1321.4	61.8	1862.9	141.7	1321.4	61.8	29%
MC-03	45	3.62582	0.15766	0.11325	0.00861	1570.2	68.3	1852.2	140.8	1570.2	68.3	15%
MC-03	46	3.67918	0.17737	0.11135	0.00848	1549.9	74.7	1821.6	138.7	1549.9	74.7	15%
MC-03	47	72.62164	4.03197	0.05114	0.00398	88.2	4.9	247.1	19.2	87.8	4.9	64%
MC-03	48	5.07614	0.42973	0.11054	0.00842	1159.2	98.1	1808.3	137.7	1159.2	98.1	36%
MC-03	49	3.63636	0.18139	0.11023	0.00839	1566.1	78.1	1803.2	137.3	1566.1	78.1	13%
MC-03	50	3.51000	0.14427	0.10800	0.00822	1616.0	66.4	1765.9	134.4	1616.0	66.4	8%

Table 7 continued

Sample	Analysis	238/206	Uncertainty (abs.)	207/206	Uncertainty (abs.)	206/238 Age (Ma)	Uncertainty (Ma)	207/206 Age (Ma)	Uncertainty (Ma)	Best Age (Ma)	Uncertainty (Ma)	Discordance (%)
MC-03	51	3.45901	0.13429	0.10110	0.00770	1637.0	63.6	1644.4	125.2	1637.0	63.6	0%
MC-03	52	4.77555	0.21936	0.10159	0.00774	1225.6	56.3	1653.4	125.9	1225.6	56.3	26%
MC-03	53	3.90778	0.15078	0.09470	0.00720	1468.8	56.7	1522.1	115.8	1468.8	56.7	4%
MC-03	54	3.46621	0.13497	0.08831	0.00674	1634.0	63.6	1389.2	106.0	1634.0	63.6	-18%
MC-03	55	3.71747	0.18360	0.08644	0.00658	1535.7	75.8	1348.0	102.7	1535.7	75.8	-14%
MC-03	56	3.42466	0.18938	0.08413	0.00641	1651.5	91.3	1295.6	98.8	1651.5	91.3	-27%
MC-03	57	3.80952	0.19717	0.08435	0.00641	1502.6	77.8	1300.6	98.9	1502.6	77.8	-16%
MC-03	58	5.37346	0.26948	0.08195	0.00624	1100.2	55.2	1244.3	94.8	1100.2	55.2	12%
MC-03	59	4.00481	0.15531	0.08143	0.00619	1436.9	55.7	1231.8	93.7	1436.9	55.7	-17%
MC-03	60	4.02253	0.19725	0.08198	0.00623	1431.3	70.2	1245.0	94.7	1431.3	70.2	-15%
MC-03	61	3.36700	0.13687	0.09547	0.00726	1676.4	68.1	1537.4	116.9	1676.4	68.1	-9%
MC-03	62	5.62746	0.28619	0.08789	0.00670	1054.4	53.6	1380.1	105.2	1054.4	53.6	24%
MC-03	63	3.93546	0.14991	0.08660	0.00658	1459.6	55.6	1351.6	102.8	1459.6	55.6	-8%
MC-03	64	6.49773	0.25774	0.08444	0.00642	922.8	36.6	1302.7	99.0	907.1	35.4	29%
MC-03	65	5.40541	0.20257	0.08834	0.00672	1094.2	41.0	1389.9	105.7	1094.2	41.0	21%
MC-03	66	3.87147	0.14605	0.09412	0.00716	1481.1	55.9	1510.5	114.9	1481.1	55.9	2%
MC-03	67	3.41181	0.13852	0.09847	0.00750	1657.0	67.3	1595.4	121.4	1657.0	67.3	-4%
MC-03	68	4.97512	0.18883	0.09988	0.00760	1180.7	44.8	1621.8	123.4	1180.7	44.8	27%
MC-03	69	28.74389	1.09792	0.04926	0.00379	220.5	8.4	160.2	12.3	220.8	8.4	-38%
MC-03	70	6.54879	0.25304	0.11425	0.00870	916.1	35.4	1868.1	142.2	868.5	33.7	51%
MC-03	71	3.52113	0.13483	0.10520	0.00807	1611.5	61.7	1717.8	131.8	1611.5	61.7	6%
MC-03	72	4.74834	0.17982	0.11412	0.00869	1232.0	46.7	1866.0	142.1	1232.0	46.7	34%
MC-03	73	22.42655	0.86419	0.15800	0.01213	281.2	10.8	2434.4	186.9	244.5	10.2	88%
MC-03	74	64.72492	2.49848	0.04470	0.00357	98.8	3.8	-72.0	-5.7	99.2	3.8	237%
MC-03	75	5.49451	0.21792	0.07467	0.00572	1077.9	42.8	1059.6	81.2	1077.9	42.8	-2%
MC-03	76	6.77048	0.26375	0.11498	0.00875	888.1	34.6	1879.6	143.1	840.1	32.9	53%
MC-03	77	3.80952	0.14630	0.09642	0.00739	1502.6	57.7	1556.0	119.2	1502.6	57.7	3%
MC-03	78	13.09072	0.49700	0.11689	0.00890	474.5	18.0	1909.2	145.4	440.0	17.1	75%
MC-03	79	5.59910	0.21835	0.10479	0.00801	1059.3	41.3	1710.6	130.7	1059.3	41.3	38%
MC-03	80	5.38503	0.20672	0.09615	0.00732	1098.0	42.2	1550.7	118.1	1098.0	42.2	29%
MC-03	81	4.69925	0.17700	0.09424	0.00718	1243.7	46.8	1512.9	115.2	1243.7	46.8	18%
MC-03	82	3.72995	0.14340	0.09232	0.00704	1531.2	58.9	1474.0	112.4	1531.2	58.9	-4%

Table 7 continued

Sample	Analysis	238/206	Uncertainty (abs.)	207/206	Uncertainty (abs.)	206/238 Age (Ma)	Uncertainty (Ma)	207/206 Age (Ma)	Uncertainty (Ma)	Best Age (Ma)	Uncertainty (Ma)	Discordance (%)
MC-03	83	5.88235	0.22375	0.09384	0.00714	1012.1	38.5	1504.9	114.5	1012.1	38.5	33%
MC-03	84	4.00641	0.15316	0.09575	0.00730	1436.4	54.9	1542.9	117.6	1436.4	54.9	7%
MC-03	85	3.54610	0.13761	0.09740	0.00747	1601.4	62.1	1574.9	120.8	1601.4	62.1	-2%
MC-03	86	3.69549	0.14093	0.09707	0.00739	1543.8	58.9	1568.6	119.5	1543.8	58.9	2%
MC-03	87	9.46611	0.35462	0.12251	0.00933	647.4	24.3	1993.1	151.7	600.2	23.1	68%
MC-03	88	3.37382	0.13249	0.10462	0.00798	1673.4	65.7	1707.6	130.2	1673.4	65.7	2%
MC-03	89	3.63636	0.13620	0.10995	0.00837	1566.1	58.7	1798.6	136.8	1566.1	58.7	13%
MC-03	90	5.71429	0.22907	0.07793	0.00598	1039.6	41.7	1145.1	87.9	1039.6	41.7	9%
MC-03	91	3.47947	0.13019	0.10896	0.00829	1628.5	60.9	1782.1	135.6	1628.5	60.9	9%
MC-03	92	3.11721	0.11680	0.11253	0.00858	1793.6	67.2	1840.7	140.3	1793.6	67.2	3%
MC-03	93	3.43761	0.12826	0.11034	0.00839	1646.0	61.4	1805.0	137.3	1646.0	61.4	9%
MC-03	94	3.43761	0.13113	0.10924	0.00833	1646.0	62.8	1786.8	136.2	1646.0	62.8	8%
MC-03	95	17.15266	0.77301	0.17790	0.01442	365.3	16.5	2633.4	213.4	309.9	15.2	86%
MC-03	96	4.42282	0.17385	0.11399	0.00869	1314.0	51.7	1864.0	142.1	1314.0	51.7	30%
MC-03	97	5.02993	0.18756	0.10874	0.00827	1168.9	43.6	1778.4	135.3	1168.9	43.6	34%
MC-03	98	3.53357	0.13909	0.10790	0.00827	1606.5	63.2	1764.3	135.3	1606.5	63.2	9%
MC-03	99	3.34225	0.13039	0.10382	0.00795	1687.3	65.8	1693.5	129.7	1687.3	65.8	0%
MC-03	100	3.47102	0.13113	0.10641	0.00810	1632.0	61.7	1738.8	132.4	1632.0	61.7	6%
MC-05	1	3.46741	0.13853	0.10419	0.00537	1633.5	65.3	1700.1	87.6	1633.5	65.3	4%
MC-05	2	3.49406	0.13784	0.10383	0.00533	1622.5	64.0	1693.7	86.9	1622.5	64.0	4%
MC-05	3	72.76961	2.88226	0.05315	0.00276	88.0	3.5	335.2	17.4	87.4	3.5	74%
MC-05	4	3.57654	0.14205	0.10904	0.00557	1589.3	63.1	1783.4	91.0	1589.3	63.1	11%
MC-05	5	3.02298	0.11992	0.10323	0.00532	1842.3	73.1	1683.0	86.7	1842.3	73.1	-9%
MC-05	6	17.68034	0.69588	0.17220	0.00886	354.7	14.0	2579.1	132.8	303.2	12.4	86%
MC-05	7	41.39073	1.64343	0.05960	0.00413	153.9	6.1	589.1	40.8	151.9	6.0	74%
MC-05	8	4.43262	0.17819	0.08927	0.00461	1311.4	52.7	1410.0	72.9	1311.4	52.7	7%
MC-05	9	63.65372	2.52966	0.04750	0.00275	100.5	4.0	74.4	4.3	100.6	4.0	-35%
MC-05	10	4.39560	0.17455	0.08975	0.00459	1321.4	52.5	1420.2	72.7	1321.4	52.5	7%
MC-05	11	6.43501	0.25854	0.10483	0.00536	931.2	37.4	1711.3	87.6	893.6	35.2	46%
MC-05	12	3.44590	0.14102	0.10151	0.00527	1642.5	67.2	1651.9	85.7	1642.5	67.2	1%
MC-05	13	3.59454	0.14255	0.10480	0.00536	1582.3	62.7	1710.8	87.5	1582.3	62.7	8%
MC-05	14	41.96391	1.68597	0.14480	0.00773	151.8	6.1	2285.4	122.1	133.7	5.5	93%

Table 7 continued

Sample	Analysis	238/206	Uncertainty (abs.)	207/206	Uncertainty (abs.)	206/238 Age (Ma)	Uncertainty (Ma)	207/206 Age (Ma)	Uncertainty (Ma)	Best Age (Ma)	Uncertainty (Ma)	Discordance (%)
MC-05	15	8.70322	0.35139	0.10647	0.00544	701.1	28.3	1739.8	88.9	664.9	26.5	60%
MC-05	16	4.26986	0.16820	0.10620	0.00543	1356.5	53.4	1735.2	88.7	1356.5	53.4	22%
MC-05	17	27.83190	1.09874	0.05087	0.00264	227.6	9.0	234.9	12.2	227.5	8.9	3%
MC-05	18	3.70508	0.14852	0.10460	0.00541	1540.3	61.7	1707.3	88.3	1540.3	61.7	10%
MC-05	19	3.66435	0.14452	0.10315	0.00530	1555.5	61.3	1681.6	86.4	1555.5	61.3	7%
MC-05	20	3.66973	0.14986	0.10500	0.00545	1553.5	63.4	1714.3	88.9	1553.5	63.4	9%
MC-05	21	4.50552	0.17656	0.09047	0.00462	1292.2	50.6	1435.5	73.3	1292.2	50.6	10%
MC-05	22	4.13223	0.16406	0.08758	0.00451	1397.1	55.5	1373.3	70.7	1397.1	55.5	-2%
MC-05	23	4.21230	0.16589	0.08894	0.00456	1373.2	54.1	1402.9	71.9	1373.2	54.1	2%
MC-05	24	3.58038	0.14133	0.10414	0.00533	1587.8	62.7	1699.2	87.0	1587.8	62.7	7%
MC-05	25	3.39789	0.13640	0.10566	0.00544	1663.0	66.8	1725.8	88.9	1663.0	66.8	4%
MC-05	26	3.30907	0.13240	0.10427	0.00540	1702.2	68.1	1701.5	88.1	1702.2	68.1	0%
MC-05	27	3.42818	0.13715	0.10192	0.00528	1650.0	66.0	1659.4	86.0	1650.0	66.0	1%
MC-05	28	8.62813	0.35951	0.11053	0.00566	706.9	29.5	1808.1	92.6	667.2	27.4	61%
MC-05	29	8.71840	0.35015	0.09940	0.00508	700.0	28.1	1612.9	82.5	669.7	26.5	57%
MC-05	30	8.62069	0.34981	0.10096	0.00518	707.5	28.7	1641.8	84.2	675.7	27.0	57%
MC-05	31	3.98406	0.15828	0.10540	0.00540	1443.6	57.4	1721.3	88.1	1443.6	57.4	16%
MC-05	32	3.46981	0.13890	0.10470	0.00537	1632.5	65.3	1709.1	87.6	1632.5	65.3	4%
MC-05	33	3.74392	0.14794	0.09792	0.00503	1526.1	60.3	1584.9	81.4	1526.1	60.3	4%
MC-05	34	4.21585	0.16629	0.09161	0.00468	1372.1	54.1	1459.3	74.6	1372.1	54.1	6%
MC-05	35	18.78287	0.76250	0.11644	0.00596	334.4	13.6	1902.3	97.3	308.5	12.6	82%
MC-05	36	3.47464	0.14058	0.10423	0.00538	1630.5	66.0	1700.8	87.7	1630.5	66.0	4%
MC-05	37	3.38066	0.13491	0.10254	0.00529	1670.4	66.7	1670.6	86.2	1670.4	66.7	0%
MC-05	38	3.46621	0.13930	0.10312	0.00532	1634.0	65.7	1681.0	86.7	1634.0	65.7	3%
MC-05	39	10.63490	0.41923	0.10750	0.00549	579.3	22.8	1757.5	89.8	546.0	21.3	67%
MC-05	40	3.35909	0.13313	0.10514	0.00540	1679.9	66.6	1716.8	88.2	1679.9	66.6	2%
MC-05	41	41.28819	1.64955	0.05140	0.00293	154.3	6.2	258.8	14.7	153.8	6.1	40%
MC-05	42	3.94945	0.15716	0.10480	0.00539	1455.0	57.9	1710.8	88.0	1455.0	57.9	15%
MC-05	43	4.34972	0.17423	0.09024	0.00468	1334.0	53.4	1430.6	74.2	1334.0	53.4	7%
MC-05	44	3.51989	0.13996	0.10610	0.00544	1612.0	64.1	1733.5	88.9	1612.0	64.1	7%
MC-05	45	4.39174	0.17370	0.09117	0.00469	1322.4	52.3	1450.2	74.6	1322.4	52.3	9%
MC-05	46	3.38868	0.13500	0.10593	0.00543	1667.0	66.4	1730.5	88.8	1667.0	66.4	4%

Table 7 continued

Sample	Analysis	238/206	Uncertainty (abs.)	207/206	Uncertainty (abs.)	206/238 Age (Ma)	Uncertainty (Ma)	207/206 Age (Ma)	Uncertainty (Ma)	Best Age (Ma)	Uncertainty (Ma)	Discordance (%)
MC-05	47	3.37496	0.14084	0.10390	0.00539	1672.9	69.8	1694.9	88.0	1672.9	69.8	1%
MC-05	48	3.64034	0.14443	0.10768	0.00551	1564.6	62.1	1760.5	90.0	1564.6	62.1	11%
MC-05	49	3.74392	0.14923	0.10812	0.00554	1526.1	60.8	1768.0	90.5	1526.1	60.8	14%
MC-05	50	3.69686	0.14917	0.10558	0.00546	1543.3	62.3	1724.4	89.2	1543.3	62.3	11%
MC-05	51	3.69959	0.14615	0.10973	0.00563	1542.3	60.9	1794.9	92.1	1542.3	60.9	14%
MC-05	52	3.76223	0.14869	0.10572	0.00541	1519.4	60.1	1726.9	88.4	1519.4	60.1	12%
MC-05	53	12.80410	0.51588	0.10223	0.00523	484.8	19.5	1665.0	85.2	458.2	18.3	71%
MC-05	54	9.98004	0.40435	0.08646	0.00442	615.6	24.9	1348.5	68.9	596.4	23.8	54%
MC-05	55	3.55619	0.14807	0.10250	0.00536	1597.4	66.5	1669.9	87.4	1597.4	66.5	4%
MC-05	56	4.22654	0.16700	0.09153	0.00468	1369.0	54.1	1457.7	74.5	1369.0	54.1	6%
MC-05	57	4.10172	0.16250	0.10672	0.00546	1406.4	55.7	1744.1	89.3	1406.4	55.7	19%
MC-05	58	6.89180	0.27381	0.10696	0.00547	873.4	34.7	1748.3	89.4	833.9	32.5	50%
MC-05	59	3.45423	0.13748	0.10644	0.00545	1639.0	65.2	1739.3	89.0	1639.0	65.2	6%
MC-05	60	4.20875	0.16870	0.09030	0.00463	1374.2	55.1	1431.9	73.4	1374.2	55.1	4%
MC-05	61	3.67512	0.14611	0.10648	0.00546	1551.5	61.7	1740.0	89.2	1551.5	61.7	11%
MC-05	62	4.93583	0.19690	0.09291	0.00479	1189.3	47.4	1486.1	76.6	1189.3	47.4	20%
MC-05	63	3.19489	0.12567	0.10664	0.00545	1755.5	69.0	1742.8	89.0	1755.5	69.0	-1%
MC-05	64	3.39789	0.13588	0.10269	0.00532	1663.0	66.5	1673.3	86.8	1663.0	66.5	1%
MC-05	65	3.48189	0.14123	0.10839	0.00556	1627.5	66.0	1772.5	90.9	1627.5	66.0	8%
MC-05	66	7.19425	0.29564	0.13384	0.00685	839.0	34.5	2149.0	110.0	773.4	31.5	61%
MC-05	67	3.28623	0.13144	0.10373	0.00532	1712.6	68.5	1691.9	86.7	1712.6	68.5	-1%
MC-05	68	3.35008	0.13550	0.10316	0.00533	1683.9	68.1	1681.7	86.8	1683.9	68.1	0%
MC-05	69	3.59066	0.14263	0.10315	0.00529	1583.8	62.9	1681.6	86.2	1583.8	62.9	6%
MC-05	70	4.48833	0.18107	0.09043	0.00465	1296.7	52.3	1434.6	73.8	1296.7	52.3	10%
MC-05	71	3.40948	0.13690	0.10365	0.00531	1658.0	66.6	1690.5	86.6	1658.0	66.6	2%
MC-05	72	4.50248	0.17977	0.10560	0.00541	1293.0	51.6	1724.8	88.3	1293.0	51.6	25%
MC-05	73	66.44518	2.63648	0.06660	0.00364	96.3	3.8	825.3	45.1	94.0	3.7	88%
MC-05	74	3.65097	0.14440	0.10294	0.00527	1560.6	61.7	1677.8	85.9	1560.6	61.7	7%
MC-05	75	5.68828	0.22522	0.07769	0.00403	1044.0	41.3	1139.0	59.0	1044.0	41.3	8%
MC-05	76	3.71747	0.15198	0.10178	0.00523	1535.7	62.8	1656.8	85.2	1535.7	62.8	7%
MC-05	77	3.63240	0.14545	0.10394	0.00531	1567.6	62.8	1695.6	86.6	1567.6	62.8	8%
MC-05	78	4.32339	0.17124	0.08643	0.00443	1341.3	53.1	1347.8	69.1	1341.3	53.1	0%

Table 7 continued

Sample	Analysis	238/206	Uncertainty (abs.)	207/206	Uncertainty (abs.)	206/238 Age (Ma)	Uncertainty (Ma)	207/206 Age (Ma)	Uncertainty (Ma)	Best Age (Ma)	Uncertainty (Ma)	Discordance (%)
MC-05	79	3.60881	0.14678	0.10680	0.00546	1576.7	64.1	1745.5	89.3	1576.7	64.1	10%
MC-05	80	3.57782	0.14406	0.10017	0.00512	1588.8	64.0	1627.2	83.1	1588.8	64.0	2%
MC-05	81	3.50631	0.14072	0.10071	0.00520	1617.5	64.9	1637.2	84.5	1617.5	64.9	1%
MC-05	82	4.14766	0.16613	0.10663	0.00544	1392.4	55.8	1742.6	88.9	1392.4	55.8	20%
MC-05	83	3.62713	0.14836	0.10002	0.00512	1569.7	64.2	1624.5	83.1	1569.7	64.2	3%
MC-05	84	3.52609	0.14072	0.09767	0.00499	1609.5	64.2	1580.1	80.8	1609.5	64.2	-2%
MC-05	85	45.68296	1.84516	0.04662	0.00243	139.6	5.6	29.8	1.6	140.0	5.6	-368%
MC-05	86	12.94331	0.51374	0.09063	0.00462	479.7	19.0	1438.8	73.4	460.1	18.1	67%
MC-05	87	7.02741	0.28523	0.10212	0.00522	857.7	34.8	1663.0	85.1	823.2	32.7	48%
MC-05	88	41.44219	1.68627	0.13220	0.00685	153.7	6.3	2127.4	110.2	137.8	5.7	93%
MC-05	89	4.50045	0.17926	0.09775	0.00500	1293.5	51.5	1581.6	80.9	1293.5	51.5	18%
MC-05	90	3.60881	0.14417	0.09637	0.00496	1576.7	63.0	1555.0	80.1	1576.7	63.0	-1%
MC-05	91	3.91696	0.15524	0.09880	0.00505	1465.8	58.1	1601.6	81.8	1465.8	58.1	8%
MC-05	92	5.65611	0.22719	0.09765	0.00500	1049.5	42.2	1579.7	80.9	1049.5	42.2	34%
MC-05	93	4.36300	0.17286	0.09591	0.00492	1330.3	52.7	1546.0	79.3	1330.3	52.7	14%
MC-07	1	3.24570	0.04814	0.10731	0.00210	1731.4	25.7	1754.2	34.3	1731.4	25.7	1%
MC-07	2	4.29738	0.07488	0.11546	0.00223	1348.6	23.5	1887.1	36.4	1348.6	23.5	29%
MC-07	3	3.32005	0.04898	0.10743	0.00217	1697.3	25.0	1756.3	35.4	1697.3	25.0	3%
MC-07	4	23.37541	0.37432	0.05542	0.00119	270.0	4.3	429.2	9.2	268.8	4.3	37%
MC-07	5	64.02049	1.01090	0.05009	0.00113	99.9	1.6	199.2	4.5	99.7	1.6	50%
MC-07	6	3.49284	0.05682	0.10868	0.00211	1623.0	26.4	1777.4	34.5	1623.0	26.4	9%
MC-07	7	6.18812	0.09460	0.07895	0.00158	965.7	14.8	1170.9	23.5	957.1	14.2	18%
MC-07	8	29.72652	0.50054	0.06224	0.00147	213.3	3.6	682.4	16.1	210.2	3.5	69%
MC-07	9	11.69044	0.18408	0.06087	0.00141	529.1	8.3	634.6	14.7	527.3	8.2	17%
MC-07	10	3.35233	0.05010	0.10598	0.00214	1682.9	25.2	1731.4	34.9	1682.9	25.2	3%
MC-07	11	6.07165	0.09048	0.07450	0.00151	982.8	14.6	1055.0	21.4	979.9	14.2	7%
MC-07	12	4.00160	0.07765	0.11260	0.00227	1438.0	27.9	1841.8	37.2	1438.0	27.9	22%
MC-07	13	3.41297	0.05372	0.10454	0.00220	1656.5	26.1	1706.2	35.9	1656.5	26.1	3%
MC-07	14	4.26258	0.06024	0.09320	0.00180	1358.6	19.2	1492.0	28.8	1358.6	19.2	9%
MC-07	15	3.54610	0.04981	0.10838	0.00219	1601.4	22.5	1772.4	35.9	1601.4	22.5	10%
MC-07	16	6.70241	0.11015	0.07330	0.00171	896.5	14.7	1022.3	23.9	891.9	14.3	12%
MC-07	17	4.64900	0.07188	0.09363	0.00202	1255.9	19.4	1500.7	32.3	1255.9	19.4	16%

Table 7 continued

Sample	Analysis	238/206	Uncertainty (abs.)	207/206	Uncertainty (abs.)	206/238 Age (Ma)	Uncertainty (Ma)	207/206 Age (Ma)	Uncertainty (Ma)	Best Age (Ma)	Uncertainty (Ma)	Discordance (%)
MC-07	18	17.24138	0.29018	0.05825	0.00127	363.5	6.1	539.2	11.7	361.5	6.0	33%
MC-07	19	6.07165	0.11584	0.10285	0.00197	982.8	18.8	1676.2	32.1	947.7	17.6	41%
MC-07	20	1.92419	0.03202	0.18910	0.00382	2697.9	44.9	2734.3	55.2	2697.9	44.9	1%
MC-07	21	6.16029	0.08830	0.07572	0.00150	969.7	13.9	1087.7	21.6	964.9	13.5	11%
MC-07	22	6.07533	0.09645	0.08218	0.00180	982.3	15.6	1249.8	27.4	970.6	15.0	21%
MC-07	23	3.47464	0.05366	0.10369	0.00210	1630.5	25.2	1691.2	34.3	1630.5	25.2	4%
MC-07	24	2.89771	0.04312	0.12833	0.00247	1911.2	28.4	2075.2	39.9	1911.2	28.4	8%
MC-07	25	3.73553	0.06887	0.10523	0.00209	1529.1	28.2	1718.3	34.1	1529.1	28.2	11%
MC-07	26	11.40641	0.18042	0.05927	0.00127	541.7	8.6	577.0	12.4	541.1	8.4	6%
MC-07	27	3.52858	0.06076	0.10420	0.00226	1608.5	27.7	1700.2	37.0	1608.5	27.7	5%
MC-07	28	29.68240	0.44001	0.05620	0.00168	213.6	3.2	460.3	13.8	212.1	3.1	54%
MC-07	29	10.12453	0.14088	0.06113	0.00124	607.2	8.4	643.8	13.1	606.5	8.3	6%
MC-07	30	3.69413	0.05891	0.11346	0.00220	1544.4	24.6	1855.6	36.0	1544.4	24.6	17%
MC-07	31	5.81058	0.08417	0.07513	0.00151	1023.7	14.8	1072.0	21.5	1023.7	14.8	5%
MC-07	32	4.35161	0.06915	0.08621	0.00175	1333.5	21.2	1342.9	27.2	1333.5	21.2	1%
MC-07	33	8.01282	0.12956	0.12311	0.00237	758.1	12.3	2001.8	38.6	705.8	11.3	62%
MC-07	34	3.92465	0.06486	0.09367	0.00193	1463.2	24.2	1501.5	30.9	1463.2	24.2	3%
MC-07	35	9.46970	0.15775	0.11860	0.00367	647.1	10.8	1935.2	59.9	603.0	10.2	67%
MC-07	36	4.45633	0.07024	0.09138	0.00179	1305.1	20.6	1454.5	28.5	1305.1	20.6	10%
MC-07	37	4.04695	0.06285	0.10549	0.00204	1423.5	22.1	1722.9	33.4	1423.5	22.1	17%
MC-07	38	10.84128	0.15707	0.06218	0.00126	568.8	8.2	680.3	13.8	566.6	8.0	16%
MC-07	39	5.84112	0.08627	0.07676	0.00163	1018.7	15.0	1115.0	23.6	1018.7	15.0	9%
MC-07	40	3.64166	0.05857	0.10519	0.00219	1564.1	25.2	1717.6	35.8	1564.1	25.2	9%
MC-07	41	3.33000	0.05814	0.10882	0.00227	1692.8	29.6	1779.8	37.1	1692.8	29.6	5%
MC-07	42	5.21105	0.09032	0.08450	0.00164	1131.7	19.6	1304.1	25.4	1131.7	19.6	13%
MC-07	43	10.05025	0.23217	0.12269	0.00240	611.5	14.1	1995.7	39.0	565.9	12.9	69%
MC-07	44	5.48246	0.08434	0.07655	0.00156	1080.1	16.6	1109.5	22.6	1080.1	16.6	3%
MC-07	45	24.25418	0.35305	0.06068	0.00138	260.5	3.8	627.9	14.2	257.5	3.7	59%
MC-07	46	4.72367	0.06994	0.08547	0.00173	1237.9	18.3	1326.2	26.9	1237.9	18.3	7%
MC-07	47	4.53515	0.07309	0.09426	0.00193	1284.5	20.7	1513.3	30.9	1284.5	20.7	15%
MC-07	48	14.60280	0.22093	0.05806	0.00132	427.0	6.5	532.0	12.1	425.6	6.3	20%
MC-07	49	3.43289	0.05413	0.10961	0.00216	1648.0	26.0	1792.9	35.4	1648.0	26.0	8%

Table 7 continued

Sample	Analysis	238/206	Uncertainty (abs.)	207/206	Uncertainty (abs.)	206/238 Age (Ma)	Uncertainty (Ma)	207/206 Age (Ma)	Uncertainty (Ma)	Best Age (Ma)	Uncertainty (Ma)	Discordance (%)
MC-07	50	4.50653	0.07493	0.09077	0.00183	1291.9	21.5	1441.8	29.1	1291.9	21.5	10%
MC-07	51	4.00962	0.07909	0.11380	0.00219	1435.4	28.3	1861.0	35.9	1435.4	28.3	23%
MC-07	52	15.48947	0.24341	0.06016	0.00140	403.3	6.3	609.3	14.1	400.7	6.2	34%
MC-07	53	6.77048	0.11169	0.10835	0.00208	888.1	14.6	1771.9	34.0	847.0	13.7	50%
MC-07	54	5.19481	0.13660	0.07660	0.00231	1134.9	29.8	1110.8	33.6	1134.9	29.8	-2%
MC-07	55	5.80383	0.08724	0.07541	0.00157	1024.8	15.4	1079.5	22.5	1024.8	15.4	5%
MC-07	56	3.57526	0.07596	0.10506	0.00213	1589.9	33.8	1715.4	34.8	1589.9	33.8	7%
MC-07	57	3.84912	0.06792	0.10399	0.00212	1488.8	26.3	1696.5	34.6	1488.8	26.3	12%
MC-07	58	3.58680	0.05814	0.10610	0.00213	1585.3	25.7	1733.5	34.8	1585.3	25.7	9%
MC-07	59	4.23012	0.07561	0.09190	0.00244	1368.0	24.5	1465.3	38.9	1368.0	24.5	7%
MC-07	60	3.52485	0.05336	0.10627	0.00214	1610.0	24.4	1736.4	35.0	1610.0	24.4	7%
MC-07	61	4.19815	0.05919	0.09441	0.00192	1377.3	19.4	1516.3	30.9	1377.3	19.4	9%
MC-07	62	4.23191	0.06664	0.11627	0.00235	1367.4	21.5	1899.6	38.4	1367.4	21.5	28%
MC-07	63	5.82751	0.08944	0.07519	0.00157	1020.9	15.7	1073.6	22.4	1020.9	15.7	5%
MC-07	64	5.87544	0.10068	0.07699	0.00168	1013.2	17.4	1120.9	24.5	1013.2	17.4	10%
MC-07	65	5.74713	0.09151	0.08690	0.00259	1034.1	16.5	1358.3	40.5	1034.1	16.5	24%
MC-07	66	3.40252	0.06239	0.10486	0.00215	1661.0	30.5	1711.9	35.0	1661.0	30.5	3%
MC-07	67	5.42005	0.08311	0.08064	0.00165	1091.5	16.7	1212.7	24.8	1091.5	16.7	10%
MC-07	68	6.43087	0.11473	0.07684	0.00153	931.7	16.6	1117.0	22.3	924.5	16.0	17%
MC-07	69	6.00601	0.09108	0.07992	0.00163	992.8	15.1	1195.0	24.3	984.0	14.5	17%
MC-07	70	3.70233	0.05608	0.10883	0.00210	1541.3	23.3	1779.9	34.4	1541.3	23.3	13%
MC-07	71	4.52284	0.07163	0.11621	0.00224	1287.7	20.4	1898.7	36.7	1287.7	20.4	32%
MC-07	72	3.37838	0.06014	0.10958	0.00217	1671.4	29.8	1792.4	35.4	1671.4	29.8	7%
MC-07	73	3.57015	0.06350	0.11289	0.00228	1591.9	28.3	1846.5	37.3	1591.9	28.3	14%
MC-07	74	16.39882	0.29163	0.05460	0.00208	381.6	6.8	395.9	15.1	381.4	6.7	4%
MC-07	75	4.27350	0.06856	0.09410	0.00192	1355.4	21.7	1510.1	30.8	1355.4	21.7	10%
MC-07	76	25.35497	0.43019	0.05308	0.00117	249.4	4.2	332.2	7.3	248.8	4.2	25%
MC-07	77	3.68324	0.06463	0.10970	0.00223	1548.4	27.2	1794.4	36.4	1548.4	27.2	14%
MC-07	78	16.60302	0.27877	0.05677	0.00120	377.0	6.3	482.6	10.2	375.8	6.2	22%
MC-07	79	5.27705	0.09198	0.10852	0.00209	1118.7	19.5	1774.7	34.1	1118.7	19.5	37%
MC-07	80	25.20797	0.38235	0.06336	0.00140	250.8	3.8	720.3	15.9	247.0	3.7	65%
MC-07	81	4.27533	0.10079	0.10778	0.00214	1354.9	31.9	1762.2	35.0	1354.9	31.9	23%

Table 7 continued

Sample	Analysis	238/206	Uncertainty (abs.)	207/206	Uncertainty (abs.)	206/238 Age (Ma)	Uncertainty (Ma)	207/206 Age (Ma)	Uncertainty (Ma)	Best Age (Ma)	Uncertainty (Ma)	Discordance (%)
MC-07	82	4.12371	0.06259	0.10963	0.00217	1399.7	21.2	1793.3	35.5	1399.7	21.2	22%
MC-07	83	4.46628	0.07400	0.09471	0.00193	1302.4	21.6	1522.3	31.0	1302.4	21.6	14%
MC-07	84	16.40151	0.25953	0.05721	0.00124	381.5	6.0	499.6	10.8	380.1	5.9	24%
MC-07	85	3.60490	0.05359	0.11359	0.00221	1578.3	23.5	1857.6	36.1	1578.3	23.5	15%
MC-07	86	6.08273	0.08893	0.07726	0.00154	981.2	14.3	1127.9	22.5	975.0	13.9	13%
MC-07	87	3.76081	0.06118	0.10786	0.00212	1520.0	24.7	1763.6	34.6	1520.0	24.7	14%
MC-07	88	7.48503	0.13616	0.11880	0.00486	808.4	14.7	1938.3	79.2	758.4	14.2	58%
MC-07	89	7.53580	0.11934	0.07556	0.00161	803.3	12.7	1083.4	23.0	794.2	12.3	26%
MC-07	90	3.84320	0.08081	0.09460	0.00222	1490.9	31.3	1520.1	35.6	1490.9	31.3	2%
MC-07	91	4.59137	0.06755	0.11088	0.00217	1270.2	18.7	1813.9	35.4	1270.2	18.7	30%
MC-07	92	9.77517	0.17771	0.13943	0.00276	627.9	11.4	2220.1	44.0	569.0	10.3	72%
MC-07	93	3.49040	0.05604	0.10906	0.00211	1624.0	26.1	1783.8	34.5	1624.0	26.1	9%
MC-07	94	3.67377	0.06175	0.10408	0.00205	1552.0	26.1	1698.1	33.5	1552.0	26.1	9%
MC-07	95	3.64697	0.05253	0.10801	0.00207	1562.1	22.5	1766.1	33.9	1562.1	22.5	12%
MC-07	96	21.19093	0.30666	0.08303	0.00163	297.2	4.3	1269.9	24.9	286.0	4.1	77%
MC-07	97	3.15557	0.04560	0.12833	0.00248	1774.6	25.6	2075.2	40.1	1774.6	25.6	14%
MC-07	98	3.70233	0.05989	0.09261	0.00194	1541.3	24.9	1479.9	31.0	1541.3	24.9	-4%
MC-07	99	13.96648	0.26649	0.12515	0.00245	445.8	8.5	2030.9	39.7	408.4	7.8	78%
MC-07	100	28.15315	0.41247	0.05319	0.00116	225.0	3.3	336.9	7.3	224.3	3.3	33%
RHC-01	1	3.50754	0.02953	0.10750	0.00337	1617.0	13.6	1757.5	55.1	1617.0	13.6	8%
RHC-01	2	4.58505	0.03784	0.09001	0.00281	1271.8	10.5	1425.7	44.5	1271.8	10.5	11%
RHC-01	3	3.76932	0.02699	0.10609	0.00332	1516.9	10.9	1733.3	54.3	1516.9	10.9	12%
RHC-01	4	4.68384	0.03510	0.09106	0.00285	1247.4	9.3	1447.9	45.3	1247.4	9.3	14%
RHC-01	5	3.78358	0.02290	0.11188	0.00347	1511.8	9.2	1830.2	56.8	1511.8	9.2	17%
RHC-01	6	10.18434	0.06846	0.11155	0.00356	603.8	4.1	1824.8	58.2	566.7	4.5	67%
RHC-01	7	4.59770	0.05285	0.08999	0.00285	1268.7	14.6	1425.3	45.1	1268.7	14.6	11%
RHC-01	8	3.74953	0.03234	0.10557	0.00329	1524.0	13.1	1724.3	53.8	1524.0	13.1	12%
RHC-01	9	4.54339	0.03509	0.09038	0.00284	1282.4	9.9	1433.6	45.0	1282.4	9.9	11%
RHC-01	10	4.60830	0.03823	0.09154	0.00286	1266.0	10.5	1457.9	45.6	1266.0	10.5	13%
RHC-01	11	7.23537	0.04188	0.12023	0.00373	834.5	4.8	1959.6	60.9	782.5	5.7	57%
RHC-01	12	4.33088	0.03376	0.08847	0.00281	1339.2	10.4	1392.7	44.2	1339.2	10.4	4%
RHC-01	13	2.09732	0.01232	0.19460	0.00613	2513.3	14.8	2781.4	87.6	2513.3	14.8	10%

Table 7 continued

Sample	Analysis	238/206	Uncertainty (abs.)	207/206	Uncertainty (abs.)	206/238 Age (Ma)	Uncertainty (Ma)	207/206 Age (Ma)	Uncertainty (Ma)	Best Age (Ma)	Uncertainty (Ma)	Discordance (%)
RHC-01	14	3.59712	0.02717	0.10615	0.00331	1581.3	11.9	1734.3	54.1	1581.3	11.9	9%
RHC-01	15	27.99552	0.26647	0.05040	0.00217	226.2	2.2	213.5	9.2	226.3	2.2	-6%
RHC-01	16	3.77501	0.02280	0.10605	0.00332	1514.9	9.1	1732.6	54.3	1514.9	9.1	13%
RHC-01	17	3.63372	0.02509	0.11133	0.00347	1567.1	10.8	1821.2	56.8	1567.1	10.8	14%
RHC-01	18	3.51865	0.01733	0.10821	0.00338	1612.5	7.9	1769.5	55.2	1612.5	7.9	9%
RHC-01	19	3.73134	0.02785	0.11029	0.00343	1530.6	11.4	1804.2	56.2	1530.6	11.4	15%
RHC-01	20	4.18410	0.02976	0.11399	0.00363	1381.5	9.8	1864.0	59.3	1381.5	9.8	26%
RHC-01	21	4.38020	0.03645	0.09013	0.00287	1325.6	11.0	1428.3	45.4	1325.6	11.0	7%
RHC-01	22	11.46526	0.06047	0.12691	0.00399	539.1	2.8	2055.6	64.6	494.6	3.7	74%
RHC-01	23	5.60853	0.10380	0.11389	0.00355	1057.7	19.6	1862.4	58.1	1057.7	19.6	43%
RHC-01	24	10.86957	0.06971	0.19090	0.00616	567.4	3.6	2749.9	88.7	477.6	5.3	79%
RHC-01	25	9.12326	0.05910	0.13839	0.00431	670.5	4.3	2207.2	68.8	609.6	5.2	70%
RHC-01	26	3.03767	0.02030	0.11735	0.00374	1834.5	12.3	1916.3	61.0	1834.5	12.3	4%
RHC-01	27	3.65764	0.02676	0.10884	0.00339	1558.0	11.4	1780.1	55.5	1558.0	11.4	12%
RHC-01	28	5.16529	0.05336	0.11121	0.00346	1140.8	11.8	1819.3	56.6	1140.8	11.8	37%
RHC-01	29	3.76081	0.02829	0.10878	0.00339	1520.0	11.4	1779.1	55.5	1520.0	11.4	15%
RHC-01	30	3.51370	0.02716	0.10426	0.00336	1614.5	12.5	1701.3	54.8	1614.5	12.5	5%
RHC-01	31	3.60881	0.02344	0.10775	0.00337	1576.7	10.2	1761.7	55.2	1576.7	10.2	10%
RHC-01	32	3.64166	0.02254	0.10732	0.00335	1564.1	9.7	1754.4	54.8	1564.1	9.7	11%
RHC-01	33	12.52505	0.08942	0.06080	0.00197	495.2	3.5	632.2	20.5	493.0	3.6	22%
RHC-01	34	28.54696	0.17114	0.05370	0.00211	222.0	1.3	358.5	14.1	221.1	1.4	38%
RHC-01	35	4.36872	0.02863	0.09005	0.00292	1328.7	8.7	1426.6	46.3	1328.7	8.7	7%
RHC-01	36	3.60881	0.02344	0.10755	0.00336	1576.7	10.2	1758.3	54.9	1576.7	10.2	10%
RHC-01	37	7.57002	0.08596	0.11435	0.00358	799.8	9.1	1869.7	58.5	754.3	9.0	57%
RHC-01	38	3.66703	0.02017	0.10710	0.00335	1554.5	8.6	1750.6	54.8	1554.5	8.6	11%
RHC-01	39	3.61533	0.02222	0.10900	0.00340	1574.2	9.7	1782.8	55.5	1574.2	9.7	12%
RHC-01	40	4.15282	0.03622	0.11242	0.00351	1390.9	12.1	1838.9	57.4	1390.9	12.1	24%
RHC-01	41	3.54108	0.03386	0.10310	0.00334	1603.4	15.3	1680.7	54.4	1603.4	15.3	5%
RHC-01	42	3.57143	0.03316	0.10571	0.00337	1591.4	14.8	1726.7	55.0	1591.4	14.8	8%
RHC-01	43	3.63769	0.02647	0.10834	0.00339	1565.6	11.4	1771.7	55.4	1565.6	11.4	12%
RHC-01	44	3.41647	0.01984	0.11010	0.00344	1655.0	9.6	1801.1	56.3	1655.0	9.6	8%
RHC-01	45	4.24448	0.03603	0.10735	0.00337	1363.8	11.6	1754.9	55.1	1363.8	11.6	22%

Table 7 continued

Sample	Analysis	238/206	Uncertainty (abs.)	207/206	Uncertainty (abs.)	206/238 Age (Ma)	Uncertainty (Ma)	207/206 Age (Ma)	Uncertainty (Ma)	Best Age (Ma)	Uncertainty (Ma)	Discordance (%)
RHC-01	46	3.45066	0.01905	0.11023	0.00345	1640.5	9.1	1803.2	56.5	1640.5	9.1	9%
RHC-01	47	4.78240	0.03202	0.10941	0.00341	1224.0	8.2	1789.6	55.8	1224.0	8.2	32%
RHC-01	48	4.40141	0.03100	0.09191	0.00290	1319.8	9.3	1465.5	46.3	1319.8	9.3	10%
RHC-01	49	3.68460	0.02308	0.10640	0.00335	1547.9	9.7	1738.6	54.8	1547.9	9.7	11%
RHC-01	50	3.67107	0.02291	0.10627	0.00334	1553.0	9.7	1736.4	54.5	1553.0	9.7	11%
RHC-01	51	4.59770	0.03171	0.09031	0.00285	1268.7	8.7	1432.1	45.2	1268.7	8.7	11%
RHC-01	52	3.63240	0.01979	0.10758	0.00337	1567.6	8.5	1758.8	55.1	1567.6	8.5	11%
RHC-01	53	4.56621	0.03753	0.09272	0.00292	1276.6	10.5	1482.2	46.6	1276.6	10.5	14%
RHC-01	54	53.21130	0.26616	0.06377	0.00203	120.0	0.6	734.0	23.3	117.7	0.7	84%
RHC-01	55	9.55110	0.10035	0.14652	0.00458	641.9	6.7	2305.7	72.0	576.6	6.9	72%
RHC-01	56	3.57654	0.01663	0.10709	0.00334	1589.3	7.4	1750.5	54.7	1589.3	7.4	9%
RHC-01	57	4.43656	0.04133	0.12030	0.00472	1310.3	12.2	1960.7	77.0	1310.3	12.2	33%
RHC-01	58	3.52113	0.02604	0.10493	0.00335	1611.5	11.9	1713.1	54.6	1611.5	11.9	6%
RHC-01	59	3.67107	0.01887	0.10906	0.00340	1553.0	8.0	1783.8	55.6	1553.0	8.0	13%
RHC-01	60	3.62845	0.01843	0.10849	0.00339	1569.2	8.0	1774.2	55.4	1569.2	8.0	12%
RHC-01	61	3.45901	0.02752	0.11143	0.00351	1637.0	13.0	1822.9	57.4	1637.0	13.0	10%
RHC-01	62	3.62188	0.02624	0.10579	0.00335	1571.7	11.4	1728.1	54.6	1571.7	11.4	9%
RHC-01	63	4.45038	0.05546	0.08990	0.00300	1306.7	16.3	1423.4	47.4	1306.7	16.3	8%
RHC-01	64	3.61011	0.02346	0.10749	0.00336	1576.2	10.2	1757.3	54.9	1576.2	10.2	10%
RHC-01	65	3.43171	0.02826	0.10481	0.00332	1648.5	13.6	1711.0	54.3	1648.5	13.6	4%
RHC-01	66	39.52569	0.37495	0.05020	0.00203	161.1	1.5	204.3	8.3	160.9	1.6	21%
RHC-01	67	3.92157	0.03537	0.10197	0.00323	1464.2	13.2	1660.3	52.6	1464.2	13.2	12%
RHC-01	68	3.70370	0.02743	0.10719	0.00336	1540.8	11.4	1752.2	54.9	1540.8	11.4	12%
RHC-01	69	3.76932	0.02699	0.10619	0.00334	1516.9	10.9	1735.0	54.6	1516.9	10.9	13%
RHC-01	70	4.47628	0.05610	0.09346	0.00293	1299.8	16.3	1497.2	47.0	1299.8	16.3	13%
RHC-01	71	3.74532	0.03367	0.10751	0.00338	1525.6	13.7	1757.6	55.3	1525.6	13.7	13%
RHC-01	72	4.64468	0.03236	0.09057	0.00283	1257.0	8.8	1437.6	45.0	1257.0	8.8	13%
RHC-01	73	3.67242	0.03237	0.10723	0.00338	1552.5	13.7	1752.9	55.3	1552.5	13.7	11%
RHC-01	74	4.46229	0.03385	0.09283	0.00293	1303.5	9.9	1484.4	46.8	1303.5	9.9	12%
RHC-01	75	3.67512	0.03242	0.11153	0.00347	1551.5	13.7	1824.5	56.8	1551.5	13.7	15%
RHC-01	76	5.95238	0.03897	0.10903	0.00340	1001.1	6.6	1783.3	55.5	1001.1	6.6	44%
RHC-01	77	3.97456	0.03633	0.10785	0.00336	1446.7	13.2	1763.4	55.0	1446.7	13.2	18%

Table 7 continued

Sample	Analysis	238/206	Uncertainty (abs.)	207/206	Uncertainty (abs.)	206/238 Age (Ma)	Uncertainty (Ma)	207/206 Age (Ma)	Uncertainty (Ma)	Best Age (Ma)	Uncertainty (Ma)	Discordance (%)
RHC-01	78	18.81468	0.17700	0.09914	0.00309	333.8	3.1	1608.0	50.2	315.0	3.2	79%
RHC-01	79	3.62976	0.04084	0.10777	0.00337	1568.7	17.7	1762.1	55.1	1568.7	17.7	11%
RHC-01	80	3.55872	0.03039	0.10679	0.00335	1596.4	13.6	1745.3	54.8	1596.4	13.6	9%
RHC-01	81	3.69549	0.02458	0.10585	0.00334	1543.8	10.3	1729.1	54.6	1543.8	10.3	11%
RHC-01	82	3.81534	0.02766	0.10966	0.00341	1500.6	10.9	1793.8	55.8	1500.6	10.9	16%
RHC-01	83	3.70096	0.01644	0.10916	0.00340	1541.8	6.8	1785.4	55.6	1541.8	6.8	14%
RHC-01	84	3.54359	0.04646	0.10924	0.00343	1602.4	21.0	1786.8	56.1	1602.4	21.0	10%
RHC-01	85	3.68053	0.02574	0.11411	0.00355	1549.4	10.8	1865.9	58.1	1549.4	10.8	17%
RHC-01	86	3.83730	0.03092	0.11202	0.00352	1492.9	12.0	1832.4	57.5	1492.9	12.0	19%
RHC-01	87	3.56252	0.02411	0.10865	0.00339	1594.9	10.8	1776.9	55.4	1594.9	10.8	10%
RHC-01	88	4.87092	0.05694	0.11157	0.00349	1203.7	14.1	1825.1	57.2	1203.7	14.1	34%
RHC-01	89	71.81844	0.45389	0.04974	0.00170	89.1	0.6	182.9	6.3	88.9	0.6	51%
RHC-01	90	4.54752	0.02895	0.09393	0.00293	1281.3	8.2	1506.7	47.0	1281.3	8.2	15%
RHC-01	91	5.16262	0.03998	0.08417	0.00269	1141.4	8.8	1296.5	41.5	1141.4	8.8	12%
RHC-01	92	13.16309	0.09183	0.12310	0.00431	472.0	3.3	2001.6	70.1	434.0	3.9	76%
RHC-01	93	76.16146	0.75407	0.05680	0.00190	84.1	0.8	483.8	16.2	83.1	0.8	83%
RHC-01	94	3.60750	0.03254	0.11178	0.00349	1577.2	14.2	1828.6	57.1	1577.2	14.2	14%
RHC-01	95	4.47427	0.03003	0.09290	0.00290	1300.3	8.7	1485.8	46.4	1300.3	8.7	12%
RHC-01	96	3.60101	0.03371	0.10599	0.00337	1579.8	14.8	1731.6	55.1	1579.8	14.8	9%
RHC-01	97	4.40917	0.04083	0.09055	0.00293	1317.7	12.2	1437.2	46.5	1317.7	12.2	8%
RHC-01	98	3.57526	0.03323	0.10663	0.00340	1589.9	14.8	1742.6	55.5	1589.9	14.8	9%
RHC-01	99	67.56757	0.68481	0.06250	0.00239	94.7	1.0	691.3	26.4	93.0	1.0	86%
RHC-01	100	4.56830	0.04174	0.09422	0.00298	1276.1	11.7	1512.5	47.9	1276.1	11.7	16%
RHC-02	1	3.57015	0.05307	0.10323	0.00189	1591.9	23.7	1683.0	30.9	1591.9	23.7	5%
RHC-02	2	3.38524	0.05169	0.10553	0.00193	1668.5	25.5	1723.6	31.6	1668.5	25.5	3%
RHC-02	3	3.60101	0.05858	0.10444	0.00194	1579.8	25.7	1704.5	31.7	1579.8	25.7	7%
RHC-02	4	72.24911	1.07725	0.05195	0.00124	88.6	1.3	283.2	6.8	88.1	1.3	69%
RHC-02	5	3.68868	0.05715	0.10430	0.00193	1546.4	24.0	1702.0	31.4	1546.4	24.0	9%
RHC-02	6	3.40484	0.05301	0.10365	0.00197	1660.0	25.8	1690.5	32.1	1660.0	25.8	2%
RHC-02	7	3.57015	0.05670	0.10853	0.00208	1591.9	25.3	1774.9	33.9	1591.9	25.3	10%
RHC-02	8	3.79075	0.07214	0.17100	0.00474	1509.3	28.7	2567.5	71.1	1509.3	28.7	41%
RHC-02	9	5.74713	0.09280	0.08330	0.00198	1034.1	16.7	1276.3	30.4	1034.1	16.7	19%

Table 7 continued

Sample	Analysis	238/206	Uncertainty (abs.)	207/206	Uncertainty (abs.)	206/238 Age (Ma)	Uncertainty (Ma)	207/206 Age (Ma)	Uncertainty (Ma)	Best Age (Ma)	Uncertainty (Ma)	Discordance (%)
RHC-02	10	3.91543	0.06778	0.10366	0.00190	1466.3	25.4	1690.7	31.0	1466.3	25.4	13%
RHC-02	11	3.74112	0.05939	0.10456	0.00191	1527.1	24.2	1706.6	31.1	1527.1	24.2	11%
RHC-02	12	3.53857	0.05668	0.10413	0.00191	1604.4	25.7	1699.0	31.1	1604.4	25.7	6%
RHC-02	13	3.71333	0.06559	0.10267	0.00194	1537.2	27.2	1672.9	31.6	1537.2	27.2	8%
RHC-02	14	4.39560	0.06802	0.08921	0.00166	1321.4	20.4	1408.7	26.2	1321.4	20.4	6%
RHC-02	15	74.53231	1.14994	0.04770	0.00148	85.9	1.3	84.4	2.6	85.9	1.3	-2%
RHC-02	16	4.56621	0.06865	0.09125	0.00166	1276.6	19.2	1451.8	26.4	1276.6	19.2	12%
RHC-02	17	3.52485	0.05898	0.10252	0.00191	1610.0	26.9	1670.2	31.2	1610.0	26.9	4%
RHC-02	18	4.14250	0.06345	0.10679	0.00194	1394.0	21.4	1745.3	31.6	1394.0	21.4	20%
RHC-02	19	3.71747	0.05829	0.10479	0.00191	1535.7	24.1	1710.6	31.2	1535.7	24.1	10%
RHC-02	20	3.72856	0.05850	0.10548	0.00192	1531.7	24.0	1722.7	31.3	1531.7	24.0	11%
RHC-02	21	4.92368	0.07794	0.10544	0.00193	1192.0	18.9	1722.0	31.6	1192.0	18.9	31%
RHC-02	22	4.62321	0.07131	0.10490	0.00191	1262.3	19.5	1712.6	31.2	1262.3	19.5	26%
RHC-02	23	3.48189	0.05391	0.10881	0.00199	1627.5	25.2	1779.6	32.5	1627.5	25.2	9%
RHC-02	24	4.53927	0.07464	0.10281	0.00188	1283.5	21.1	1675.5	30.6	1283.5	21.1	23%
RHC-02	25	3.46741	0.05222	0.10193	0.00197	1633.5	24.6	1659.6	32.0	1633.5	24.6	2%
RHC-02	26	3.49284	0.05312	0.10711	0.00199	1623.0	24.7	1750.8	32.5	1623.0	24.7	7%
RHC-02	27	3.55492	0.06107	0.09880	0.00204	1597.9	27.4	1601.6	33.1	1597.9	27.4	0%
RHC-02	28	3.62976	0.05608	0.10555	0.00192	1568.7	24.2	1723.9	31.3	1568.7	24.2	9%
RHC-02	29	4.47427	0.07129	0.08993	0.00164	1300.3	20.7	1424.0	26.0	1300.3	20.7	9%
RHC-02	30	4.82393	0.08764	0.11347	0.00216	1214.4	22.1	1855.7	35.3	1214.4	22.1	35%
RHC-02	31	4.62321	0.07223	0.09029	0.00165	1262.3	19.7	1431.7	26.2	1262.3	19.7	12%
RHC-02	32	15.37043	0.22656	0.12190	0.00223	406.3	6.0	1984.2	36.3	373.2	5.5	80%
RHC-02	33	3.48675	0.05750	0.10306	0.00201	1625.5	26.8	1679.9	32.7	1625.5	26.8	3%
RHC-02	34	3.68324	0.05407	0.10528	0.00191	1548.4	22.7	1719.2	31.1	1548.4	22.7	10%
RHC-02	35	4.18410	0.06350	0.10494	0.00190	1381.5	21.0	1713.3	31.0	1381.5	21.0	19%
RHC-02	36	3.39905	0.06171	0.10580	0.00231	1662.5	30.2	1728.3	37.7	1662.5	30.2	4%
RHC-02	37	3.25945	0.05506	0.11656	0.00215	1724.9	29.1	1904.1	35.1	1724.9	29.1	9%
RHC-02	38	5.79710	0.09063	0.07755	0.00144	1025.9	16.0	1135.4	21.1	1025.9	16.0	10%
RHC-02	39	4.07498	0.06519	0.10631	0.00195	1414.7	22.6	1737.1	31.8	1414.7	22.6	19%
RHC-02	40	4.63607	0.08030	0.08818	0.00177	1259.1	21.8	1386.4	27.8	1259.1	21.8	9%
RHC-02	41	5.55556	0.08615	0.11148	0.00203	1067.0	16.5	1823.7	33.3	1067.0	16.5	41%

Table 7 continued

Sample	Analysis	238/206	Uncertainty (abs.)	207/206	Uncertainty (abs.)	206/238 Age (Ma)	Uncertainty (Ma)	207/206 Age (Ma)	Uncertainty (Ma)	Best Age (Ma)	Uncertainty (Ma)	Discordance (%)
RHC-02	42	60.79027	0.95967	0.04799	0.00105	105.2	1.7	98.8	2.2	105.2	1.7	-6%
RHC-02	43	4.15973	0.06604	0.10816	0.00200	1388.8	22.0	1768.7	32.6	1388.8	22.0	21%
RHC-02	44	4.30663	0.06984	0.09161	0.00180	1346.0	21.8	1459.3	28.6	1346.0	21.8	8%
RHC-02	45	4.56204	0.07109	0.09110	0.00170	1277.6	19.9	1448.7	27.0	1277.6	19.9	12%
RHC-02	46	5.29661	0.08668	0.10486	0.00190	1114.9	18.2	1711.9	31.0	1114.9	18.2	35%
RHC-02	47	3.37382	0.05896	0.10315	0.00195	1673.4	29.2	1681.6	31.7	1673.4	29.2	0%
RHC-02	48	12.54233	0.19575	0.07327	0.00143	494.5	7.7	1021.4	19.9	484.9	7.4	52%
RHC-02	49	4.58085	0.07144	0.10604	0.00193	1272.9	19.9	1732.4	31.5	1272.9	19.9	27%
RHC-02	50	3.52983	0.05427	0.10244	0.00199	1608.0	24.7	1668.8	32.4	1608.0	24.7	4%
RHC-02	51	3.41997	0.05279	0.10531	0.00193	1653.5	25.5	1719.7	31.5	1653.5	25.5	4%
RHC-02	52	4.53515	0.07797	0.09113	0.00170	1284.5	22.1	1449.3	27.1	1284.5	22.1	11%
RHC-02	53	3.46861	0.07273	0.10130	0.00230	1633.0	34.2	1648.1	37.4	1633.0	34.2	1%
RHC-02	54	29.76190	0.45276	0.05015	0.00106	213.0	3.2	202.0	4.3	213.1	3.2	-5%
RHC-02	55	19.96805	0.29679	0.10449	0.00194	315.0	4.7	1705.4	31.6	295.0	4.4	82%
RHC-02	56	6.96573	0.10426	0.14308	0.00261	864.8	12.9	2264.8	41.3	788.8	11.8	62%
RHC-02	57	3.49162	0.05635	0.10433	0.00198	1623.5	26.2	1702.5	32.4	1623.5	26.2	5%
RHC-02	58	35.46099	0.57456	0.14063	0.00259	179.3	2.9	2235.0	41.1	159.0	2.6	92%
RHC-02	59	3.68460	0.05708	0.11217	0.00205	1547.9	24.0	1834.9	33.5	1547.9	24.0	16%
RHC-02	60	61.34969	1.02783	0.14970	0.00466	104.2	1.7	2342.5	72.9	91.0	1.6	96%
RHC-02	61	8.12348	0.15077	0.10263	0.00194	748.4	13.9	1672.2	31.5	714.5	13.0	55%
RHC-02	62	10.83893	0.17430	0.10554	0.00191	568.9	9.1	1723.7	31.2	537.2	8.5	67%
RHC-02	63	4.35730	0.07729	0.10609	0.00195	1331.9	23.6	1733.3	31.8	1331.9	23.6	23%
RHC-02	64	42.93688	0.69573	0.05049	0.00120	148.4	2.4	217.6	5.2	148.1	2.4	32%
RHC-02	65	3.91696	0.07259	0.10557	0.00201	1465.8	27.2	1724.3	32.9	1465.8	27.2	15%
RHC-02	66	11.17318	0.20013	0.10575	0.00196	552.6	9.9	1727.4	32.0	521.4	9.2	68%
RHC-02	67	44.03347	0.74966	0.04930	0.00141	144.8	2.5	162.1	4.6	144.7	2.5	11%
RHC-02	68	3.51741	0.05568	0.10300	0.00211	1613.0	25.5	1678.9	34.3	1613.0	25.5	4%
RHC-02	69	4.14766	0.07027	0.10338	0.00191	1392.4	23.6	1685.7	31.2	1392.4	23.6	17%
RHC-02	70	3.68189	0.05703	0.10594	0.00195	1548.9	24.0	1730.7	31.9	1548.9	24.0	11%
RHC-02	71	69.49270	1.10848	0.04702	0.00104	92.1	1.5	50.2	1.1	92.2	1.5	-83%
RHC-02	72	3.46981	0.05533	0.10597	0.00194	1632.5	26.0	1731.2	31.8	1632.5	26.0	6%
RHC-02	73	4.29369	0.06542	0.08971	0.00167	1349.7	20.6	1419.4	26.4	1349.7	20.6	5%

Table 7 continued

Sample	Analysis	238/206	Uncertainty (abs.)	207/206	Uncertainty (abs.)	206/238 Age (Ma)	Uncertainty (Ma)	207/206 Age (Ma)	Uncertainty (Ma)	Best Age (Ma)	Uncertainty (Ma)	Discordance (%)
RHC-02	73	4.29369	0.06542	0.08971	0.00167	1349.7	20.6	1419.4	26.4	1349.7	20.6	5%
RHC-02	74	14.33897	0.22554	0.09402	0.00170	434.6	6.8	1508.5	27.3	414.3	6.5	71%
RHC-02	75	3.53107	0.05379	0.10452	0.00201	1607.5	24.5	1705.9	32.8	1607.5	24.5	6%
RHC-02	76	3.50385	0.05380	0.10427	0.00192	1618.5	24.9	1701.5	31.4	1618.5	24.9	5%
RHC-02	77	3.47947	0.05336	0.10697	0.00198	1628.5	25.0	1748.4	32.3	1628.5	25.0	7%
RHC-02	78	3.37382	0.05635	0.10323	0.00204	1673.4	28.0	1683.0	33.2	1673.4	28.0	1%
RHC-02	79	4.26439	0.06898	0.10299	0.00208	1358.0	22.0	1678.7	34.0	1358.0	22.0	19%
RHC-02	80	4.67290	0.07866	0.09285	0.00170	1250.1	21.0	1484.8	27.2	1250.1	21.0	16%
RHC-02	81	69.54103	1.15891	0.06710	0.00152	92.0	1.5	840.9	19.1	89.8	1.5	89%
RHC-02	82	3.60881	0.05745	0.11002	0.00202	1576.7	25.1	1799.7	33.0	1576.7	25.1	12%
RHC-02	83	4.27899	0.06669	0.11691	0.00216	1353.9	21.1	1909.5	35.2	1353.9	21.1	29%
RHC-02	84	4.00962	0.06316	0.09486	0.00182	1435.4	22.6	1525.3	29.2	1435.4	22.6	6%
RHC-02	85	26.56748	0.44264	0.05018	0.00126	238.2	4.0	203.3	5.1	238.4	3.9	-17%
RHC-02	86	3.66703	0.05859	0.10796	0.00199	1554.5	24.8	1765.3	32.6	1554.5	24.8	12%
RHC-02	87	3.67918	0.06730	0.10728	0.00201	1549.9	28.4	1753.7	32.8	1549.9	28.4	12%
RHC-02	88	3.63769	0.05866	0.10750	0.00197	1565.6	25.2	1757.5	32.2	1565.6	25.2	11%
RHC-02	89	4.59770	0.07085	0.10877	0.00197	1268.7	19.5	1778.9	32.2	1268.7	19.5	29%
RHC-02	90	26.49709	0.40458	0.05177	0.00115	238.8	3.6	275.3	6.1	238.6	3.6	13%
RHC-02	91	70.92199	1.27810	0.04852	0.00116	90.3	1.6	124.7	3.0	90.2	1.6	28%
RHC-02	92	4.19112	0.06839	0.10732	0.00203	1379.4	22.5	1754.4	33.2	1379.4	22.5	21%
RHC-02	93	9.93443	0.15755	0.11091	0.00202	618.3	9.8	1814.4	33.0	581.1	9.1	66%
RHC-02	94	3.85654	0.06026	0.11529	0.00210	1486.3	23.2	1884.4	34.3	1486.3	23.2	21%
RHC-02	95	3.77216	0.06068	0.11139	0.00205	1515.9	24.4	1822.2	33.5	1515.9	24.4	17%
RHC-02	96	8.47458	0.18082	0.10885	0.00200	719.0	15.3	1780.3	32.7	680.4	14.2	60%
RHC-02	97	3.36927	0.06241	0.11522	0.00217	1675.4	31.0	1883.3	35.4	1675.4	31.0	11%
RHC-02	98	3.60231	0.06068	0.10604	0.00196	1579.3	26.6	1732.4	32.1	1579.3	26.6	9%
RHC-02	99	4.34594	0.07476	0.11121	0.00216	1335.0	23.0	1819.3	35.3	1335.0	23.0	27%
RHC-02	100	4.57876	0.07439	0.10713	0.00198	1273.4	20.7	1751.2	32.3	1273.4	20.7	27%

REFERENCES

Akyuz, I., Warny, S., Famubode, O., and Bhattacharya, J.P., 2016, Palynology of the Upper Cretaceous (Turonian) Ferron Sandstone Member, Utah, USA: Identification of marine flooding surfaces and Milankovitch cycles in subtropical, ever-wet, paralic to non-marine palaeoenvironments: Palynology, v. 40, p. 122–136, doi: 10.1080/01916122.2015.1014525.

Allen, J.R.L., 1978, Studies in fluviatile sedimentation: an exploratory quantitative model for the architecture of avulsion-controlled alluvial suites: Sedimentary Geology, v. 21, p. 129–147, doi: 10.1016/0037-0738(78)90002-7.

Allen, P.A., and Heller, P.L., 2012, Dispersal and preservation of tectonically generated alluvial gravels in sedimentary basins, *in* Busby, C.J. and Ingersoll, R. V. eds., Tectonics of Sedimentary Basins, John Wiley & Sons, Ltd, p. 111–130, doi: 10.1002/9781444347166.ch6.

Allen, J.L., and Johnson, C.L., 2011, Architecture and formation of transgressive-regressive cycles in marginal marine strata of the John Henry Member, Straight Cliffs Formation, Upper Cretaceous of southern Utah, USA: Sedimentology, v. 58, p. 1486–1513, doi: 10.1111/j.1365-3091.2010.01223.x.

Allen, J.L., and Johnson, C.L., 2010a, Facies control on sandstone composition (and influence of statistical methods on interpretations) in the John Henry Member, Straight Cliffs Formation, Southern Utah, USA: Sedimentary Geology, v. 230, p. 60–76, doi: 10.1016/j.sedgeo.2010.06.023.

Allen, J.L., and Johnson, C.L., 2010b, Sedimentary facies, paleoenvironments, and relative sea level changes in the John Henry Member, Cretaceous Straight Cliffs Formation, Southern Utah, USA: Utah Geological Association Publication 39, p. 225–247.

Amorosi, A., Pavesi, M., Ricci Lucchi, M., Sarti, G., and Piccin, A., 2008, Climatic signature of cyclic fluvial architecture from the Quaternary of the central Po Plain, Italy: Sedimentary Geology, v. 209, p. 58–68, doi: 10.1016/j.sedgeo.2008.06.010.

Anderson, P.B., and Ryer, T.A., 2004, Regional stratigraphy of the Ferron Sandstone, *in* Chidsey, T.C., Adams, R.D., and Morris, T.H. eds., Regional to Wellbore Analog for Fluvial-Deltaic Reservoir Modeling: Ferron Sandstone of Utah: AAPG Studies in Geology 50, p. 211–224.

Armitage, J.J., Burgess, P.M., Hampson, G.J., and Allen, P.A., 2016, Deciphering the origin of cyclical gravel front and shoreline progradation and retrogradation in the stratigraphic record: Basin Research, p. 1–21, doi: 10.1111/bre.12203.

Armstrong, R.L., 1968, Sevier orogenic belt in Nevada and Utah: Geological Society of America Bulletin, v. 79, p. 429–458, doi: 10.1130/0016-7606(1968)79[429:SOBINA]2.0.CO;2.

Barth, A.P., and Wooden, J.L., 2006, Timing of magmatism following initial convergence at a passive margin, southwestern U.S. Cordillera, and ages of lower crustal magma sources: The Journal of Geology, v. 114, p. 231–245, doi: 10.1086/499573.

Barth, A.P., Wooden, J.L., Jacobson, C.E., and Probst, K., 2004, U-Pb geochronology and geochemistry of the McCoy Mountains Formation, southeastern California: A Cretaceous retroarc foreland basin: Geological Society of America Bulletin, v. 116, p. 142–153, doi: 10.1130/B25288.1.

Bilodeau, W.L., 1986, The Mesozoic Mogollon Highlands, Arizona: An Early Cretaceous rift shoulder: The Journal of Geology, v. 94, p. 724–735, doi: 10.2307/30078336.

Bobb, M.C., 1991, The Calico bed, Upper Cretaceous, southern Utah: A fluvial sheet deposit in the Western Interior foreland basin and its relationship to eustasy and tectonics [M.S. thesis]: University of Colorado, 166 p.

Bohacs, K., and Suter, J., 1997, Sequence stratigraphic distribution of coaly rocks: Fundamental controls and paralic examples: American Association of Petroleum Geologists Bulletin, v. 81, p. 1612–1639, doi: 10.1306/7834E192-1721-11D7-8645000102C1865D.

Bourman, R.P., and Ollier, C.D., 2002, A critique of the Schellmann definition and classification of “laterite”: Catena, v. 47, p. 117–131, doi: 10.1016/S0341-8162(01)00178-3.

Bridge, J.S., and Leeder, M.R., 1979, A simulation model of alluvial stratigraphy: Sedimentology, v. 26, p. 617–644, doi: 10.1111/j.1365-3091.1979.tb00935.x.

Bridge, J.S., and Tye, R.S., 2000, Interpreting the dimensions of ancient fluvial channel bars, channels, and channel belts from wireline-logs and cores: American Association of Petroleum Geologists Bulletin, v. 84, p. 1205–1228, doi: 10.1306/E4FD4B07-1732-11D7-8645000102C1865D.

Bromley, R.G., Pemberton, S.G., and Rahmani, R.A., 1984, A Cretaceous woodground: The Teredolites ichnofacies: Journal of Paleontology, v. 58, p. 488–498, doi: 10.2307/1304797.

Brozovic, N., and Burbank, D.W., 2000, Dynamic fluvial systems and gravel progradation in the Himalayan foreland: Geological Society of America Bulletin, v. 112, p. 394–412, doi: 10.1130/0016-7606(2000)112<394:DFSAGP>2.0.CO;2.

Bryant, M., Falk, P., and Paola, C., 1995, Experimental study of avulsion frequency and rate of deposition: Geology, v. 23, p. 365–368, doi: 10.1130/0091-7613(1995)023<0365:ESOAFA>2.3.CO.

Burbank, D.W., 1992, Causes of recent Himalayan uplift deduced from deposited patterns in the Ganges basin: Nature, v. 357, p. 680–683, doi: 10.1038/357680a0.

Burbank, D.W., Beck, R.A., and Mulder, T., 1996, The Himalayan foreland basin, *in* Lin, A. and Harrison, T.M. eds., The Tectonic Evolution of Asia, Cambridge University Press, p. 149–188.

Burbank, D.W., Beck, R.A., Raynolds, R.G.H., Hobbs, R., and Tahirkheli, R.A.K., 1988, Thrusting and gravel progradation in foreland basins: A test of post-thrusting gravel dispersal: Geology, v. 16, p. 1143–1146, doi: 10.1130/0091-7613(1988)016<1143:TAGPIF>2.3.CO;2.

Catuneanu, O., 2004, Retroarc foreland systems—evolution through time: Journal of African Earth Sciences, v. 38, p. 225–242, doi: 10.1016/j.jafrearsci.2004.01.004.

Catuneanu, O., 2002, Sequence stratigraphy of clastic systems: Concepts, merits, and pitfalls: Journal of African Earth Sciences, v. 35, p. 1–43, doi: 10.1016/S0899-5362(02)00004-0.

Cecil, M.R., Rotberg, G., Ducea, M.N., Saleeby, J.B., and Gehrels, G.E., 2012, Magmatic growth and batholithic root development in the northern Sierra Nevada, California: Geosphere, v. 8, p. 592–606, doi: 10.1130/GES00729.1.

Chen, J.H., and Moore, J.G., 1982, Uranium-lead isotopic ages from the Sierra Nevada batholith, California: Journal of Geophysical Research, v. 87, p. 4761–4784, doi: 10.1029/JB087iB06p04761.

Chentnik, B.M., Johnson, C.L., Mulhern, J.S., and Stright, L., 2015, Valleys, estuaries, and lagoons: Paleoenvironments and regressive-transgressive architecture of the Upper Cretaceous Straight Cliffs Formation: Journal of Sedimentary Research, v. 85, p. 1166–1196, doi: 10.2110/jsr.2015.70.

Cleveland, D.M., Atchley, S.C., and Nordt, L.C., 2007, Continental sequence stratigraphy of the Upper Triassic (Norian-Rhaetian) Chinle strata, northern New Mexico, U.S.A.: Allocyclic and autocyclic origins of paleosol-nearing alluvial successions: Journal of Sedimentary Research, v. 77, p. 909–924, doi: 10.2110/jsr.2007.082.

Cobban, W.A., Merewether, E.A., Fouch, T.D., and Obradovich, J.D., 1994, Some Cretaceous shorelines in the western interior of the United States, *in* Cuputo, M. V, Peterson, J.A., and Franczyk, K.J. eds., Mesozoic Systems of the Rocky Mountain Region, U.S.A., Denver, Rocky Mountain Section SEPM, p. 393–414.

Coleman, D.S., Carl, B.S., Glazner, A.F., and Bartley, J.M., 2000, Cretaceous dikes within the Jurassic Independence dike swarm in eastern California: Geological Society of America Bulletin, v. 112, p. 504–511, doi: 10.1130/0016-7606(2000)112<504:CDWTJI>2.0.CO;2.

Colombera, L., Mountney, N.P., and McCaffrey, W.D., 2015, A meta-study of relationships between fluvial channel-body stacking pattern and aggradation rate: Implications for sequence stratigraphy: Geology, v. 43, p. 283–286, doi: 10.1130/G36385.1.

Corfu, F., Hanchar, J.M., Hoskin, P.W.O., and Kinny, P., 2003, Atlas of zircon textures: Reviews in Mineralogy and Geochemistry, v. 53, p. 469–500, doi: 10.2113/0530469.

Currie, B.S., 1997, Sequence stratigraphy of nonmarine Jurassic-Cretaceous rocks, central Cordilleran foreland-basin system: Geological Society of America Bulletin, v. 109, p. 1206–1222, doi: 10.1130/0016-7606(1997)109<1206.

Dalrymple, R.W., and Choi, K., 2007, Morphologic and facies trends through the fluvial–marine transition in tide-dominated depositional systems: A schematic framework for environmental and sequence-stratigraphic interpretation: Earth-Science Reviews, v. 81, p. 135–174, doi: 10.1016/j.earscirev.2006.10.002.

Davidson, S.K., Hartley, A.J., Weissmann, G.S., Nichols, G.J., and Scuderi, L.A., 2013, Geomorphic elements on modern distributive fluvial systems: Geomorphology, v. 180-181, p. 82–95, doi: 10.1016/j.geomorph.2012.09.008.

Davis, S.J., Dickinson, W.R., Gehrels, G.E., Spencer, J.E., Lawton, T.F., and Carroll, A.R., 2010, The Paleogene California River: Evidence of Mojave-Uinta paleodrainage from U-Pb ages of detrital zircons: Geology, v. 38, p. 931–934, doi: 10.1130/G31250.1.

DeCelles, P.G., 2004, Late Jurassic to Eocene evolution of the Cordilleran thrust belt and foreland basin system, western U.S.A.: American Journal of Science, v. 304, p. 105–168, doi: 10.2475/ajs.304.2.105.

DeCelles, P.G., and Cavazza, W., 1999, A comparison of fluvial megafans in the Cordilleran (Upper Cretaceous) and modern Himalayan foreland basin systems: Geological Society of America Bulletin, v. 111, p. 1315–1334, doi: 10.1130/0016-7606(1999)111<1315:ACOFMI>2.3.CO;2.

DeCelles, P.G., and Coogan, J.C., 2006, Regional structure and kinematic history of the Sevier fold-and-thrust belt, central Utah: Geological Society of America Bulletin, v. 118, p. 841–864, doi: 10.1130/B25759.1.

DeCelles, P.G., and Currie, B.S., 1996, Long-term sediment accumulation in the Middle Jurassic-early Eocene Cordilleran retroarc foreland-basin system: Geology, v. 24, p. 591–594, doi: 10.1130/0091-7613(1996)024<0591:LTSAIT>2.3.CO;2.

Decelles, P.G., and Giles, K.A., 1996, Foreland basin systems: Basin Research, v. 8, p. 105–123.

Dickinson, W.R., Beard, L.S., Brakenridge, G.R., Erjavec, J.L., Ferguson, R.C., Inman, K.F., Knepp, R.A., Lindberg, F.A., and Ryberg, P.T., 1983, Provenance of North American Phanerozoic sandstones in relation to tectonic setting: Geological Society of America Bulletin, p. 222–235, doi: 10.1130/0016-7606(1983)94<222.

Dickinson, W.R., and Gehrels, G.E., 2008a, Sediment delivery to the Cordilleran foreland basin: Insights from U-Pb ages of detrital zircons in Upper Jurassic and Cretaceous strata of the Colorado Plateau: American Journal of Science, v. 308, p. 1041–1082, doi: 10.2475/10.2008.01.

Dickinson, W.R., and Gehrels, G.E., 2008b, U-Pb ages of detrital zircons in relation to paleogeography: Triassic paleodrainage networks and sediment dispersal across southwest Laurentia: Journal of Sedimentary Research, v. 78, p. 745–764, doi: 10.2110/jsr.2008.088.

Dickinson, W.R., and Gehrels, G.E., 2009, Use of U–Pb ages of detrital zircons to infer maximum depositional ages of strata: A test against a Colorado Plateau Mesozoic database: Earth and Planetary Science Letters, v. 288, p. 115–125, doi: 10.1016/j.epsl.2009.09.013.

Dickinson, W.R., Lawton, T.F., Pecha, M., Davis, S.J., Gehrels, G.E., and Young, R.A., 2012, Provenance of the Paleogene Colton Formation (Uinta Basin) and Cretaceous–Paleogene provenance evolution in the Utah foreland: Evidence from U-Pb ages of detrital zircons, paleocurrent trends, and sandstone petrofacies: Geosphere, v. 8, p. 854, doi: 10.1130/GES00763.1.

Dickinson, W.R., and Suczek, C.A., 1979, Plate Tectonics and sandstone compositions: American Association of Petroleum Geologists Bulletin, v. 63, p. 2164–2182.

Dooling, P.R., 2013, Tidal Facies, stratigraphic architecture, and along-strike variability of a high energy, transgressive shoreline, Late Cretaceous, Kaiparowits Plateau, Southern Utah [M.S. thesis]: University of Utah, 142 p.

Eaton, J.G., 1991, Biostratigraphic framework for the Upper Cretaceous rocks of the Kaiparowits Plateau, southern Utah, *in* Nations, J.D. and Eaton, J.G. eds., Stratigraphy, Depositional Environments, and Sedimentary Tectonics of the Western Margin, Cretaceous Western Interior Seaway: Geological Society of America Special Paper 260, p. 47–63, doi: 10.1130/SPE260-p47.

Eaton, J.G., and Nations, J.D., 1991, Introduction: Tectonic setting along the margin of the Cretaceous Western Interior Seaway, southwestern Utah and northern Arizona, *in* Nations, J.D. and Eaton, J.G. eds., Stratigraphy, Depositional Environments, and Sedimentary Tectonics of the Western Margin, Cretaceous Western Interior Seaway: Geological Society of America Special Paper 260, p. 1–8, doi: 10.1130/SPE260-p1.

Eisele, J., and Isachsen, C.E., 2001, Crustal growth in southern Arizona: U-Pb geochronologic and Sm-Nd isotopic evidence for addition of the Paleoproterozoic Cochise block to the Mazatzal province: American Journal of Science, v. 301, p. 773–797, doi: 10.2475/ajs.301.9.773.

Elston, D.P., and Young, R. a., 1991, Cretaceous-Eocene (Laramide) landscape development and Oligocene-Pliocene drainage reorganization of Transition Zone and Colorado Plateau, Arizona: Journal of Geophysical Research, v. 96, p. 12,389–12,406, doi: 10.1029/90JB01978.

Ethridge, F.G., Wood, L.J., and Schumm, S.A., 1998, Cyclic variables controlling fluvial sequence development problems and perspectives, *in* Shanley, K.W. and McCabe, P.J. eds., Relative Role of Eustasy, Climate, and Tectonism in Continental Rocks: Society for Sedimentary Geology Special Publication 59, p. 17–29.

Famubode, O.A., and Bhattacharya, J.P., 2016, Sequence stratigraphic analysis of the youngest nonmarine sequence in the Cretaceous Ferron Notom Delta, south central Utah, U.S.A.: Journal of Sedimentary Research, v. 86, p. 168–198, doi: 10.2110/jsr.2016.8.

Fanti, F., and Catuneanu, O., 2010, Fluvial sequence stratigraphy: The Wapiti Formation, west-central Alberta, Canada: Journal of Sedimentary Research, v. 80, p. 320–338, doi: 10.2110/jsr.2010.033.

Fielding, C.R., 2015, Anatomy of falling-stage deltas in the Turonian Ferron Sandstone of the western Henry Mountains Syncline, Utah: Growth faults, slope failures and mass transport complexes: Sedimentology, v. 62, p. 1–26, doi: 10.1111/sed.12136.

Fielding, C.R., 2011, Foreland basin structural growth recorded in the Turonian Ferron Sandstone of the Western Interior Seaway Basin, USA: Geology, v. 39, p. 1107–1110, doi: 10.1130/G32411.1.

Fielding, C.R., 2010, Planform and facies variability in asymmetric deltas: facies analysis and depositional architecture of the Turonian Ferron Sandstone in the western Henry Mountains, south-central Utah, U.S.A.: Journal of Sedimentary Research, v. 80, p. 455–479, doi: 10.2110/jsr.2010.047.

Fillmore, R.P., 1991, Tectonic influence on sedimentation in the southern Sevier foreland, Iron Springs Formation (Upper Cretaceous), southwestern Utah, *in* Nations, J.D. and Eaton, J.G. eds., Stratigraphy, Depositional Environments, and Sedimentary Tectonics of the Western Margin, Cretaceous Western Interior Seaway: Geological Society of America Special Paper 260, p. 9–26.

Fleck, R.J., and Carr, M.D., 1990, The age of the Keystone Thrust: laser-fusion 40Ar/39Ar dating of foreland basin deposits, southern Spring Mountains, Nevada: Tectonics, v. 9, p. 467–476, doi: 10.1029/TC009i003p00467.

Franczyk, K.J., 1988, Stratigraphic revision and depositional environments of the Upper Cretaceous Toreva Formation in the northern Black Mesa area, Navajo and Apache counties, Arizona:, doi: 10.1017/CBO9781107415324.004.

Friend, P.F., Slater, M.J., and Williams, R.C., 1979, Vertical and lateral building of river sandstone bodies, Ebro Basin, Spain: Journal of the Geological Society, v. 136, p. 39–46, doi: 10.1144/gsjgs.136.1.0039.

Fürsich, F.T., 1975, Trace fossils as environmental indicators in the Corallian of England and Normandy: Lethaia, v. 8, p. 151–172, doi: 10.1111/j.1502-3931.1975.tb01309.x.

Gallin, W.N., Johnson, C.L., and Allen, J.L., 2010, Fluvial and Marginal Marine Architecture of the John Henry Member, Straight Cliffs Formation, Kelly Grade of the Kaiparowits Plateau, South-Central Utah, *in* Carney, S.M., Tabet, D.E., and Johnson, C.L. eds., Geology of South-Central Utah: Utah Geological Society Publication 39, p. 248–275.

Garcia-Castellanos, D., 2002, Interplay between lithospheric flexure and river transport in foreland basins: Basin Research, v. 14, p. 89–104, doi: 10.1046/j.1365-2117.2002.00174.x.

Gardner, M.H., 1995, Tectonic and eustatic controls on the stratal architecture of mid-Cretaceous stratigraphic sequences, central western interior foreland basin of North America, *in* Dorobek, S.L. and Ross, G.M. eds., Stratigraphic Evolution of Foreland Basins: Society for Sedimentary Geology Special Publication 52, p. 243–281, doi: 10.2110/pec.95.52.0243.

Gardner, M.H., and Cross, T.A., 1994, Middle Cretaceous paleogeography of Utah, *in* Caputo, M.V., Peterson, J.A., and Francyzk, K.J. eds., Mesozoic Systems of the Rocky Mountain Region, USA, Rocky Mountain Section SEPM, p. 471–502.

Gingras, M.K., and MacEachern, J.A., 2012, Tidal ichnology of shallow-water clastic settings, *in* Davis, R.A. and Dalrymple, R.W. eds., Principles of Tidal Sedimentology, Dordrecht, Springer Netherlands, p. 335–369, doi: 10.1007/978-94-007-0123-6.

Goldstrand, P.M., 1994, Tectonic development of Upper Cretaceous to Eocene strata of southwestern Utah: Geological Society of America Bulletin, v. 106, p. 145–154, doi: 10.1130/0016-7606(1994)106<0145.

Gooley, J.T., Johnson, C.L., and Pettinga, L., 2016, Spatial and temporal variation of fluvial architecture within a prograding clastic wedge of the Late Cretaceous Western Interior Basin (Kaiparowits Plateau), U.S.A.: Journal of Sedimentary Research, p. 125–147, doi: 10.2110/jsr.2016.11.

Hajek, E.A., Heller, P.L., and Sheets, B.A., 2010, Significance of channel-belt clustering in alluvial basins: Geology, v. 38, p. 535–538, doi: 10.1130/G30783.1.

Hajek, E.A., and Wolinsky, M.A., 2012, Simplified process modeling of river avulsion and alluvial architecture: Connecting models and field data: Sedimentary Geology, v. 257-260, p. 1–30, doi: 10.1016/j.sedgeo.2011.09.005.

Haq, B.U., Hardenbol, J., and Vail, P.R., 1987, Chronology of fluctuating sea levels since the Triassic: Science, v. 235, p. 1156–1167, doi: 10.1126/science.235.4793.1156.

Hartley, A.J., Owen, A., Swan, A., Weissmann, G.S., Holzweber, B.I., Howell, J.A., Nichols, G.J., and Scuderi, L.A., 2015, Recognition and importance of amalgamated sandy meander belts in the continental rock record: Geology, v. 43, p. 679–682, doi: 10.1130/G36743.1.

Hartley, A.J., Weissmann, G.S., Bhattacharyya, P., Nichols, G.J., Scuderi, L.A., Davidson, S.K., Leleu, S., Chackraborty, T., and Ghosh, P., 2013, Soil development on modern distributive fluvial systems: Preliminary observations with implications for interpretation of paleosols in the rock record, *in* Driese, S.G., Nordt, L.C., and McCarthy, P.J. eds., New Frontiers in Paleopedology and Terrestrial Paleoclimatology: Society for Sedimentary Geology Special Publication 104, p. 149–158, doi: 10.2110/sepmsp.104.10.

Hartley, A.J., Weissmann, G.S., Nichols, G.J., and Scuderi, L.A., 2010, Fluvial form in modern continental sedimentary basins: Distributive fluvial systems: Geology, v. 38, p. 39–42, doi: 10.1130/G31588Y.1.

Heller, P.L., Angevine, C.L., Winslow, N.S., and Paola, C., 1988, Two-phase stratigraphic model of foreland-basin sequences: Geology, v. 16, p. 501–504.

Hettinger, R.D., McCabe, P.J., and Shanley, K.W., 1993, Detailed facies anatomy of transgressive and highstand systems tracts from the Upper Cretaceous of southern Utah, U.S.A., *in* Weimer, P. and Posamentier, H.W. eds., Siliciclastic Sequence Stratigraphy: American Association of Petroleum Geologists, Memoir 58, p. 235–257.

Hettinger, R.D., Roberts, L.N.R., Biewick, L.R.H., and Kirschbaum, M.A., 2009, Geologic overview and resource assessment of coal in the Kaiparowits Plateau, southern Utah, *in* Kirschbaum, M.A., Roberts, L.N.R., and Biewick, L.R.H. eds., Geologic Assessment of Coal in the Colorado Plateau: Arizona, Colorado, New Mexico, and Utah: U.S. Geological Survey Professional Paper 1625-B, p. 73.

Hettinger, R.D., Roberts, L.N.R., Biewick, L.R.H., and Kirschbaum, M.A., 1996, Preliminary investigations of the distribution and resources of coal in the Kaiparowits Plateau, southern Utah: U.S. Geological Survey, Open-File Report 96-539, p. 49.

Heumann, M.J., Johnson, C.L., Webb, L.E., Taylor, J.P., Jalbaa, U., and Minjin, C., 2012, Paleogeographic reconstruction of a late paleozoic arc collision zone, Southern Mongolia: Geological Society of America Bulletin, v. 124, p. 1514–1534, doi: 10.1130/B30510.1.

Horton, B.K., Constenius, K.N., and DeCelles, P.G., 2004, Tectonic control on coarse-grained foreland-basin sequences: An example from the Cordilleran foreland basin, Utah: Geology, v. 32, p. 637–640, doi: 10.1130/G20407.1.

Ingersoll, R. V., Bullard, T.F., Ford, R.L., Grimm, J.P., Pickle, J.D., and Sares, S.W., 1984, The effect of grain size on detrital modes: A test of the Gazzi-Dickinson point-counting method: Journal of Sedimentary Research, v. 54, p. 103–116, doi: 10.1306/212F83B9-2B24-11D7-8648000102C1865D.

Jackson, R.G., 1976, Depositional model of point bars in the Lower Wabash River: Journal of Sedimentary Research, v. 46, p. 579–594.

Jones, H.L., and Hajek, E.A., 2007, Characterizing avulsion stratigraphy in ancient alluvial deposits: Sedimentary Geology, v. 202, p. 124–137, doi: 10.1016/j.sedgeo.2007.02.003.

Jordan, T.E., 1995, Retroarc foreland and related basins, *in* Busby, C.J. and Ingersoll, R. V. eds., Tectonics of Sedimentary Basins, Cambridge, MA, Blackwell Science, p. 331–362.

Knapp, J.H., and Heizler, M.T., 1990, Thermal history of crystalline nappes of the Maria fold and thrust belt, west central Arizona: Journal of Geophysical Research, v. 95, p. 20049–20073.

Kominz, M.A., Browning, J. V., Miller, K.G., Sugarman, P.J., Mizintseva, S.F., and Scotese, C.R., 2008, Late Cretaceous to Miocene sea-level estimates from the New Jersey and Delaware coastal plain coreholes: An error analysis: Basin Research, v. 20, p. 211–226, doi: 10.1111/j.1365-2117.2008.00354.x.

Kraus, M.J., 1999, Paleosols in clastic sedimentary rocks: Their geologic applications: Earth-Science Reviews, v. 47, p. 41–70, doi: 10.1016/S0012-8252(99)00026-4.

Kraus, M.J., and Hasiotis, S.T., 2006, Significance of different modes of rhizolith preservation to interpreting paleoenvironmental and paleohydrologic settings: Examples from Paleogene paleosols, Bighorn Basin, Wyoming, USA: Journal of Sedimentary Research, v. 76, p. 633–646, doi: 10.2110/jsr.2006.052.

Kraus, M.J., and Wells, T.M., 1999, Recognizing avulsion deposits in the ancient stratigraphical record, *in* Smith, N.D. and Rogers, J. eds., Fluvial Sedimentology VI: International Association of Sedimentologists Special Publication 28, Oxford, UK, Blackwell Publishing Ltd., p. 251–268, doi: 10.1002/9781444304213.ch19.

Kreisa, R.D., and Moiola, R.J., 1986, Sigmoidal tidal bundles and other tide-generated sedimentary structures of the Curtis Formation, Utah: Geological Society of America Bulletin, v. 97, p. 381–387, doi: 10.1130/0016-7606(1986)97<381:STBAOT>2.0.CO;2.

Laskowski, A.K., DeCelles, P.G., and Gehrels, G.E., 2013, Detrital zircon geochronology of Cordilleran retroarc foreland basin strata, western North America: Tectonics, v. 32, p. 1027–1048, doi: 10.1002/tect.20065.

Lawton, T.F., and Bradford, B.A., 2011, Correlation and provenance of Upper Cretaceous (Campanian) fluvial strata, Utah, U.S.A., from zircon U-Pb geochronology and petrography: Journal of Sedimentary Research, v. 81, p. 495–512, doi: 10.2110/jsr.2011.45.

Lawton, T.F., Hunt, G.J., and Gehrels, G.E., 2010, Detrital zircon record of thrust belt unroofing in Lower Cretaceous synorogenic conglomerates, central Utah: Geology, v. 38, p. 463–466, doi: 10.1130/G30684.1.

Lawton, T.F., Pollock, S.L., and Robinson, R.A.J., 2003, Integrating sandstone petrology and nonmarine sequence stratigraphy: Application to the Late Cretaceous fluvial systems of southwestern Utah, U.S.A.: Journal of Sedimentary Research, v. 73, p. 389–406, doi: 10.1306/100702730389.

Lawton, T.F., Schellenbach, W.L., and Nugent, A.E., 2014, Megafan and axial-river systems in the southern Cordilleran foreland basin: Drip Tank Member of Straight Cliffs Formation and adjacent strata, southern Utah, USA: Journal of Sedimentary Research, v. 84, p. 407–434, doi: 10.2110/jsr.2014.33.

Leclair, S.F., and Bridge, J.S., 2001, Quantitative interpretation of sedimentary structures formed by river dunes: Journal of Sedimentary Research, v. 71, p. 713–716.

Leeder, M.R., 1978, A quantitative stratigraphic model for alluvium with special reference to channel deposit density and interconnectedness, *in* Miall, A.D. ed., Fluvial Sedimentology: Canadian Society of Petroleum Geologists Memoir 5, p. 587–596.

Li, Y., and Bhattacharya, J.P., 2013, Facies-architecture study of a stepped, forced regressive compound incised valley in the Ferron Notom Delta, southern central Utah, U.S.A: Journal of Sedimentary Research, v. 83, p. 206–225, doi: 10.2110/jsr.2013.19.

Li, W., Bhattacharya, J.P., and Campbell, C., 2010, Temporal evolution of fluvial style in a compound incised-valley fill, Ferron "Notom Delta", Henry Mountains region, Utah (U.S.A.): Journal of Sedimentary Research, v. 80, p. 529–549, doi: 10.2110/jsr.2010.053.

Li, W., Bhattacharya, J.P., Zhu, Y., Garza, D., and Blankenship, E., 2011, Evaluating delta asymmetry using three-dimensional facies architecture and ichnological analysis, Ferron "Notom Delta", Capital Reef, Utah, USA: Sedimentology, v. 58, p. 478–507, doi: 10.1111/j.1365-3091.2010.01172.x.

Little, W.W., 1997, Tectonic and eustatic controls on cyclical fluvial patterns, Upper Cretaceous strata of the Kaiparowits Basin, Utah, *in* Hill, L.M. ed., Learning from the Land: Grand Staircase-Escalante National Monument Science Symposium Proceedings, Salt Lake City, Bureau of Land Management, p. 489–504.

Ludwig, K.R., 2012, Isoplot 3.75: A Geochronological Toolkit for Microsoft Excel: 75 p.

Macaulay, C.I., Fallick, A.E., and Haszeldine, R.S., 1993, Textural and isotopic variations in diagenetic kaolinite from the magnus oilfield sandstones: Clay Minerals, v. 28, p. 625–639.

McCarthy, P.J., and Plint, A.G., 1998, Recognition of interfluve sequence boundaries: Integrating paleopedology and sequence stratigraphy: Geology, v. 26, p. 387–390, doi: 10.1130/0091-7613(1998)026<0387:ROISBI>2.3.CO;2.

McLaurin, B.T., and Steel, R.J., 2007, Architecture and origin of an amalgamated fluvial sheet sand, lower Castlegate Formation, Book Cliffs, Utah: Sedimentary Geology, v. 197, p. 291–311, doi: 10.1016/j.sedgeo.2006.10.005.

Miall, A.D., 1985, Architectural-element analysis: A new method of facies analysis applied to fluvial deposits: Earth-Science Reviews, v. 22, p. 261–308, doi: 10.1016/0012-8252(85)90001-7.

Miall, A., 2014, Fluvial Depositional Systems: Springer, 332 p., doi: 10.1007/978-3-319-00666-6.

Miall, A.D., 1978, Lithofacies types and vertical profile models in braided river deposits: a summary, *in* Miall, A.D. ed., Fluvial Sedimentology: Canadian Society of Petroleum Geologists Memoir 5, p. 597–600.

Miall, A.D., 2006, Reconstructing the architecture and sequence stratigraphy of the preserved fluvial record as a tool for reservoir development: A reality check: American Association of Petroleum Geologists Bulletin, v. 90, p. 989–1002, doi: 10.1306/02220605065.

Miller, G.M., 1963, Outline of structural-stratigraphic units of the Wah Wah Mountains, southwest Utah, *in* Guidebook to the Geology of Southwestern Utah: Transition Between Basin-Range and Colorado Plateau Provinces, Intermountain Association of Petroleum Geologists, p. 96–102.

Miller, K.G., 2009, Sea level change, last 250 million years, *in* Gornitz, V. ed., Encyclopedia of Paleoclimatology and Ancient Environments, Springer Netherlands, p. 879–887, doi: 10.1007/978-1-4020-4411-3_206.

Miller, G.M., 1966, Structure and stratigraphy of southern part of Wah Wah Mountains, southwest utah: American Association of Petroleum Geologists Bulletin, v. 50, p. 858–900.

Miller, J.S., Glazner, A.F., Walker, J.D., and Martin, M.W., 1995, Geochronologic and isotopic evidence for Triassic-Jurassic emplacement of the eugeoclinal allochthon in the Mojave Desert region, California: Geological Society of America Bulletin, v. 107, p. 1441–1457, doi: 10.1130/0016-7606(1995)107<1441:GAIEFT>2.3.CO;2.

Miller, K.G., Kominz, M.A., Browning, J. V., Wright, J.D., Mountain, G.S., Katz, M.E., Sugarman, P.J., Cramer, B.S., Christie-Blick, N., and Pekar, S.F., 2005, The Phanerozoic record of global sea-level change: Science, v. 310, p. 1293–1298, doi: 10.1126/science.1116412.

Miller, C.F., and Wooden, J.L., 1994, Anatexis, hybridization and the modification of ancient crust: Mesozoic plutonism in the Old Woman Mountains area, California: Lithos, v. 32, p. 111–133, doi: 10.1016/0024-4937(94)90025-6.

Moore, J.N., Allis, R.G., Nemčok, M., Powell, T.S., Bruton, C.J., Wannamaker, P.E., Raharjo, I.B., and Norman, D.I., 2008, The evolution of volcano-hosted geothermal systems based on deep wells from Karaha-Telaga Bodas, Indonesia: American Journal of Science, v. 308, p. 1–48, doi: 10.2475/10.2008.01.

Newell, A.J., Tverdokhlebov, V.P., and Benton, M.J., 1999, Interplay of tectonics and climate on a transverse fluvial system, Upper Permian, southern Uralian Foreland Basin, Russia: Sedimentary Geology, v. 127, p. 11–29, doi: 10.1016/S0037-0738(99)00009-3.

Nummedal, D., and Riley, G.W., 1991, Origin of Late Turonian and Coniacian unconformities in the San Juan Basin, *in* Van Wagoner, J.C., Jones, C.R., Taylor, D.R., Nummedal, D., Jennette, D.C., and Riley, G.W. eds., Sequence Stratigraphy Applications to Shelf Sandstone Reservoirs: Outcrop to Subsurface Examples: AAPG Field Conference Guide, p. 8:1–8:12.

Ollier, C.D., and Galloway, R.W., 1990, The laterite profile, ferricrete, and unconformity: Catena, v. 17, p. 97–109.

Olsen, T., Steel, R.J., Høgseth, K., Skar, T., and Røe, S.-L., 1995, Sequential architecture in a fluvial succession: Sequence stratigraphy in the Upper Cretaceous Mesaverde Group, Price Canyon, Utah: Journal of Sedimentary Research, v. B65, p. 265–280.

Owen, A., Nichols, G.J., Hartley, A.J., and Weissmann, G.S., 2015, Vertical trends within the prograding Salt Wash distributive fluvial system, SW United States: Basin Research, p. 1–17, doi: 10.1111/bre.12165.

Owen, A., Nichols, G.J., Hartley, A.J., Weissmann, G.S., and Scuderi, L.A., 2015, Quantification of a distributive fluvial system: The Salt Wash DFS of the Morrison Formation, SW U.S.A.: Journal of Sedimentary Research, v. 85, p. 544–561, doi: 10.2110/jsr.2015.35.

Peterson, F., 1969a, Cretaceous sedimentation and tectonism in the southeastern Kaiparowits region, Utah: U.S. Geological Survey, Open-File Report 69-202, p. 259.

Peterson, F., 1969b, Four new members of the Upper Cretaceous Straight Cliffs Formation in the southeastern Kaiparowits region, Kane County, Utah: U.S. Geological Survey Bulletin 1274-J, p. J1-J28.

Peterson, F., and Kirk, A.R., 1977, Correlation of the Cretaceous rocks in the San Juan, Black Mesa, Kaiparowits and Henry Basins, Southern Colorado Plateau: San Juan Basin III: New Mexico Geological Society 28th Field Conference Guidebook, p. 167–178.

Peterson, F., and Ryder, R.T., 1975, Cretaceous rocks in the Henry Mountains region, Utah and their relation to neighboring regions, *in* Fassett, J.E. ed., Canyonlands Country: Four Corners Geological Society 8th Field Conference Guidebook, p. 167–189.

Petrus, J.A., and Kamber, B.S., 2012, VizualAge: A novel approach to laser ablation ICP-MS U-Pb geochronology data reduction: Geostandards and Geoanalytical Research, v. 36, p. 247–270, doi: 10.1111/j.1751-908X.2012.00158.x.

Pettinga, L.A., 2013, Tectonic controls on alluvial architecture in the Upper Cretaceous John Henry Member, Straight Cliffs Formation, Southern Utah [M.S. thesis]: University of Utah, 292 p.

Raines, M.K., Hubbard, S.M., Kukulski, R.B., Leier, A.L., and Gehrels, G.E., 2013, Sediment dispersal in an evolving foreland: Detrital zircon geochronology from Upper Jurassic and lowermost Cretaceous strata, Alberta Basin, Canada: Geological Society of America Bulletin, v. 125, p. 741–755, doi: 10.1130/B30671.1.

Reineck, H.-E., and Wunderlich, F., 1968, Classification and origin of flaser and lenticular bedding: Sedimentology, v. 11, p. 99–104, doi: 10.1111/j.1365-3091.1968.tb00843.x.

Roberts, E.M., 2007, Facies architecture and depositional environments of the Upper Cretaceous Kaiparowits Formation, southern Utah: Sedimentary Geology, v. 197, p. 207–233, doi: 10.1016/j.sedgeo.2006.10.001.

Roberts, L.N.R., and Kirschbaum, M.A., 1995, Paleogeography of the Late Cretaceous of the Western Interior of middle North America: Coal distribution and sediment accumulation: U.S Geological Survey Professional Paper 1561, 115 p.

Ryer, T.A., 1981, Deltaic coals of Ferron Sandstone Member of Mancos Shale: predictive model for Cretaceous coal-bearing strata of Western Interior: American Association of Petroleum Geologists Bulletin, v. 65, p. 2323–2340, doi: 10.1306/2F917F05-16CE-11D7-8645000102C1865D.

Ryer, T.A., 2004, Previous Studies of the Ferron Sandstone, *in* Chidsey, T.C., Adams, R.D., and Morris, T.H. eds., Regional to Wellbore Analog for Fluvial-Deltaic Reservoir Modeling: Ferron Sandstone of Utah: American Association for Petroleum Geologists Studies in Geology 50, v. 50, p. 2–38.

Ryer, T.A., 1984, Transgressive-regressive Cycles and the occurrence of coal in some Upper Cretaceous strata of Utah, U.S.A., *in* Rahmani, R.A. and Flores, R.M. eds., Sedimentology of Coal and Coal-Bearing Sequences: International Association of Sedimentologists Special Publication 7, p. 217–227, doi: 10.1002/9781444303797.ch12.

Salem, A.C., 2009, Mesozoic tectonics of the Maria fold and thrust belt and McCoy Basin, southeastern California: an examination of polyphase deformation and synorogenic response [Ph.D. thesis]: University of New Mexico, 283 p.

Schmitt, J.G., Jones, D.A., and Goldstrand, P.M., 1991, Braided stream deposition and provenance of the Upper Cretaceous-Paleocene(?) Canaan Peak Formation, Sevier foreland basin, southwestern Utah, *in* Nations, J.D. and Eaton, J.G. eds., Stratigraphy, Depositional Environments, and Sedimentary Tectonics of the Western Margin, Cretaceous Western Interior Seaway: Geological Society of America Special Paper 260, p. 27–45.

Schoene, B., 2014, U–Th–Pb Geochronology, *in* Holland, H. and Turekian, K. eds., Treatise on Geochemistry, 2nd Edition, Oxford, Elsevier, v. 4, p. 341–378, doi: 10.1016/B978-0-08-095975-7.00310-7.

Schumm, S.A., and Ethridge, F.G., 1994, Origin, evolution and morphology of fluvial valleys, *in* Dalrymple, R.W., Boyd, R., and Zaitlin, B.A. eds., Incised-valley Systems: Origin and Sedimentary Sequences: Society for Sedimentary Geology, Special Publication 51, p. 11–27.

Shanley, K.W., and McCabe, P.J., 1993, Alluvial architecture in a sequence stratigraphic framework: A case history from the Upper Cretaceous of southern Utah, USA, *in* Flint, S.S. and Bryant, I.D. eds., The Geological Modelling of Hydrocarbon Reservoirs and Outcrop Analogues: International Association of Sedimentologists Special Publication 15, Blackwell Publishing Ltd., p. 21–56.

Shanley, K.W., and McCabe, P.J., 1994, Perspectives on the sequence stratigraphy of continental strata: American Association of Petroleum Geologists Bulletin, v. 78, p. 544–568, doi: 10.1306/BDFF9258-1718-11D7-8645000102C1865D.

Shanley, K.W., and McCabe, P.J., 1991, Predicting facies architecture through sequence stratigraphy: An example from the Kaiparowits Plateau, Utah: Geology, v. 19, p. 742–745, doi: 10.1130/0091-7613(1991)019<0742:PFATSS>2.3.CO;2.

Shanley, K.W., and McCabe, P.J., 1995, Sequence stratigraphy of Turonian–Santonian strata, Kaiparowits Plateau, southern Utah, U.S.A.: Implications for regional correlation and foreland basin evolution, *in* Van Wagoner, J.C. and Bertram, G.T. eds., Sequence Stratigraphy of Foreland Basin Deposits: Outcrop and Subsurface Examples from the Cretaceous of North America: American Association of Petroleum Geologists Memoir 64, p. 103–136.

Shanley, K.W., McCabe, P.J., and Hettinger, R.D., 1992, Tidal influence in Cretaceous fluvial strata from Utah, USA: A key to sequence stratigraphic interpretation: Sedimentology, v. 39, p. 905–930, doi: 10.1111/j.1365-3091.1992.tb02159.x.

Shearer, J.C., Staub, J.R., and Moore, T.A., 1994, The conundrum of coal bed thickness: a theory for stacked mire sequences: The Journal of Geology, v. 102, p. 611–617.

Sheets, B.A., Paola, C., and Kelberer, J.M., 2007, Creation and preservation of channel-form sand bodies in an experimental alluvial system, *in* Nichols, G.J., Williams, E., and Paola, C. eds., Sedimentary Processes, Environments and Basins: A Tribute to Peter Friend: International Association of Sedimentologists Special Publication 38, Oxford, UK, Blackwell Publishing Ltd., p. 555–567, doi: 10.1002/9781444304411.ch22.

Sláma, J., Košler, J., Condon, D.J., Crowley, J.L., Gerdes, A., Hanchar, J.M., Horstwood, M.S.A., Morris, G.A., Nasdala, L., Norberg, N., Schaltegger, U., Schoene, B., Tubrett, M.N., and Whitehouse, M.J., 2008, Plešovice zircon: A new natural reference material for U–Pb and Hf isotopic microanalysis: Chemical Geology, v. 249, p. 1–35, doi: 10.1016/j.chemgeo.2007.11.005.

Slingerland, R., Kump, L.R., Arthur, M.A., Fawcett, P.J., Sageman, B.B., and Barron, E.J., 1996, Estuarine circulation in the Turonian Western Interior seaway of North America: Geological Society of America Bulletin, v. 108, p. 941–952, doi: 10.1130/0016-7606(1996)108<0941:ECITTW>2.3.CO;2.

Smith, N.D., Cross, T.A., Dufficy, J.P., and Clough, S.R., 1989, Anatomy of an avulsion: Sedimentology, v. 36, p. 1–23, doi: 10.1111/j.1365-3091.1989.tb00817.x.

Steel, R.J., Plink-Björklund, P., and Aschoff, J.L., 2011, Tidal Deposits of the Campanian Western Interior Seaway, Wyoming, Utah, and Colorado, *in* Davis, R.A. and Dalrymple, R.W. eds., Principles of Tidal Sedimentology, Dordrecht, Springer Netherlands, p. 437–471.

Szwarc, T.S., Johnson, C.L., Stright, L.E., and McFarlane, C.M., 2015, Interactions between axial and transverse drainage systems in the Late Cretaceous Cordilleran foreland basin: Evidence from detrital zircons in the Straight Cliffs Formation, southern Utah, USA: Geological Society of America Bulletin, v. 127, p. 372–392, doi: 10.1130/B31039.1.

Tibert, N.E., and Leckie, R.M., 2004, High-Resolution estuarine sea level cycles from the Late Cretaceous: amplitude constraints using agglutinated foraminifera: Journal of Foraminiferal Research, v. 34, p. 130–143, doi: 10.2113/0340130.

Tibert, N.E., Leckie, R.M., Eaton, J.G., Kirkland, J.I., Colin, J.-P., Leithold, E.L., and McCormic, M.E., 2003, Recognition of relative sea-level change in Upper Cretaceous coal-bearing strata: A paleoecological approach using agglutinated foraminfera and ostracodes to detect key stratigraphic surfaces, *in* Olson, H.C. and Leckie, R.M. eds., Micropaleontologic Proxies for Sea-Level Change and Stratigraphic Discontinuities: Society for Sedimentary Geology Special Publication 75, p. 263–299, doi: 10.2110/pec.03.75.0263.

Titus, A.L., Powell, J.D., Roberts, E.M., Sampson, S.D., Pollock, S.L., Kirkland, J.I., and Albright, L.B., 2005, Late Cretaceous stratigraphy, depositional environments, and macrovertebrate paleontology of the Kaiparowits Plateau, Grand Staircase–Escalante National Monument, Utah, *in* Pederson, J. and Dehler, C.M. eds., Interior Western United States: Geological Society of America, Field Guide 6, p. 101–128, doi: 10.1130/2005.fld006(05).

Titus, A.L., Roberts, E.M., and Albright, L.B.I., 2013, Geologic overview, *in* Titus, A.L. and Loewen, M.A. eds., At the Top of the Grand Staircase: The Late Cretaceous of Southern Utah, Indiana University Press, p. 13–41.

Trendell, A.M., Atchley, S.C., and Nordt, L.C., 2012, Depositional and diagenetic controls on reservoir attributes within a fluvial outcrop analog: Upper Triassic Sonsela member of the Chinle Formation, Petrified Forest National Park, Arizona: American Association of Petroleum Geologists Bulletin, v. 96, p. 679–707, doi: 10.1306/08101111025.

Uygur, K., and Picard, M.D., 1980, Reservoir characteristics of Jurassic Navajo Sandstone, southern Utah, *in* Picard, M.D. ed., Henry Mountain Symposium: Utah Geological Association Publication 8, p. 277–286.

Van Wagoner, J.C., 1995, Sequence Stratigraphy and Marine to Nonmarine Facies Architecture of Foreland Basin Strata, Book Cliffs, Utah, U.S.A., *in* Van Wagoner, J.C. and Bertram, G.T. eds., Sequence Stratigraphy of Foreland Basin Deposits: Outcrop and Subsurface Examples from the Cretaceous of North America: American Association of Petroleum Geologists Memoir 64, p. 137–223, doi: 10.1306/1D9BCB1F-172D-11D7-8645000102C1865D.

Weissmann, G.S., Hartley, A.J., Nichols, G.J., Scuderi, L.A., Olson, M., Buehler, H., and Banteah, R., 2010, Fluvial form in modern continental sedimentary basins: Distributive fluvial systems: Geology, v. 38, p. 39–42, doi: 10.1130/G30242.1.

Weissmann, G.S., Hartley, A.J., Nichols, G.J., Scuderi, L.A., Olson, M.E., Buehler, H.A., and Massengill, L.C., 2011, Alluvial facies distributions in continental sedimentary basins: Distributive fluvial systems, *in* Davidson, S.K., Leleu, S., and North, C.P. eds., From River to Rock Record: The Preservation Of Fluvial Sediments And Their Subsequent Interpretation: Society for Sedimentary Geology Special Publication 97, p. 327–355.

Weissmann, G.S., Hartley, A.J., Scuderi, L.A., Nichols, G.J., Davidson, S.K., Owen, A., Atchley, S.C., Bhattacharyya, P., Michel, L., and Tabor, N.J., 2013, Prograding distributive fluvial systems: Geomorphic models and ancient examples, *in* New Frontiers in Paleopedology and Terrestrial Paleoclimatology.: Society for Sedimentary Geology Special Publication 104, p. 131–147, doi: 10.2110/sepmsp.104.16.

Weissmann, G.S., Hartley, A.J., Scuderi, L.A., Nichols, G.J., Owen, A., Wright, S., Felicia, A.L., Holland, F., and Anaya, F.M.L., 2015, Fluvial geomorphic elements in modern sedimentary basins and their potential preservation in the rock record: A review: Geomorphology, v. 250, p. 187–219, doi: 10.1016/j.geomorph.2015.09.005.

White, T., Furlong, K.P., and Arthur, M.A., 2002, Forebulge migration in the Cretaceous western interior basin of the central United States: Basin Research, v. 14, p. 43–54, doi: 10.1046/j.1365-2117.2002.00165.x.

Whitmeyer, S.J., and Karlstrom, K.E., 2007, Tectonic model for the Proterozoic growth of North America: Geosphere, v. 3, p. 220–259, doi: 10.1130/GES00055.1.

Widdowson, M., 2007, Laterite and ferricrete, *in* Nash, D.J. and McLaren, S.J. eds., Geochemical Sediments and Landscapes, Oxford, UK, Blackwell Publishing Ltd, p. 45–94, doi: 10.1002/9780470712917.ch3.

Wiedenbeck, M., Allé, P., Corfu, F., Griffin, W.L., Meier, M.F., Oberli, F., Von Quadt, A., Roddick, J.C., and Speigel, W., 1995, Three natural zircon standards for U-Th-Pb, Lu-Hf, trace element and REE analyses: Geostandards Newsletter, v. 19, p. 1–23, doi: DOI 10.1111/j.1751-908X.1995.tb00147.x.

Wiedenbeck, M., Hanchar, J.M., Peck, W.H., Sylvester, P., Valley, J., Whitehouse, M., Kronz, A., Morishita, Y., Nasdala, L., Fiebig, J., Franchi, I., Girard, J.-P., Greenwood, R.C., Hinton, R., et al., 2004, Further characterisation of the 91500 zircon crystal: Geostandards and Geoanalytical Research, v. 28, p. 9–39, doi: DOI 10.1111/j.1751-908X.2004.tb01041.x.

Wright, V.P., and Marriott, S.B., 1993, The sequence stratigraphy of fluvial depositional systems: The role of floodplain sediment storage: Sedimentary Geology, v. 86, p. 203–210.

Young, R.A., and Mckee, E.H., 1978, Early and middle Cenozoic drainage and erosion in west-central Arizona: Geological Society of America Bulletin, v. 89, p. 1745–1750, doi: 10.1130/0016-7606(1978)89<1745:EAMCDA>2.0.CO;2.

Zaitlin, B.A., Dalrymple, R.W., and Boyd, R., 1994, The stratigraphic organization of incised-valley systems associated with relative sea-level change, *in* Dalrymple, R.W., Boyd, R., and Zaitlin, B.A. eds., Incised-Valley Systems: Origin and Sedimentary Sequences, Society for Sedimentary Geology, Special Publication 51, p. 45–60.

Zhu, Y., Bhattacharya, J.P., Li, W., Lapen, T.J., Jicha, B.R., and Singer, B.S., 2012, Milankovitch-scale sequence stratigraphy and stepped forced regressions of the Turonian Ferron Notom Deltaic Complex, south-central Utah, U.S.A: Journal of Sedimentary Research, v. 82, p. 723–746, doi: 10.2110/jsr.2012.63.

Zuffa, G.G., 1985, Optical analyses of arenites: Influence of methodology on compositional results, *in* Zuffa, G.G. ed., Provenance of Arenites, Dordrecht, Springer Netherlands, p. 165–189, doi: 10.1007/978-94-017-2809-6_8.